STRUCTURAL, ELASTIC AND VIBRATIONAL PROPERTIES OF Fe$_2$P-TYPE MATERIALS FOR MAGNETIC REFRIGERATION: A DENSITY FUNCTIONAL THEORY (DFT) STUDY

THIRIKA ANNE MWENDE

A Thesis Submitted to the Graduate School in Partial Fulfillment of the Requirements for the Doctor of Philosophy Degree in Physics of Egerton University

EGERTON UNIVERSITY

AUGUST, 2023

DECLARATION AND RECOMMENDATION

Declaration

This thesis is my original work and has not been presented in this university or any other for the award of a degree.

Signature: ~~RM~~   Date: 5/8/2023

THIRIKA ANNE MWENDE

SD13/16524/18

Recommendation

This thesis has been submitted with our approval as university supervisors.

Signature: Date: 7/8/2023

DR. WINFRED M MULWA, PhD

Department of Physics,

Egerton University.

Signature: Date: 7/8/2023

DR. NICHOLAS W. MAKAU, PhD

Department of Physics,

University of Eldoret.

Signature: Date: 7/8/2023

DR. ADETUNJI BAMIDELE IBRAHIM, PhD

Department of Physics,

Bells University of Technology, Ota, Ogun State, Nigeria.

DEDICATION

This thesis is dedicated to my beloved parents Mr. Albert Thirika and Mrs. Evelyn Thirika for their endless support in making my dream a reality. To my nieces Lynn Mukami, Leer Nkantha, Trishelle Thirika and nephews Leon Muthomi, Brovins Thirika, Carson Mwenda, Sean Makali, Liam Mawira and Tristan Thirika for being my greatest cheer leaders throughout this academic journey.

ACKNOWLEDGEMENTS

Above all my deepest gratitude goes to the Lord God the Almighty for giving me the wisdom, strength and knowledge to pursue this study.

ABSTRACT

Magnetic refrigeration, also known as adiabatic magnetisation is a physical process that makes use of the magnetic properties of some type of materials to attain extremely low temperatures, through a process defined as the magnetocaloric effect (MCE). The advantages of this technology over the traditional gas compressor-based refrigeration are that, it is low in energy consumption, has a higher refrigeration efficacy and it is ecologically friendly. Hexagonal Fe_2P-type materials have been established to exhibit good magnetocaloric properties however, their poor structural, mechanical and dynamical stability along the phase transition limits their application in practical devices. Modifying these material characteristics by alloying or doping is crucial for finely-tuning their performance. Here, a study was conducted into the theoretical aspects of the structural, elastic, and vibrational attributes of $FeMnP_{1-x}A_x$ compounds (where A = Si, Se, In, Sn, and x = 0.33). The primary aim was to assess the viability of employing these compounds as solid-state magnetic refrigerants. To achieve this, first principle computations based on Density Functional Theory (DFT) were executed via the Quantum Espresso software. The investigation encompassed diverse dimensions such as structural parameters (including lattice dimensions and bond lengths), which were determined by iteratively adjusting atomic positions along the x, y, and z axes until the system reached its lowest energy configuration following defined convergence criteria. The calculations of elastic characteristics, including elastic constants, was accomplished using the Thermo_pw software coupled with quantum espresso. The assessment of bulk moduli (B) and shear moduli (G) involved the implementation of the Voigt-Reuss-Hill (VRH) approximation method. The Vibrational properties such as phonon frequency, phonon density of states, phonon band structure and phonon thermal properties were calculated using harmonic approximation by the frozen phonon approach using the phonopy code interfaced with quantum espresso. From study results, the calculated elastic constants were found to fulfill the four Born conditions essential for ensuring elastic stability. The small percentage deviations of the values of lattice constants and bond lengths from the experimental data for $FeMnP_{0.66}Si_{0.33}$ indicated the accuracy of these calculations. There is also occurrence of phonon anomaly (pseudo gap) which is fundamentally a measure of thermal conductivity and it confirmed that the investigated materials were good thermal conductors. The nonappearance of negative frequencies from the phonon dispersion graphs indicate that all the compounds were dynamically stable in their ferromagnetic phases.

TABLE OF CONTENTS

LIST OF FIGURES

LIST OF TABLES

LIST OF ABBREVIATIONS AND ACRONYMS

AFM	Anti-Ferro Magnetic
AMR	Active Magnetic Regenerator
CFC	Chlorofluorocarbon
DFT	Density Function Theory
DOS	Density of State
EOS	Equation of State
ESPRESSO	opEn-Source Package for Research in Electronic Structure, Simulation, and Optimisation
FM	Ferro Magnetic
GGA	Generalised Gradient Approximation
GRACE	Graphing Advanced Computing and Exploration of data
HFC	Hydrofluorocarbon
IBZ	Irreducible Brillouin zone
MCE	Magneto Caloric Effect
PBE	Perdew Burke Ernzerhof
PM	Para Magnetic
Pw	Plane waves
Pwscf	Plane wave self-consistent field
QE	Quantum ESPRESSO
XCrySDen	X-window Crystalline Structure and density
SCF	Self-consistent field
USPP	Ultra-Soft Pseudopotentials
VRH	Voigt-Reuss-Hill

LIST OF SYMBOLS

As	Arsenic
CO_2	Carbon dioxide
Fe	Iron
Ga	Gallium
Ge	Germanium
Gd	Gadolinium
In	Indium
La	Lanthanum
Mn	Manganese
P	Phosphorus
Si	Silicon
Se	Selenium
Sn	Tin

CHAPTER ONE

INTRODUCTION

1.1 Background Information

The rising energy demand has turned out to be a chief alarm in the world since conservative sources of energy are inadequate. In both domestic and in industrial environments, refrigeration is a main source of energy consumption (Aprea *et al*., 2016). Cooling systems are very vital in food transportation and storage. This implies that in the absence of refrigeration in the supply of food would result in a seasonal and limited supply of non-perishable and locally produced food items only. Short of cooling systems, medical practices such as cryo-surgery, organ transportation, tissue and organ cryo- storage would not be possible. Hospitals, Laboratories and Pharmacies also depend on cold storage systems to preserve drugs, vaccines, blood and serum. Air conditioning units in buildings, vehicles and aircraft also rely on refrigeration. The traditional refrigerators use refrigerants such as chlorofluorocarbons and hydro fluorocarbons which has raised major environmental concerns with depletion of the ozone layer and global warming respectively (Drake *et al*., 2001; Protocol, 1987). In order to improve energy efficiency, minimise energy consumption, and reduce the ozone layer exhaustion and in turn global heating there is a need to replace the current cooling systems with more energy-efficient and environment friendly cooling technologies (Ekanth & Kishor, 2016).

The field of magnetic refrigeration, an electronic process which involves magnetisation and demagnetisation of magnetic materials, has caught the attention of numerous researchers (Balli *et al*., 2012). This technology depends on the magnetocaloric effect and is used in refrigerators to achieve remarkably low temperatures with a higher cooling efficiency, low energy consumption and non-reliance on detrimental and ozone-depleting coolant gases. Hence, it poses no impairment to the environment by limiting discharge of greenhouse gases (CO_2) and avoiding the use of ozone layer depletion and hazardous chemicals such as CFCs and HCFs (Mezaal *et al*., 2017). Zimm *et al*. (1998) reported that the cooling efficiency of a gas compression refrigerator was about 40% whereas that of a magnetic refrigerator based on Gadolinium was 60% of the theoretical limit. Moreover, magnetic refrigeration is a cost-effective technology that has been shown to save up to 30% of energy in comparison with the traditional gas compression technology (Dieckmann *et al*., 2007).

Research into magnetic refrigeration has led to the discovery of magnetic materials with extraordinary changes in temperature upon adiabatic magnetisation around the room temperature (Dung *et al.*, 2011). The most commonly utilized materials for room temperature refrigeration are rare-earth-based substances, such as alloys containing Gd, $Gd_5(Ge_{1-x}Si_x)_4$ where (where $0 < x < 0.5$) and La (Fe, Si)$_{13}$ (Dan'kov *et al.*, 1998). These materials show paramagnetic to ferromagnetic transition at Curie temperatures of around 276K to 299K. The limitation of these rare-earth based materials is that they contain expensive rare-earth metals which limit their application in practical devices (Franco *et al.*, 2018). In addition, their admirable magnetocaloric characteristics are tough to advance upon. Other materials such as β-MnAs and Heusler alloys have also been studied as possible candidates for magnetic cooling. However, the β-MnAs compound contains a toxic element (As) and has poor mechanical properties (Jiles, 2015). Pecharsky and Schneider (1997) reported that for Heusler alloys, the temperature range for the magneto structural transition is 280–310 K but are dynamically unstable. Other interesting compounds that have been reported as probable candidates for good performance in magnetic cooling are hexagonal Fe$_2$P-type materials.

In the past decade, samples of different Si content in the $FeMnP_{1-x}Si_x$ ($0 < x < 1$) system were carefully explored. The crystals were reported to be structurally unstable for $0.5 < x < 1$ in that they changed from hexagonal to cubic structure at phase transition (Hoglin *et al.,* 2015). However, for $FeMnP_{1-x}Si_x$ ($0.3 < x < 0.5$) structural stability was reported (Torun *et al.*, 2016). These materials were found to crystallise in $P\bar{6}2m$ (189) space group where the transition metals, Iron and Manganese occupy the 3f and 3g sites while the Phosphorus and Silicon atoms occupy the sites 2c and 1b respectively (Balli *et al.*, 2012). In proximity to room temperature, this category of materials was observed to undergo a first-order magnetoelastic transition, leading to alterations in the ratio of lattice parameters (c/a), while the overall volume remained relatively unchanged. At the Curie temperature, the best performance of FeMn-based materials was found to be influenced by the frequency of the elastic and the magnetic transition concurrently (Ou *et al.*, 2013). Deprived mechanical and dynamical stability along with poor phase transition restricts the application of $FeMnP_{1-x}Si_x$ ($0.3 < x < 0.5$)   as a magnetic refrigerant on practical devices (Zhu *et al.*, 2017). The current literature shows there are gaps in the understanding of these magnetocaloric materials. Further research, therefore, needs to be done in order to identify non-toxic, readily available, structurally, mechanically and dynamically stable magnetic refrigerant materials (Berreta *et al.,* 2019).

Several efforts to improve the performance of $FeMnP_{1-x}A_x$ (A = Si,) for practical device application have been made through alteration of the crystal parameters, transition temperature, magnetic properties, transition order and hysteresis, among others (Vincent *et al.,* 2021). This has been achieved by alloying with elements such as Cobalt, Nickel, Copper, Chromium and Boron, together with changing the ratio of the transition metals (Fe: Mn) occupying the 3f and 3g sites as well as (P: A=Si) at the 2c and 1b sites, respectively. Some of the available options for optimisation of the structural, mechanical and dynamical stability of magnetocaloric materials include replacing the atoms at the A site in $FeMnP_{1-x}A_x$ (A = Si) with other viable elements that are not toxic in nature. The principal goal of alloying is to imitate the bonding between atoms which could eventually raise o lower the stability, enhance magnetic behaviour, transition order and decrease the thermal hysteresis. Examples in this direction can be found for Ge and Ga replacement of A in $FeMnP_{1-x}A_x.$ This has already been observed in a recent study where Wu *et al*. (2017) established through Density Functional Theory calculations that $FeMnP_{1-x}A_x$ (A= Ga, Si, Ge; x = 0.33) indeed maintained their hexagonal structure in both ferromagnetic and paramagnetic states hence structurally stable. In addition, Wu *et al.* (2017) reported a high magnetisation effect, little thermal hysteresis and a phase transition close to room temperature T_C for these compounds.

Apart from having their phase transition near the room temperature, a good magnetocaloric material should also be; structurally stable, mechanically stable, dynamically stable, a good thermal conductor, environmentally friendly, energy efficient, less toxic and made from readily available materials. From the current literature, a number of materials that have been studied so far do not fulfill the many of the requirements for a magnetic refrigeration and hence there need for extensive research to improve the known materials. Therefore, there is need to replace the A site atom in $FeMnP_{1-x}A_x$ (x = 0.33) with other viable metalloids in order to provide more understanding on the structural mechanical and vibrational properties of these magnetocaloric alloys. Building on this, structural, elastic and vibrational calculations of the host material, $FeMnP_{1-x}A_x$ (A=Si, x = 0.33) were carried out using first principle DFT. In addition, $FeMnP_{1-x}A_x$ (A = Sn, Se and In, x = 0.33) were investigated as possible candidates for room temperature magnetic refrigeration by analysing their structural, elastic and vibrational properties and comparing the results with those of the host crystal.

1.2. Statement of the Problem

The current energy crisis coupled with environmental concerns has put clean energy research on the urgent agenda worldwide. This aims at increasing the use of renewable energy, which in turn reduces environmental pollution, that would otherwise result in ozone layer exhaustion and global warming. Domestic utilisations such as refrigerators and air conditioners are some of the major energy consumers. These depend on refrigerants such as chlorofluorocarbons, hydrofluorocarbons and other chemicals to complete the vapor-compression refrigeration cycle. In the process, they react with oxygen and release CO_2, which is a major greenhouse gas that poses harmful effects on the ecosystem, biodiversity and human livelihood. There is an urgent need to replace the current refrigeration methodologies with more energy-efficient and environmentally friendly refrigeration methods. This work aims at modelling a magnetic refrigerant that is non-toxic, inexpensive, structurally, mechanically and dynamically stable. Insights from this work will allow future studies to appreciate, comprehend and forecast better magnetocaloric materials and fabricate the same.

1.3. Objectives

1.3.1 General Objective

To investigate the structural, elastic and vibrational properties of $FeMnP_{1-x}A_x$ (A= Si, Se, Sn and In, x = 0.33) for near –room- temperature magnetic refrigeration, using Density Functional Theory (DFT).

1.3.2 Specific Objectives

i. To determine the effect of the substitutional atoms (Se, Sn and In) on the structural properties of $FeMnP_{1-x} A_x$ (A = Si, x = 0.33) using DFT

ii. To determine the effect of the substitutional atoms (Se, Sn, In) on the elastic properties of $FeMnP_{1-x} A_x$ (A = Si, x = 0.33) using DFT

iii. To determine the effect of the substitutional atoms (Se, Sn and In) on the vibrational properties of $FeMnP_{1-x} A_x$ (A = Si, x = 0.33) using DFT

1.4. Research Questions

i.   What is the effect on the structural properties of $FeMnP_{1-x}A_x$ (A=Si, x = 0.33), when the A site of this alloy is substituted with atoms (Se, Sn and In)?

ii. What is the effect on the Elastic properties of $FeMnP_{1-x}A_x$ (A=Si, x = 0.33), when the A site of this alloy is substituted with atoms (Se. Sn and In)?

iii. What is the effect on the Vibrational properties of $FeMnP_{1-x}A_x$ (A=Si, x = 0.33), when the A site of this alloy is substituted with atoms (Se. Sn and In)?

1.5. Justification

Currently, hexagonal Fe_2P-type magnetocaloric materials have garnered substantial research attention due to their promising application in magnetic refrigeration. Recent studies indicate that these materials offer energy-efficient and environmentally friendly alternatives to conventional gas compressor-based refrigeration methods. However, working under recurrent magnetic and thermal cycles, these polycrystalline samples experience significant local strains. Thus, they necessitate robust architectural, dynamic, and mechanical stability across phase transitions to endure these external stresses. Many of the magnetocaloric compounds considered for magnetic cooling candidates suffer from drawbacks such as toxicity, high cost, limited dynamic stability, poor mechanical strength, and architectural fragility. Consequently, comprehensive research is required to develop alloys that exhibit enhanced performance in magnetic refrigeration, overcoming the aforementioned limitations. This study aims to investigate $FeMnP_{1-x}A_x$ (A = Si, x = 0.33) materials with the intention of surpassing the properties previously reported in the literature. Moreover, viable and non-toxic atoms (In, Se, Sn) will be introduced to replace the atoms at the A site of $FeMnP_{1-x}A_x$ (A = Si, x = 0.33). The analysis encompassed an examination of their structural, elastic, and vibrational attributes.

1.6. Definition of Terms

1.6.1 P-type materials

A P-type material is a semiconductor whose majority of charge carriers are holes which exhibit properties of positive charges. It is achieved by doping an intrinsic semiconductor with a trivalent atom.

1.6.2 Refrigeration

This cooling process is of artificial origin, orchestrated by humans. In this method, thermal energy is extracted from a low-temperature reservoir and transferred to a higher-temperature reservoir by applying external work to the system. It encompasses the act of reducing the temperature of a space, substance, or system, or sustaining it at a level lower than the surrounding ambient temperature.

1.6.3 Magnetic refrigeration

Magnetic refrigeration is an evolving, environment-friendly knowledge for the cooling at room temperature. It is grounded on a magnetic solid state refrigerant that works using the principle of the magneto-caloric effect.

1.6.4 Magnetic field

Magnetic field is a vector field in the neighbourhood of an electric current, a magnet, a magnetic material or a changing electric field that describes the effects magnetic forces. It is used as a tool to visualise how the magnetic force is spread in the areas around and within a magnetic material.

1.6.5 Refrigerant

A refrigerant is a working substance that is used in the refrigeration heat cycle. It extracts heat from a low temperature reservoir and rejects the same heat to a high temperature medium.

1.6.6 Near room temperature refrigeration

Magnetocaloric effect only works around a materialsferromagnetc to paramagnetic phase transition temperature and is maximum at a materials curies temperature T_C. Near room temperature refrigeration signifies the refrigeration achieved at a materials curies temperature which is between 293 K to 300 K depending on climatic conditions of the given environment at a specific time.

1.6.7 Magnetocaloric effect (MCE)

MCE is the heating or cooling of a magnetic material when an applied magnetic field changes. This outcome is characterised by an adiabatic alteration in temperature ΔT_{ad} and isothermal change in magnetic entropy, ΔS_m arising from the application of external magnetic field H.

1.6.8 Curie temperature

This is temperature at which some magnetic materials exhibit a sharp variation in their magnetic properties. Above this temperature these magnetic materials lose their permanent magnetic properties. In other words it is the temperature above which there is a transtition between a ferromagnetic phase and a paramagnetic phase.

1.6.9 Computational physics

Computational physics is a field that involves the learning and application of numerical analysis to solve problems in physics for which a quantitative theory already exists. It involves both arithmetic and non-arithmetic calculations following well defined models with computers using programming languages such as FORTRAN, C, C++, and Python.

1.6.10 Density functional theory

 Density functional theory is a quantum mechanical modelling method used to solve the Schrödinger equation of a many body system using the idea ofelectron density as a functional to give ground state properties. It is based on two important mathematical statements demonstrated by Hohenberg – Kohn and a set of equations derived by Kohn and Sham.

1.6.11 Metalloids

Metalloids also known as semi metals are chemical elements that lie between groups 13 to 17 of the periodic table. They have a mixture of both metallic and non-metallic properties and form alloys easily with metals.

1.6.12 Alloys

An alloy is a mixture of two or more elements and whose the primary constituent is a metal. Most commonly it has one or two metallic elements that stand for 90% of the composition. Alloys are

formed by combining desired elements in secific proportions to create a material with better properties.

1.6.13 Paramagnetic materials

Paramagnetic materials are those materials that tend to get weakly magnetised in the direction of the magnetising field when placed in a magnetic field. They become magnetised when put in a magnetic field but when the field is removed the magnetism disappears. Some examples of these materials are Copper and Aluminum.

1.6.14 Ferromagnetic materials

Ferromagnetic materials are those whose magnetic domains align parallel to the applied magnetic field resulting to a spontaneous positive net magnetisation at the atomic level. They retain their magnetism even in the absence of an external magnetic field. Some examples of these materials are Iron and Nickel.

1.6.15 Antiferromagnetic materials

Antiferromagnetic materials are those whose magnetic moments align anti parallel to the applied magnetic field resulting to zero total magnetism at the atomic level. Some examples of these materials are Manganese and Chromium.

1.6.16 Doping

Doping is the process of adding impurities to an intrinsic semiconductor to make it an extrinsic semi conductor with the aim of imroving or modifying its electronic properties.These impurities constitute atoms of differing valence,inorder to alter the Fermi level. This process manipulates the extent to which electrons go from the valence band to the conduction band or create holes in the valence band.

1.6.17 Alloying

Alloying is a complex process characterized by mechanical, heat transfer, mass transfer, and chemical events that involve intricate phase transformations and multifaceted interactions among solid, liquid, and gaseous phases

1.6.18 Entropy (S)

Entropy is a measurable physical property, commonly associated with a state of randomness, uncertainty and disorder of a thermodynamic system. It is defined as the measure of a system's thermal energy per unit temperature that is unavailable for doing useful work.

1.6.19 Enthalpy (H)

Enthalpy is a thermodynamic concept that is used to calculate the total heat content of an open system in science and engineering. It is the sum of the internal energy added to the work (product of pressure and volume) of the system.

1.6.20 Free Energy (G)

Free energy is a thermodynamic quantity equivalent to the capacity of a system to do work or energy that is ot dissipated. Gibbs free energy is the energy that may be converted into work in a systen that is at a constant pressure and temperature. Gibbs free energy is equal to Enthalpy minus the product of entropy and temperature of a system ($G = H – TS$). Helmholtz free energy (A) is that which may be converted into work at a contant temperature and volume. It is equivalent to the internal energy of the system minus the product of entropy and absolute temperature of the system ($A = U – TS$).

1.6.21 Schrodinger equation

Schrodinger equation is a mathematical expression that describes the energy and position of an electron in space and time. This is a key equation in Quantum mechanics and it takes into account the matter wave nature of an electron inside an atom.

1.6.22 Phonons

A phonon is a definite discrete unit or quantum of vibrational mechanical energy that arises from oscillating atoms within a crystal lattice.

1.6.23 Adiabatic process

An adiabatic process is a thermodynamic process that involvres the transfer of energy without the transfer of heat or mass between the system and its sorrounding. For this to happen, the system

must be perfectly insulated from the sorrounding. In addition the process must be carried out so quickly that there is not enough time for appreciable heat flow.

1.6.24 Isothermal process

An Isotherma process is a themodynamic process that occurs at a constant temperature. For this to happen, any heat flow into or out of the system must occur slowly enough that thermal equilibrium is mantained.

1.6.25 Elasticity

Elasticity implies to the ability of a deformed material body to return to its original shape and size when the forces causing the deformation are removed. Elastic modulus and elastic limit are the 2 parameters that define the elasticity of a material.

1.6.26 Plasticity

This is the the ability of a solid material to undergo a non reversible change in shape and size in response to applied forces. A material undergoes plastic deformation when the stress is increased beyond the elastic limit.

1.6.27 Global warming

Global warming is the phenomenon of gradual increase in the earths temperature generally due to greenhouse effect caused by increased levels of carbon dioxide, Chlorofluoral carbons and other pollutants. This happens when carbon dioxide (CO_2) and other air pollutants collect in the atmosphere and absorb sunlight and solar radiation that have bounced off the earth's surface leading to long term shift in temperatures and weather patterns.

1.6.28 Ozone layer depletion

Ozone layer depletion is the reduction or thinning of the ozone layer present in the upper atmosphere caused by relese of of chemical compounds containing gaseous chlorine or Bromine from industries and human activities. This is a major environmental concern because it it increase the amount of ultra violet radiation that reaches the earth surface and cause damage to both living things and the environment.

1.6.29 First order magnetic phase transition

First order magnetic phase transition is when the first derivative of the system's Gibbs free-energy with intensive parameters /temperature, pressure, magnetic field exhibit a discontinuity at the critical values of the parameters. It results from the strong change of the exchange interactions as a function of the interatomic distances and the associated changes in the elastic energy of the material.

1.6.30 Second order magnetic phase transition

At the second order magnetic phase transition, the order parameter increases continuously from zero starting at the critical temperature of the phase transition. Here there is a discontinous change in the second derivative of the Gibbs free energy hence a reversible magnetic transition from a low temperature ferromagnetic state to a high temperature paramagnetic state.This does not have any latent heat associated with it but the entropy is continous at the critical temperature T_C.

1.6.31 Pseudopotential

A pseudopotential also known as an effective core potential is a reliable and convenient technique used to incooperate the major scalar relativistic effects into quantum mechanics calculations. This helps in excluding the inactive atom core electrons from an explicit treatment during these calculations therefore, providing an approximation for a simplified description of many body or complex systems.

1.6.32 Self consistent field

A self consistent field is an iterative concept in quantum mechanics that is used to find an approximate solution to the many body problem. It involves the selection of an approximate Hamiltonian, solving the schrodinger equation to obtain a set of orbitals that are more accurate and then repeating the whole process until the system attains a convergence.

1.6.33 k-points

k-points are defined as a set of discrete sampling points in the first brillouin zone in the reciprocal or fourier space. The number of k -points to be used in any calculation is determined by the size

of the unit cell in that the bigger the cell the less the number of k-points required. Also to note is that the higher the number of k-points, the more the convergence and the finer the precision.

1.6.34 First brilloin zone

The first brillouin zone also known as the primitive wigner seitz cell is defined as the specific region of the reciprocal space closest to the gamma point or the origin defined by coordinates (0,0,0). This is where the propertis of the bloch electrons (electrons present in the periodic potential or crystals) are usually studied.

1.6.35 Lattice parameters

A lattice parameter also known as a lattice constant is the length between two points on the corners of a unit cell. A crystals lattice parameters a,b and c have the dimensions of length. The periodic arrangement of atoms in a crystal is reffered to as a lattice.

1.6.36 Bond Length

Bond length also known as bond distance is the mean length between nuclei of two bonded atoms in a molecule. It is connected to the bond order in that the more the electrons participating in the bond formation the shorter the bond length. Bond length also has an inverse proportionality to both the bond strength and the bond dissociation energy.

1.6.37 Structural optimisation

Structural optimisation in density functional theory calculations involves moving the atoms of a molecule to achieve the most stable structure with the lowest possible ground state energy. This helps predict the 3 -dimensional arrangement of the atoms in the molecule by minimising the stresses weight or compliance for a given amount of materials boundary conditions.

1.6.38 Structural relaxation.

Structural relaxation is the process of minimising the interatomic forces in density functional theory calculations. Relaxation is done prior to a property calculation as a critical precaution inorder to ensure fast convergence and give accurate final result in the material property that is being computed.

1.6.39 A supercell

A super cell is defined as a repeating unit cell of the crystal that contains several primitive cells.It is used in calculation of properties that cannot be determined using the unit cell for example during phonon calculations.

1.6.40 Electron density

Electron density is the degree of the likelyhood of an electron being present at a certain distance from the nucleus. Density functional theory uses the idea of of electron density to reduce many body problem to a many one body problem. The former has many degrees of freedom with 3N coordinate system where N is the number of atoms in the unit cell. While the latter reduces the degrees of freedom to only a 3 coordinate (x,y,z) system.

CHAPTER TWO
LITERATURE REVIEW

2.1 Introduction

Over the recent past, researchers drawn from different parts of the globe have developed a great interest towards the magnetic refrigeration field of study mainly due to the conventional cooling technique which operates by vapor compression (Botoc *et al*., 2021). Magnetic refrigeration idea came about from the magnetocaloric effect discovery by Warburg in 1881. However, the discovery of the principle related to the cooling near room temperature was done later by Brown in the year 1976 (Tishin & Spichkin, 2016). The close to room temperature cooling by magnetism is a technology that has got the ability to attain higher efficiency as compared to the usual approach of vapor compression. Additionally, magnetic refrigeration entails the concept of magnetic effect which can basically be said to be the nature of a magnetic material to absorb or emit heat as a way of responding to the changes in the magnetic field (Romero *et al.,* 2013).

2.2 Magnetic Refrigeration

Magnetic refrigeration is an emerging and environmentally friendly technology that relies on a magnetic solid material functioning as a refrigerant through the utilization of the magnetocaloric effect (Aprea *et al*., 2015; Ekanth & Kishor, 2016). The magnetocaloric effect (MCE) is a magneto-thermodynamic phenomenon wherein a suitable material undergoes a reversible temperature change when subjected to a varying magnetic field. This process generates a warming effect during field creation and a cooling effect during field removal (Nagalakshmi *et al*., 2015; Wali *et al*., 2015). The MCE operates effectively around a material's transition temperature and is most pronounced at its Curie temperature (Tc), which is the temperature above which a ferromagnetic compound transitions to paramagnetic due to atomic vibrations (Kitanovski *et al*., 2014; Kitanovski & Egolf, 2009).
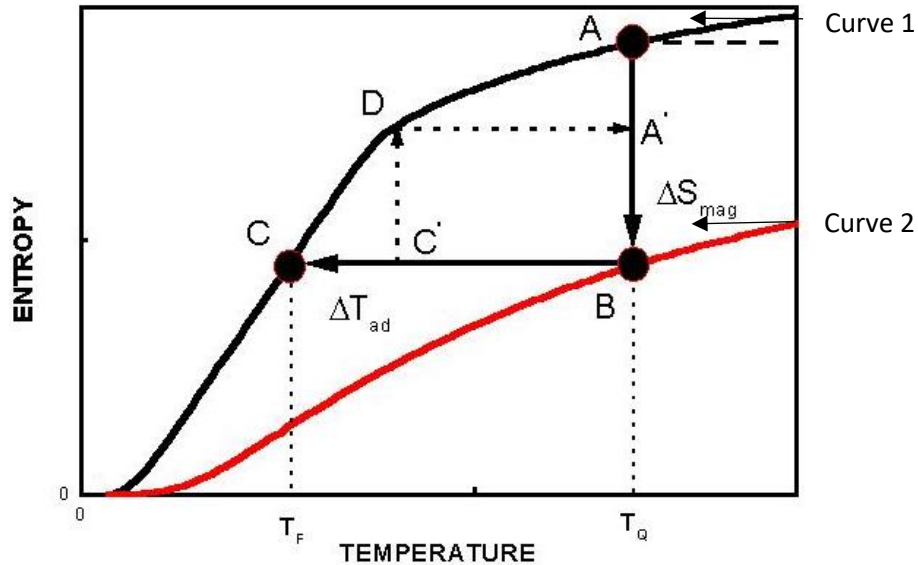
Figure 2. 1: Graph of temperature dependence on magnetic entropy. Curves 1 and 2 represent the normal magnetic behaviours with zero field, and with applied magnetic field respectively
Source: Ranke *et al*. (2000).

The Magnetocaloric effect is depicted in figure 2.1. This process is characterised by a temperature change in an adiabatic process – one that happens without transfer of heat between a system and its environs. This is shown by the section B to C of the graph where along the constant entropy path the temperature drops from T_Q to T_F. Another feature of MCE can be seen from the section A to B of the same graph where there is a magnetic entropy change in an isothermal process. An isothermal process is one whose temperature remains constant for example what is happening along the isotherm T_Q (Huang *et al*., 2015). The isothermal magnetisation of a paramagnetic material decreases the entropy and in the reverse course, demagnetisation restores the zero-field magnetic entropy of the system. All of this arises due to the interaction between the magnetic sublattice and the applied magnetic field, leading to alterations in the magnetic contribution to the entropy of the soli (Wand & Bi, 2009).

2.2.1 The Benefits of the Use of Magnetic Refrigeration.

Magnetic refrigeration has advantages over vapour compression refrigeration in that it is an environmentally friendly technology. This is because it eliminates the refrigerants found within the vapor compression system, primarily composed of chlorofluorocarbons and hydrofluorocarbons that cause the depletion of the ozone layer. Instead, it makes use of solid-state

magnetocaloric material and a heat transfer fluid such as water or ethanol, which are less harmful to the environmentally (Pecharsky & Gschneidner, 1997). Secondly, magnetic refrigeration has a high thermodynamic efficiency that come near to a reversed Carnot cycle significantly improved than the conventional system and reduces the power consumption by 20 to 30 % (Aprea *et al*., 2016). In addition, it is free of noise pollution. The compressor, used in a conventional system brings a few disadvantages such as the noise and vibrations. In a magnetic system, this component is replaced by magnets, which operates in silent without noise and vibrations (Mezaal *et al*., 2017). Lastly, a Magnetic cooling arrangement guarantees inexpensive running and insignificant maintenance as there are no moving parts. Disposal of such systems is also simple and cost-effective (Aprea *et al*., 2016; Gschneidner & Pecharsky, 2008).

2.2.2 The Magnetisation and Demagnetisation Cycles on the Crystal Structures.

The magnetisation cycle involves the process of an external magnetic field application to a material and observing how its magnetisation changes as a function of the field strength. In the context of MCE, this cycle is essential for understanding how the crystal structure responds to magnetic fields and how this response influences the temperature change of the said material. During the magnetisation cycle, the material undergoes transitions between different magnetic phases, which are closely related to its crystal structure. On the other hand, the demagnetisation cycle involves reducing or removing the external magnetic field from the material, causing its magnetisation to change again. In the context of MCE, the demagnetisation cycle is crucial because it allows the material to release heat and return to its original temperature. This process is often carefully controlled to ensure efficient cooling. As the magnetic field decreases, the material absorbs heat from its surroundings, resulting in a cooling effect (Nayak & Nigam, 2009).

Magnetic refrigeration relates to the concept of magnetocaloric effect (MCE). Adiabatic temperature change (ΔT_{ad}) or rather a Magnetocaloric effect is usually detected as the cooling and heating of magnetic materials as a result of changing magnetic field, was initially discovered in iron by a scientist known as Warburg. The MCE thermodynamics was first comprehended by Giauque and Debye who both suggested that this effect could be applied to arrive at low temperatures through an adiabatic demagnetisation process. Later after this discovery, a refrigerator employing the concept of adiabatic demagnetisation was set up and the utilised by McDougal and Giauque upon application of magnetic field of 0.8T on $Gd_2(SO_4)_3.8H_2O$ (Gschneidner *et al.,* 2000). For a ferromagnetic material close to magnetic Neel temperature,

16

subjecting a solid to an adiabatic magnetic field results in a reduction of its magnetic entropy, prompting an increase in lattice entropy to maintain a constant overall entropy within a closed system. In a reversible scenario, the cooling of a ferromagnet involves a simultaneous rise in magnetic entropy, followed by a decline in lattice entropy upon adiabatic removal of the magnetic field (Cakir & Acet, 2012).

The refrigeration of a magnetic material while responding to a varying magnetic field resembles how a gas medium behaves when it is warmed and cooled as a response to adiabatic expansion and compression. As a result, magnetic refrigeration works by magnetising or demagnetising the involved magnetic material. In the meantime, the said refrigerant is a solid, mostly in thin sheets form or spherically shaped, provision of heat transfer is done with a fluid such as inert gas, water or water incorporated with antifreeze based on the temperature under which the refrigerator operates (Zoontens *et al.,* 2009). Despite the need for refrigerants that are friendly to the environment, the efficiency of energy for air conditioning and refrigeration also needs to be improved. To some extent, this can be realised using vapor compression. Nevertheless, the fact that vapor compression potential is limited calls for the exploration of alternate mechanically or electrically driven systems. Many researchers have suggested that ferroic/caloric refrigeration as well as heat-pumping technologies are the most appropriate future options and are currently under study (Kitanovski, 2020).

Magnetic refrigerators work by utilisation of magnetocaloric materials. These materials display the phenomenon referred to as the MCE which happens in the instance when a magnetic field that is applied externally varies (Zverev & Tishin, 2016). This changes how materials are aligned in a magnetic order which leads to a reduction in the entire entropy contained by the magnetic portion. Under isentropic circumstances, the material will exhibit no change in total entropy. This implies that the lattice entropy change compensates for the change in magnetic entropy, and is linked with the magnetocaloric material changing its temperature (Barcza *et al*., 2013). Since adiabatic conditions accompany isentropic conditions and not the other way around, the isentropic temperature change exhibited by the magnetocaloric material is as well-known as an adiabatic change in temperature, ΔT_{ad} (Yin *et al.,* 2011).

Kitanovski (2020) also suggested that in the event that magnetocaloric material is magnetised under an isothermal environment, there will be no change in lattice entropy. Consequently, change in magnetic entropy will lead to isothermal complete change in entropy. To exploit magnetocaloric

17

effect and apply it in heat pumping and refrigeration, it is important to work on the thermodynamic cycle nearer to the magnetocaloric material's curie temperature in this case the near -room temperature. It is the point where MCE is said to be maximum (Gottschall *et al*., 2019)

2.2.3 The Advancement of Magnetic Refrigeration Systems.

The earliest design of a magnetic coolant was built in Santa Catarina by the Federal University whereby the refrigerator had a rotating part. It was made in such a way that its magnetic circuit was optimised and had a two-pole system which were fixed in a rotor-stator configuration that had regions of maximum flux density of about 1 T. The performance of this system was analysed based on the second law efficiency and Coefficient of Performance. It was discovered that a 7.1 K temperature span was generated by the device which was corresponding to an 80.4 W thermal load (Lozano *et al.,* 2016). A prototype which was named the FAME cooler was designed to study how various magnetocaloric materials performed in an environment that is practical and realistic. When the performance test was carried out, it was observed that when the hot side of the system had a fixed temperature of 295 K, under a 0.25 T utilisation condition, the prototype attained a 162.4 W maximum cooling power, and a zero-power 11.6 K temperature span. Under a 0.15 T utilisation condition, the prototype achieved a COP of 1.85 which was its maximum value (Huang *et al.,* 2019).

Later an experiment was conducted to determine how an AMR refrigerator performed between a temperature of 77 K and 20 K with a detailed analysis of energy transfer (Park *et al.,* 2014). A multi-layered AMR which comprised of four distinct intermetallic compounds belonging to the rare earth category was used. The working fluid utilised in this case was helium and it oscillated in the AMR as the variation in magnetic field was applied in controlling its flow. The ability of the prototype to attain a 25.4 K no-load temperature and a 77 K temperature at the warm end was confirmed by the experimental results (Park & Jeong, 2017). Magnetic refrigeration technology which depended on a unique feature of certain materials referred to as magnetocaloric effect (MCE) is a fascinating and a superior one in relation to the traditional refrigeration techniques. (Alahmer *et al.,* 2021).

A deeper understanding of various technologies of magnetic refrigeration was explored by applying different models to assess the COP and the outputs of particular cooling capacities. The models applied in the study of magnetic refrigeration are categorised into four main classes, namely: reciprocating, rotating, magnetic refrigeration designed in a C shape and an active or

working magnetic regenerator (He e*t al.,* 2015). Magnetisation area, magnetic refrigeration efficiency cycles, thermodynamic processes and magnetocaloric effect impact were the sections that were discussed and examined in order to attain extreme cooling capacity. From this study, Alahmer *et al.* (2021) discovered that whereas magnetic refrigeration can be considered to be a refrigeration system that is extremely effective and friendly to environment, it still needs improvement in many sections before recommending it for use in a wide range of applications, like air conditioners and domestic refrigerators. This is due to the fact that its cooling capacity and temperature are limited (Desideri *et al*., 2009).

A publication by Gao *et al.* (2020) reported a study that delved into comparing recent developments undergone by AMR refrigerators. Results and findings submitted to the literature were weighed based on geometric parameters, magnetocaloric materials and operating parameters. Factors such as no-load temperature duration, COP and cooling capacity which are all performance indicators were also put into consideration (Shoukourian & Kranzlmüller, 2020). They found out that the maximum temperature duration to be applied highly determined the performance and they found the range of the temperature to be between 0.05 to 0.2K. Also, they obtained the highest thermal rejection temperature of between 25-30 °C for all the prototypes They equally confirmed that the non-inclusion of the compression stage in the AMR refrigerator makes it extremely efficient in terms of energy consumption, even though more research still needs to be done to make its cooling performance to be effective enough to increase its chances of being embraced in the commercial field of the current technology examined (Capozzoli & Primiceri, 2015).

Smedley and Abravomitz (2011) presented a lumped parameter prototype aimed at envisaging the temporary and steady-state temperature of the cabinet, efficiency parameters and the energy consumed by a magnetic fridge. The magnetic cooler is designed with a small capacity and is made up of a wine cooler cupboard which is retrofitted and thermally insulated (Peixer *et al.,* 2022). The model is categorised into hydraulic and magnetic circuits, heat exchanger assemblies and autonomous, experimentally authenticated mini-models for the AMR. The geometric characteristics and dimensions of the component, speed and frequency of power sources (axial fans, inductor motor and hydraulic pump) and properties and composition of magnetic materials (Nakashima *et al.,* 2021). Special focus is set on the lumped model of AMR, which precisely predicts how the first-order and second-order materials work on the basis of the rate of heat rejection, magnetic work and the cooling capacity. The model was used to forecast the

experimental temperature of the cabinet of the prototype in the steady-state condition to around 1.5 °C while making an estimate of the COP with an average error of 6.5%. This study also determined that at the point of temperature pull-down, the model correctly reproduced the time response obtained from the magnetic wine cooler. This made it possible to apply the model in the designing of future heat pumping structures or systems (Nakashima *et al.*, 2022).

2.3 Early Models of Magnetocaloric Materials

Recently, magnetic cooling has been of great interest to researchers all over the world due to its numerous recompences over the orthodox vapor compression cooling system (Gutfleisch *et al.*, 2011). The idea of magnetic cooling started in 1881 when Warburg discovered the principle of magnetocaloric effect. He noticed that under the effect of a magnetic field intensity, iron metal would either heat up or cool down. He concluded that changes in internal energy resulted in change in temperature of the iron metal as a result of the influence of magnetic field intensity (Smith, 2013). In 1905, Langevin showed that the magnetisation changes of a paramagnet resulted in a reversible change of temperature of a sample (Sucksmith *et al.*, 1938). While working independently of each other, two American scientists, Peter Debye and William Giaque first tried the practical use of magnetic cooling. Their main aim was to achieve temperatures which were under the boiling point of helium (Bleaney, 1990). In 1933, Jiok and Mc Dougall were the first to demonstrate a basic experiment on magnetic refrigeration. Later de Haas and Kurt also did the same experiment. During this experiment, they applied magnetocaloric effect to obtain a sub-Kelvin temperature of 0.25K. To achieve this, a paramagnetic $Gd_2(SO_4)_3$ $8H_2O$ salt was used. This was cooled using liquid helium at a temperature of 1.5 K and magnetised in 0.8T magnetic field intensity. The demagnetisation and cooling of the Gd- containing salt was achieved by simply removing the magnetic field intensity (Carlin *et al.*, 1977).

Brown constructed a reciprocal magnetic cooler to validate the possibility of having a near room temperature magnetic refrigeration. He used a Gd metal to obtain a temperature span of 47 K with 50 cycles minus a heat load. Though his work was promising, it was not followed up for the next two decades (Brown, 1976). The research on MCE and magnetic refrigeration was later revived by Pecharsky and Gschneidner much later when they reported on the GMCE (giant magnetocaloric effect) in $Gd_5Si_2Ge_2$. The magnetocaloric effect was highly improved in

$Gd_5Si_2Ge_2$ as a result of the transformation that accompanied the magnetic transformation. Zimm *et al.* (1999) constructed a rotary magnetic cooler that used Gd spheres as a functional cooling material and $Nd_2Fe_{14}B$ permanent magnets to supply 1.5T fields. This had a predicted efficiency improvements of between 20 -30% above the traditional vapor cooling systems. The principle of applying active magnetic regenerator (AMR) in refrigeration gadget to enhance heat transfer was presented by Steyert two years later following the earlier work by Brown. Steyert evaluated the Stirling cycles for magnetic refrigeration and heat engines (Steyert, 1978). The AMR cycle was further developed by Steyert and Barclays in 1983 and later by Barclays in 1984. In his seminar paper in 1984, Barclays demonstrated that a much larger temperature lift is achievable than just adiabatic temperature increase of the magnetic refrigerant when using an active magnetic component and a regenerator at the same time (Pecharsky & Johnson, 2016).

2.3.1 Magnetocaloric Effect in the Rare – Earth Transition Materials.

The original magnetic material that was available as a refrigerant was the rare earth metal lanthanide gadolinium (Gd). It was reported that at T_c of 29K, Gd exhibited a second order ferromagnetic to paramagnetic phase transition (Hadimani, 2008). Many researchers have studied the magnetocaloric effect and heat capacity of Gd. Because of its high thermal conductivity, Gd was first proposed as a candidate for magnetic refrigeration. This was later dropped when it was discovered that it oxidises easily and does not exhibit a strong magnetocaloric effect at room temperature. In attempt to advance the MCE of Gd. Yin *et al.* (2015) studied some Gd based compounds and reported that $Gd_{0.74}Tb_{0.26}$ and $Gd_{0.5}Dy_{0.5}$ presented magnetocaloric effect equivalent to Gd at approximately 280K and 265k respectively. It was later found out that $(Gd_4 Bi_xSb_{1-x})_3$ had a maximum magnetocaloric effect of about 50% of pure Gd for a 10T field change with the width of the peaks reaching 60 – 100K at half maximum. This enabled it to provide a reasonable cooling power over a reasonable temperature range of approximately 240 to 340K (Gschneidner & Pecharsky, 2000).

After the discovery of MCE in pure iron, the study on magnetocaloric materials was narrowed down to rare earth metals and their compounds. The first breakthrough came when reversible giant MCE in GdSiGe was detected in Ames Laboratory (Yu *et al.*, 2003). Later a sub-room temperature giant magnetocaloric effect in $Gd_5(Ge_{1-x}Si_x)_4$ for $0.3 \leq x \leq 0.55$ was discovered. This brought a lot of interest from both practical and fundamental point of view in searching for magnetocaloric effect in these materials. The most remarkable characteristic observed in these compounds was

their capacity to undergo a primary magnetic and structural phase transition, resulting in an extensive alteration in magnetic field intensity-induced entropy at their ordering temperature (Li, 2009). In their investigation, Balema *et al*. (2002) highlighted that at significantly low temperatures, regardless of the values of x, $Gd_5(Ge_{1-x}Si_x)_4$ demonstrates an orthorhombic structure akin to Gd_5Si_4, and this state exhibits ferromagnetic properties. Furthermore, they observed that at room temperature, three distinct crystallographic phases exist, contingent on the x values. Specifically, when x is at a certain level, Gd_5Si_4 maintains stability. As x shifts, Gd_5Si_4 adopts a structure akin to Sm_5Ge_4, characterized by the same space group, a larger volume, and moderately distinct atomic arrangements. When x reaches a different threshold, the monoclinic structure of Gd5Si2Ge2 forms, with a space group of P1121/a. This particular structure is reported to remain stable at temperatures below 570K (Levin, 2002).

Pecharsky *et al.* (1997) noted that the unit cell of $Gd_5(Ge_{1-x}Si_x)_4$ contained four formula units which basically differed in the way the similar building blocks were arranged. These blocks are connected by either none, one or two covalent like Si – Ge bond, giving successive increase in unit cell volume. They also reported that the giant magnetocaloric effect was present in compounds and that it showed instantaneous paramagnetic to ferromagnetic and physical stage transition which was brought about by applied pressure, temperature change or applied magnetic field intensity (Morellon *et al.,* 1998). Transition metals as well as elements in the lanthanide-series experience the MCE effect. Gadolinium, which is one of the rare earth metals, is known to exhibit the greatest magnetocaloric effect. This explains why it was a critical component of many early designs of magnetic refrigeration (Grunner *et al.*, 2015). Inability to display a robust room temperature magnetocaloric effect is the major reason as to why pure gadolinium is not an efficient refrigerant.

According to studies, however, arc-melted alloys of silicon, germanium and gadolinium give satisfactory results when applied to refrigeration under room temperature. The enormous magnetocaloric effect (GMCE) discovery in $Gd_5Ge_2Si_2$ (Dan'Kov *et al.,* 1998) has led to the concept of room-temperature cooling being an authentic idea. In the previous years, numerous categories of materials such as La (Fe, Si)$_{13}$ (Gutfleisch *et al*., 2005; Han & Miller, 2008), $MnFeP_{1-x} A_x$ (A=Si, Ge, and As) (Tegus *et al*., 2002) as well as their hydrides (Fujieda *et al*., 2004). Heusler alloys (Planes *et al*., 2007), Mn (As, Sb), FeRh (Roy *et al*., 2006) and also Mn_2Sb have attained recommendations as promising prospects of magnetic refrigerants. The largest MCE

was experienced to be approximately lower than the room temperature, whereas a conventional refrigerator necessitates the dissipation of heat at a minimum of approximately 320 K. The extent of the magnetocaloric effect and the presence of thermal hysteresis are closely connected to the initial phase transition, which is significantly influenced by the material's quality and the preparation of samples (Schamberger & Ohuchi, 2009). In the case of the compound $Gd_5(Ge_{1-x}Si_x)4$, where x is roughly 0.5, a limited quantity of impurities, such as Al, Co, Bi, Mn, C, or Sn, can disrupt the creation of the monoclinic structure around room temperature. Interestingly, these alloys exhibited exclusively a second-order phase transition at elevated temperatures, albeit with a substantially lower MCE (Franco *et al.,* 2009).

Shull *et al*. (2006) remarked that among impurities, Pb stood out as the sole one to amplify the magnetocaloric effect and elevate the magnetic ordering temperature. The responsiveness to impurities like oxygen, carbon, and iron has a profound impact on the production expenses of the material, potentially impeding widespread application. In the context of $Gd_5(Ge_{1-x}Si_x)_4$, the magneto-structural transition displayed a comparatively slower pace when compared to its thermal and field hysteresis. This disparity could influence the upper limit of operational frequency and efficiency achievable in a magnetic refrigerator. Compounds slated as contenders for room temperature refrigeration must tackle issues such as elevated costs, susceptibility to oxidation, and complexities in preparation before being deemed suitable. Aksoy *et al*. (2008) conducted research on the effects of introducing 3d (Co and Mn) and p (Ga and B) orbit alloys to $Gd_5(Si_{2-z}Ge_{2-z}R_{2z})$ compounds. They found that substituting Si and Ge allowed for the tuning of the compound's Curie temperature, Tc, ranging from 20K to 286K. Meanwhile, Chen *et al*. (2005) explored the magnetic properties of $Gd_5Si_{2-x}Ge_{2-x}Sn_{2x}$ alloys (x = 0.05, 0.10, 0.15, and 0.5) and observed a gradual augmentation in the absolute magnetic entropy of these alloys as Sn content increased from x = 0 to x = 0.25. For the case of x = 0.25, the alloy exhibited a dominant monoclinic $Gd_5Si_2Ge_2$-type crystal structure alongside a minor presence of the Gd_5Si_4-type phase at room temperature.
 (Her *et al*., 2005).

Oestereicher and Parker while studying the magnetic effect of rare - earth transition metal compounds that have Curie temperature within the room temperature, noted that it was possible to use $Y_2F_{17-x}CO_x$ and $Y_2F_{17-x}Ni_x$ as a room temperature magnetic refrigerant (Oesterreicher & Parker, 1984). The investigations done on $Ce_{2x}Dy_xFe_{17}$ alloys found that the absolute change in magnetic entropy within 1.4T magnetic field intensity was approximately 1.67, 1.41 and 1.18JKg⁻

$^1K^{-1}$ with x = 0.0, 0.3 and 0.5 with the corresponding temperature being approximately 234K, 267K and 286K respectively (Chen *et al*., 2012). Wang *et al*. (2004) observed that the maximum adiabatic temperature in $Ce_2Fe_{17-x}Co_x$ and $Er_2Fe_{17-x}Ni_x$ (x = 0.3) are 4.75K and 4.51K with corresponding T_c values being 294.2K and 293.5K respectively, which is near Gd metal though much cheaper than that of Gd metal (Chen *et al.,* 1999). Hu *et al*. (2000) observed that the change in magnetic entropy of $Ni_{52.6}Mn_{23.1}Ga_{24.3}$ (a Heusler alloy metal) at 300K is approximately $18.0JKg^{-1}K^{-1}$ which is close to that of $Gd_5Si_2Ge_2$ and a bit higher than that of Gd near room temperature.

It's important to highlight that Heusler metals typically undergo a first-order temperature-induced transition from a martensitic to an austenitic phase. Webster *et al*. (1984) noted that the Heusler alloy Ni_2MnGa exhibited a ferromagnetic transition with a Curie temperature of 376K. The magnetic moment was largely associated with Mn atoms, while Ni atoms possessed a moment of 0.3 Bohr magneton. In their research, Krenke *et al*. (2005) observed a substantial magnetocaloric effect in NiMnSn, attributing it to the increased magnetization with rising temperatures during the martensitic transition. Additionally, they found that substituting Ni with Co led to a near-room temperature shift in the transition temperature. Duan *et al*. (2008) pointed out that substituting Mn with Co resulted in a non-modulated tetragonal martensitic structure at room temperature. They also reported that substituting Ni with Co led to a monotonic reduction in the transition temperature with increasing Co concentration, as confirmed in a different study (Nayak *et al*., 2009). In another study, Labo *et al*. (2014) observed that substituting Fe for Mn in the Heusler metal NiMnSn led to a decrease in Mn-antiferromagnetic interactions due to the presence of Fe atoms. This systematic change contributed to a lower martensitic temperature.

Earlier research had shown that single materials with temperature range which were not wide enough could not meet the needs of a magnetic Ericsson cycle. To solve this, Brown came up with a method of getting composite materials. He achieved this by combining a few, of these into one new composite material with its absolute change in entropy fitting into a suitable magnetic range (Brown, 1976). Hashimoto *et al*. (1987) confirmed that the combination of a number of magnetic materials had promising magnetocaloric effect and could be used as a future magnetic refrigerant. They achieved this by constructing a layer designed sintered comprising of ErAl, DyAl and (DyHo)Al alloys in the low temperature range (Hashimoto *et al*., 1987). Following this, Smaili and Chahin recorded two sets of composite materials with the temperature range of 240 – 290 K

and 210 – 290 K respectively from GdDy alloys. This showed that the resulting absolute magnetic entropy was constant and fell within the required temperature range (Smaili & Chalin, 1997).

Another interesting material for magnetic refrigeration is a rare-earth transition metal compounds of crystallising in the cubic $NaZn_{13}$ type structure. Burdett and Miller, (1990) noted that this structure can be stabilised by adding iron and nickel or by adding at least 10% of Si or Al. Another compound which has been of interest is La $(Fe, Si)_{13}$. This compound has unraveled performance with the Neel temperature, that is, the temperature above which the transition from anti-ferromagnetic to paramagnetic takes place, being between 200K to 262K with lower iron content. As opposed to $Gd_5Ge_2Si_2$, this phase transition metal does not show any structural change, thus above and below Curie temperature, the material remains cubic. Recently a large magnetocaloric effect was reported in (La, Fe, -Si, Al) system after several investigations by different researchers (Liu *et al*., 2013; Shao *et al*., 2020; Zhong *et al*., 2021). Though the magnetic property of $LaFe_{13-x}Si_x$ had been extensively researched on, it was not until the year 2000 when its magnetocaloric property was discovered (Hu *et al*., 2002). They noted that $LaFe_{13-x}si_x$ had an entropy change which was as high as 20 $JKg^{-1}K^{-1}$ in a field change of 0 - 5T and a very low concentration of Si.

In their later work, they reported that the large change in entropy in $LaFe_{13-x}Si_x$ was related to the metamagnetic behaviour and negative lattice expansion. The supreme value of variation in magnetic entropy of the fields 1T, 2T and 5T are given as 10.5, 14.3 and 19.4 $JKg^{-1}K^{-1}$ respectively. To take care of change in Curie temperature that could significantly affect the change of magnetic entropy, they proposed that Fe should be replaced by the correct amount of Co (Feng, 2000). In other studies, it was observed that the extreme absolute variation in magnetic entropy value of $LaFe_{11.2}Co_{0.7}Si_{1.1}$ near T_c of 274K within the field change of 0 -5T was 20.3$JKg^{-1}K^{-1}$ which was more than the value recorded for Gd by almost a factor of 2 and almost equivalent to the values of $Gd_5Si_2Ge_2$ and $MnFeP_{0.45}As_{0.55}$. Further they noted that in La $(Fe_{1-x}Co_x)_{11.9}Si_{1.1}$ for (x = 0.04, 0.06 and 0.08), the T_c increased from 243K to 301K with x increasing from 0.04 to 0.08. At the same time, the absolute magnetic entropy decreased gradually from 23 to 15.6 $JKg^{-1}K^{-1}$ for the field that changed from 0 – 5T (Hu *et al.,* (2002).

Jun *et al.* (2009) studied the magnetocaloric effect of $La_{0.5}Pr_{0.5}Fe_{11.5-x}Co_xsi_{1.5}$ for values of ranging from 0 to 1. They found out that when Co is substituted in $La_{0.5}Pr_{0.5}Fe_{11.5}si_{1.5}$, the phase transition at T_c changed from first order to second order when the value of is 0.6. They also noted

that magnetic entropy decreased as Co concentration increased and T_c also increased from 181K when to 295K when. It is worth noting that when, the maximum values of the absolute change in magnetic entropy at T_c is 295K with specific heat capacity of 6.0 and 11.7 $JKg^{-1}J^{-1}$ for a magnetic field intensity change of 0 - 2 T and 0- 5T respectively. These values are almost 20% higher than that of Gd (Jun et al., 2009). Other researchers have studied how substituting Fe with Co affects the magnetocaloric effect in $LaFe_{11.7-x}Co_xSi_{1.3}$, $LaFe_{11.9-x}Co_xSi_{1.1}$, $LaFe_{11.8-x}Co_xSi_{1.2}$ and $LaFe_{11.4-x}Co_xSi_{1.6}$ (Balli et $al.$, 2007; Liu et $al.$, 2005; Yan et al., 2008). A year later, Shen et $al.$ (2009) studied the magnetocaloric effect of $La_{0.7}Pr_{0.3}Fe_{13-x}Si_x$. They showed that the magnetocaloric effect has an increase in Curie temperature and a reduction in absolute change in magnetic entropy when Si is replaced with Fe. The effect of substituting Mn with Fe on La $(Fe_{1-x}Mn_x)_{11.7}Si_{1.3}$ for $0 \leq x \leq 0.03$ had been earlier studied (Wang et $al.$, 2004). They reported that T_c was decreasing at the rate of 174K per 1% of Mn. They also noted that there was a large absolute change in magnetic entropy for a wide range of temperature. There was also a tendency to degenerate as increases with the values given as 17 $JKg^{-1}K^{-1}$ for T_c =130K and 25 $JKg^{-1}K^{-1}$ for T_c = 188K over a field range of $0 - 5T$ (Wang et al., 2004).

Anh et $al.$ (2003) studied the effect of substituting Nd on magnetocaloric effect. They found that the increase in Curie temperature resulted into a reduction in MCE in $La_{1-x}Nd_xFe_{11.44}Si_{1.56}$ for values given as $0 \leq x \leq 0.4$ (Anh et $al.$, 2003). Shen et $al.$ (2009) found that when R is substituted with La in $La_{1-x}R_xFe_{11.5}Si_{1.5}$ there was a monotonic decrease in Curie temperature. The absolute change in magnetic entropy for variation in magnetic field intensity from $0 - 5T$ also changed from 23.7 $JKg^{-1}K^{-1}$ for to 32.4 $JKg^{-1}K^{-1}$ when for $La_{1-x}Pr_xFe_{11.5}Si_{1.5}$ and 32.0 $JKg^{-1}K^{-1}$ for $La_{1-x}Nd_xFe_{11.5}Si_{1.5}$ for but remained constant at 24 $JKg^{-1}K^{-1}$ for $La_{1-x}Ce_xFe_{11.5}Si_{1.5}$ for $0 \leq x \leq 0.3$. Fujita et $al.$ (2002) and Chen et al. (2003) independently studied the consequence of hydrogenation on magnetocaloric effect. They observed that when interstitial hydrogen was added to $LaFe_{13-x}Si_x$, Curie temperature moved to higher temperature but large magnetocaloric effect remained. There was also a change of entropy of 17 $JKg^{-1}K^{-1}$ in $LaFe_{11.5}Si_{1.5}H_{1.3}$ at a temperature of 288K (Chen et al., 2003; Fujita et al., 2002). Fujieda et $al.$ (2004) controlled the concentration of interstitial hydrogen by changing the annealing temperature under which they prepared the sample (Fujieda et al., 2004). Fang et $al.$ (2003) while studying the magnetocaloric effect of La $(Fe_{1-x}Mn_x)_{11.7}Si_{1.3}Hy$ observed that tuning Curie temperature around room temperature was possible by controlling hydride concentration (Fang et al., 2003).

Tian *et al*. (2013) did research on how interstitial carbon affects $LaFe_{13-x}Si_x C_\sigma$ carbides. They reported that for $LaFe_{11.6}Si_{1.4} C_\sigma$ with $\sigma = 0$, 0.2, 0.4 and 0.6, the entropy change was almost constant when σ is below 0.2 but decreased rapidly when σ is greater than 0.4. They reported that the maximum value of the absolute change in magnetic entropy for a magnetic field intensity of range between 0 -5T were given as 24.2 $JKg^{-1}K^{-1}$ for $\sigma = 0.2$, 18.8 $JKg^{-1}K^{-1}$ for $\sigma = 0.4$ and 12.1 $JKg^{-1}K^{-1}$ for $\sigma = 0.6$. Chen *et al*. (2003) investigated the change of entropy and the loss of hysteresis in $Lafe_{11.7}(Si_{1-x}Cu_x)_{1.3}$. They found that when the Cu content increased from 0 to 0.2, the Curie temperature changed from 185 to 200K and the absolute change of magnetic entropy dropped. However, the absolute change in magnetic entropy was approximately 20 $JKg^{-1}K^{-1}$ which was considered to be large when the value of was 0.2. They further noted that the introduction of Cu reduced both the thermal and magnetic hysteresis. They noted that $LaFe_{1-x}Al_x$ compounds are rich in magnetic properties as compared with $LaFe_{1-x}Si_x$ compounds (Tian *et al*., 2013).

Hu *et al.* (2007) conducted a study involving the manipulation of Al content in $LaFe_{1-x} Al_x$ and documented a gradual transition from the ferromagnetic (FM) to antiferromagnetic states. Subsequently, they investigated alterations in magnetic entropy within Co-doped compounds: $La(Fe, Al)_{13}$, $La(Fe_{0.98}Co_{0.02})_{11.7}A_{l1.3}$, and $LaFe_{11.12}C_{0.71} A_{11.17}$. They found that these compounds exhibited second-order ferromagnetic behavior, undergoing a magnetic transition at Curie temperatures of around 198K and 279K, respectively. The changes in magnetic entropy were approximately 5.9 and 10.6 JKg-1K-1 for $La(Fe_{0.98}Co_{0.02})_{11.7} A_{l1.3}$ and 4.6 and 9.1 JKg-1K-1 for $LaFe_{11.12} Co_{0.71} A_{11.17}$, with field variations of 0 to 2T and 0 to 5T. Their findings also indicated that the introduction of Co through doping could transform antiferromagnetic coupling into ferromagnetic coupling, resulting in a shift of the Curie temperature towards higher values with an increase in Co concentration. Additionally, it was noted that the alteration in magnetic entropy for $La(Fe_{1-x}Co_x)_{11.83}A_{11.7}$ closely resembled that observed near room temperature for Gd (Hu *et al*., 2000). In a separate investigation, Wang *et al*. (2004) explored the impact of interstitial elements on the magnetic entropy change and magnetic properties of $La(Fe,Al)_{13}$ alloys. With $LaFe_{11.5}Al_{11.5}$, they observed that the Curie temperature increased from 191K to 262K as the carbon concentration rose from 0.1 to 0.5. This change was accompanied by a slight augmentation in saturation magnetization.

The first synthetisation of the distorted perovskite structure of manganites with formula given as $R_{1-x}M_xMnO_3$ was done in 1950 by Jonker and Van Santen. In the formula, R is the trivalent rare-earth elements like Y, Tb, Ho, Gd, Sm, Pr, Eu etc., and M is the divalent alkaline earth ions like Ba, Pb, Sr or K^{1+}, Ag^{1+} etc. The perovskite A-site are formed from homogeneous solid solution. Some advantages of this compound over GdSiGe and Gd alloys are that they are cheap, have good chemical stability, large electrical resistivity and small coercive force. These compounds are highly doping dependent since their Curie temperature could easily be tuned to any needed range by simply adding some special types of metal. These compounds were proposed as candidates for room temperature refrigeration (Jonker, 1950). However, it was later discovered that their absolute change in magnetic entropy would decrease significantly when their doping levels were increased hence making their practical application impossible. For example, the absolute change in entropy of $La_{0.8}Ca_{0.2}MnO_3$ with a magnetic field intensity change of 1.5T reached 5.5 $JKg^{-1}K^{-1}$ which was about 1.5 times that of Gd but with Curie temperature of only 230K (Wang *et al.*, 2004).

It was also reported that the Curie temperature increased to 263 K when the ratio of Ca was adjusted to $La_{0.6}Ca_{0.4}MnO_3$ but the absolute magnetic entropy reduced 70% of Gd value at 3.0T. Their Curie temperature was improved by adding Pb and Sr which increased it to 327 and 296 respectively but the absolute change in magnetic entropy decreased significantly (Bohigas *et al.*, 200). The magnetocaloric effect of $(La_{1-x}Ca_x)$ MnO_3 is the most extensively researched on compound among the manganite family. Moreli *et al.* (1996) investigated the magnetocaloric effect of $(La_{1-x}M_x)$ MnO_3 with M = (Ca, Sr, Ba). They reported that the values of the absolute change in magnetic entropy were not large. They noted that varying doping concentrations would enable tuning of the magnetocaloric effect peak temperature within the temperature range of 250 to 350K (Morelli *et al.*, 1996). Guo *et al.* (1997) reported the presence of a large magnetocaloric effect in $(La_{1-x}Ca_x)$ MnO_3 polycrystalline samples with $0.20 \le x \le 0.33$. They noted that for a change of magnetic field intensity of 1.5 T, the absolute change in magnetic entropy reached its peaks of 5.5 $JKg^{-1}K^{-1}$ at 230K, 4.7 $JKg^{-1}K^{-1}$ at 224K and 4.3 $JKg^{-1}K^{-1}$ at 260K for the values of 0.2, 0.25 and 0.33 respectively.

The reported values were larger than that of Gd which had a change in magnetic entropy of 4.2 $JKg^{-1}K^{-1}$ for the same magnetic field intensity of 1.5T (Guo *et al.*, 1997; Guo *et al.*, 1998). Zang *et al.* (2012) later discovered a smaller value of absolute change in magnetic entropy 0.6 $JKg^{-1}K^{-1}$

with a change of magnetic field intensity of 1T having a wider breadth of magnetocaloric effect peak δT_{FWHM} of 62K in $La_{0.67}Ca_{0.33}MnO_3$ for = 0.33 than the one reported by (Guo *et al*.,1997). They suggested that the observed discrepancy could have been as a result difference in chemical composition and/or the way the samples were prepared (Zang *et al*., 1996). Szymczak *et al*. (2010) investigated the effect of hydrostatic pressure on the change of entropy, the crucial components and Curie temperature in $La_{0.7}Ca_{0.3}MnO_3$. They observed that when pressure is applied, the magnetic entropy of a solid could change significantly without magnetic variation. They concluded that combined effects of applied hydrostatic pressure and magnetic field intensity on the manganite calorie properties are promising candidates for refrigerators. Among the compositions, $La_{0.67}Ca_{0.33}MnO_3$ had the largest magnetocaloric effect (Szymczak *et al.,* 2010).

Hernández *et al*. (2014) took the measurement of magnetocaloric effect of $La_{0.67}Ca_{0.3}MnO_3$ and found the variation in adiabatic temperature of 2.4K for a change of magnetic field intensity of 2.02T. This value was less than that of Gd. It was reported that $La_{0.54}Ca_{0.32}MnO_3 - \delta$ had a large absolute change of magnetic entropy of 2.9 $JKg^{-1}K^{-1}$ for a change of magnetic field intensity of 0.9T. The sample Curie temperature was recorded as 272K which was approximately 10K higher than that of $La_{0.67}Ca_{0.33}MnO_3$. This suggested that $La_{0.54}Ca_{0.32}MnO$ could possibly be used as a magnetic refrigerant for a sub-room temperature refrigerator (Xu *et al*., 2001). Hueso *et al.* (2002) showed that the magnetocaloric effect peak temperature could be tuned without suppressing the values of magnetocaloric effect of $La_{0.67}Ca_{0.33}MnO_{3-\delta}$ nanoparticles synthesised using sol-gel technique. They also found out that the change of magnetic entropy was inversely proportional to the size of the grain (Hueso *et al*., 2002).

Phan *et al.* (2003) while investigating the magnetic and magnetocaloric properties of $(La_{1-x})_{0.8}Ca_{0.2}MnO_3$ with $0.05 \leq x \leq 0.3$ noted that decrease in Lanthanum favored not only magnetocaloric effect but also raised the Curie temperature to a higher temperature which is favorable to magnetic refrigeration at various temperatures (Phan *et al*., 2003). The magnetocaloric effect of $La_{0.67-x}Ca_{0.33}MnO_3$ for, x equal to 0.02, 0.06 and 0.1 was investigated. It was found that the largest value for change of magnetic entropy was 2.78 $JKg^{-1}K^{-1}$ at 272 K over a change of magnetic field intensity of 1T which was noted to be good for a sub-room temperature magnetic refrigeration (Hou *et al*., 2004). Several efforts have been made to fit MCE in the room temperature range by exploring the MCE of $(La_{1-x}Sr_x)MnO_3$ manganites. For example, Szewczyk *et al.* (2000) reported the magnetocaloric effect of $La_{0.845}Sr_{0.55}MnO_3$ polycrystalline manganites, which had

phase transition at 234K. The absolute change in magnetic entropy and the change in adiabatic temperature reached 6.6 JKg^{-1}K^{-1} and 3.3 K respectively for a change of magnetic field intensity of 7T. Later they measured the magnetocaloric effect of (La$_{1-x}$Sr$_x$) MnO$_3$ for x values equal to 0.135, 0.155, 0.185 and 0.200. They observed that the increase in magnetocaloric effect was directly proportional the increase in Sr doping. The change in adiabatic temperature reached 4.15 K which was the highest for a change in magnetic field intensity of 7T (Szwczyk *et al*., 2000).

Demin *et al*. (2004) observed that the MCE increased in (La$_{1-x}$Sr$_x$) MnO$_3$ for $0.1 \leq x \leq 0.3$ where Sr was added for a variation in magnetic field intensity of 0.82T. Mira *et al*. (2002) observed an absolute change in magnetic entropy of 1.5 JKg^{-1}K^{-1} at 370 K for a change in adiabatic temperature of 1 T in La$_{0.67}$Sr$_{0.33}$MnO$_3$ sample. This result was analogous to the one recorded by (Xu *et al*., 2001). Phan *et al*. (2003) reported a large absolute variation in magnetic entropy value of 2.12 JKg^{-1}K^{-1} at 305K for the change of magnetic intensity of 1 T in La$_{0.65}$Sr$_{0.35}$MnO$_3$. Measurement of magnetocaloric effect of La$_{0.8}$Sr$_{0.2}$MnO$_3$ which was synthesised using carbonate precursor method were taken and the recorded absolute change in magnetic entropy was 1.7 JKg^{-1}K^{-1} at 275K for a variation of magnetic intensity of 2 T. Later, they measured the magnetocaloric effect in nano size form of La$_{0.8}$Sr$_{0.2}$MnO$_3$ prepared using sol-gel process. They recorded a Curie temperature of approximately 295K and 301K respectively. The absolute change of magnetic entropy recorded were 0.5 and 2.2 JKg^{-1}K^{-1} for a change of magnetic intensity of 2T. Again, they prepared the same manganite in carbonate precipitation and measured. They also recorded the absolute change of magnetic entropy value of 2.0 JKg^{-1}K^{-1} at 331K for a change of magnetic intensity of 2T which made the material a possible applicant for magnetic refrigeration (Pekala *et al*., 2008)

The researchers Phan *et al*. (2003), Zhong *et al*. (2012) and Xu *et al*. (2001) have studied the magnetocaloric effect properties of La$_{1-x}$Ba$_x$MnO$_3$. Phan *et al*. (2003) determined the MCE of La$_{0.7}$Ba$_{0.3}$MnO$_3$ polycrystalline manganite and found an absolute change of magnetic entropy of 0.6 JKg^{-1}K^{-1} at 336 K for a change of magnetic intensity of 1 T. Zhong *et al*. (2012) looked at how oxygen stoichiometry affects the magnetocaloric and magnetic properties of La$_{0.67}$Ba$_{0.33}$MnO$_{3-\delta}$ with $\delta = 0.00, 0.02, 0.05, 0.08$ and 0.10. They noted that oxygen deficiency is directly proportional to the reduction of magnetocaloric effect in the sample. They also reported that La$_{0.67}$Ba$_{0.33}$MnO$_{3-\delta}$ at $\delta = 0.00$ had a large absolute change in magnetic entropy of 2.7 JKg^{-1}K^{-1} at 350 K for a change of magnetic intensity of 1 T. Xu *et al*. (2001) got a different result for the La$_{0.67}$Ba$_{0.33}$MnO$_3$ composition. This was attributed to differences in chemical composition and sample preparation

method (Phan *et al*., 2003; Xu *et al*, 2001; Zhong *et al.,* 2012). Koubaa *et al.* (2009) also did some research on $La_{0.65}Ba_{0.3}M_{0.05}MnO_3$ with M being replaced with Na, Ag and K. They noted that the highest change in the absolute magnetic entropy values were 2.65, 2.82 and 2.66 $JKg^{-1}K^{-1}$ for M = Na, Ag and K at 310, 300 and 290 K respectively (Koubaa *et al*., 2009).

The measurement of magnetocaloric effect of $La_{0.7-x}Eu_xBa_{0.3}MnO_3$ for 0.05, 0.10 and 0.15 was done by Dhahri *et al*. (2009). They reported a highest MCE of 298 K with absolute change of magnetic entropy value of approximately 2.3 $JKg^{-1}K^{-1}$ for a magnetic field intensity of 1 T when. In conclusion, they noted that $La_{0.67}Ba_{0.33}MnO_3$ materials are generally suitable for a room-temperature magnetic refrigeration (Dhahri *et al*., 2009) Several researchers have also studied the magnetocaloric effect of $(La_{1-x}Pb_x)$ MnO_3 manganites. The magnetocaloric properties of $La_{1-x}Pb_xMnO_3$ manganites with, 0.2, 0.3, 0.4 and 0.5 was studied by Chau *et al.* (2003). They reported that the absolute change in magnetic entropy value was directly proportional to the increase in Pb concentration up to when. Thereafter decreased for a larger Pb doping levels. The highest value of absolute change in magnetic entropy recorded was 1.53 $JKg^{-1}K^{-1}$ at 358 K for a change of a magnetic field of 1.35 T for $La_{0.7}Pb_{0.3}MnO_3$ (Chau *et al*., 2003).

Min *et al.* (2005) later measured both the variations in the adiabatic temperature and magnetic field intensity of $La_{1-x}Pb_xMnO_3$ with, 0.2 and 0.3. They reported that the largest value of absolute variation of magnetic entropy was recorded for composition. However, for a variation of magnetic field intensity of 1.5 T, the change of adiabatic temperature obtained was approximately 0.68 K and 1 K for and at 292 and 349 K respectively (Min *et al*., 2005). Tozri *et al.* (2010) studied the MCE of $La_{0.8}Pb_{0.1}MnO_3$ and $La_{0.8}Pb_{0.1}Na_{0.1}MnO_3$ and noted that the absolute change of magnetic entropy values was much lower than the ones discussed earlier. The recorded values were 0.43 and 0.68 $JKg^{-1}K^{-1}$ at 201 and 247 K for a change of magnetic field intensity of 1 T. It was therefore concluded that though the absolute change in magnetic entropy value and the adiabatic temperature change could be obtained in the room-temperature range, the values were very small and therefore not suitable for room temperature magnetic refrigeration (Tozri *et al*., 2010).

In a study conducted by Zhong et al. in 1998, it was found that the magnetocaloric effect's peak temperatures can be adjusted within specific ranges. For La1-xNaxMnO3 compounds, these temperatures span from 195 to 334K, while for La1-xKxMnO3 compounds, they span from 230 to 334K. The maximum absolute alteration in magnetic entropy for La1-xNaxMnO3, resulting from a 1T magnetic field adjustment, are 1.32, 1.53, 2.11, and 1.96 J Kg-1K-1 when x equals

0.075, 0.10, 0.165, and 0.20, respectively, according to Zhong et al.'s work. Subsequently, Das et al. (2006) explored the magnetocaloric effect of La1-xKxMnO3 (with x values of 0.05, 0.1, and 0.15), prepared using a pyrophoric method. Their findings indicated that the introduction of potassium into Lanthanum manganite elevates the system's Curie temperature. For instance, the Curie temperature increased from 264K to 310K as x changed from 0.05 to 0.15. Notably, the La0.85K0.15MnO3 samples exhibited the highest absolute magnetic entropy of 3 J Kg-1K-1 at 310K, as reported by Das et al. 2006). In 2011, Juan et al. delved into the correlation between magnetocaloric characteristics and the calcination temperature of La1-xKxMnO3 nanoparticles. Their findings revealed that for La0.85K0.15MnO3 samples, the most substantial absolute modification in magnetic entropy values occurred when samples were calcined at 600°C, 800°C, and 1000°C. Specifically, these values were measured at 2.02, 3.06, and 3.56 J Kg-1K-1 at 274K for a magnetic field alteration of 2T, respectively (Juan *et al*., 2011).

Tang *et al.* (2000) observed a GMCE in $La_{1-x}Ag_xMnO_3$ for $0 \leq x \leq 0.3$. They noted that for a revolution of magnetic field of 1T the absolute variation in magnetic entropy value reached a peak of 3.4 J $Kg^{-1}K^{-1}$ for $La_{0.8}Ag_{0.2}MnO_3$ which was larger than that detected in Gd (Tang *et al*., 2000). Hien *et al.* (2002) discovered that when the Ag concentration of $La_{1-x}Ag_xMnO_3$ is varied, the magnetocaloric effect could be tuned in the range of room temperature and the highest absolute magnetic entropy value was 0.22 (Hien *et al*., 2002). In their investigations, Gamzatov *et al.* (2007) found out that the magnetocaloric effect of $La_{0.9}Ag_{0.1}MnO_3$, $La_{0.8}Ag_{0.2}MnO_3$ and $La_{0.8}Ag_{0.15}MnO_3$. They reported that for a change of magnetic field of 2.6T, the absolute magnetic entropy value reached a peak of 2.8 J $Kg^{-1}K^{-1}$ at 270 K for $La_{0.8}Ag_{0.15}MnO_3$ when sintered at 1373 K and Po_2 of 1 bar. This indicated that $La_{1-x}Ag_xMnO_3$ (x = 0.2, 0.22) have the potential to be candidates for room temperature refrigeration (Gamzatov *et al*., 2007).

Multiple researchers have highlighted that La1-xCaxMnO3 phases exhibit an exceptional magnetocaloric effect compared to other manganites. However, their Curie temperatures fall well below room temperature, restricting their practical use as magnetic refrigerants within that range. To address this limitation, researchers have proposed substituting Ca with other elements like Sr, Ba, Pb, Na, K, and Ag. This substitution leads to an increase in the Curie temperature, enabling the retention of a substantial magnetocaloric effect (Guo et al., 1997; Hou et al., 2004; Jonker et al., 1950; Morelli et al., 1996). In the work of Phan et al. (2005), significant magnetocaloric effects were observed in single crystals of La0.7Ca0.3-xSrxMnO3 (x = 0.05, 0.10, 0.20, 0.25). Notably,

for a magnetic field variation of 5T, the absolute change in magnetic entropy reached its peak at 10.5 J Kg-1K-1 at 275 K for x = 0.05. Remarkably, this value exceeded that of Gd, which possesses an absolute magnetic entropy of 10.2 J Kg-1K-1 at 294 K. These findings suggest the potential of these single crystals for magnetic refrigeration applications close to room temperature. However, a decline in the magnetocaloric effect was observed in La2/3(Ca1-xSrx)1/3MnO3 polycrystalline samples (x = 0.05, 0.15, 0.25, 0.50, 0.75, 1.0) with an increase in Sr substitution (Mira *et al.*, 2002).

Kim et al. (2007) conducted an investigation into the magnetocaloric properties of La0.7Ca0.2Sr0.1MnO3 and determined that, when exposed to a magnetic field of 2 T, the absolute magnetic entropy reached 2.85 J Kg-1K-1 at 315 K. In a separate study, Li et al. examined La0.5Ca0.3Sr0.2MnO3, recording an absolute magnetic entropy value of 1.52 J Kg-1K-1 at 317 K under a 2 T magnetic field (Sun et al., 2006). To account for lattice structure influences on magnetocaloric behavior, Sun et al. (2006) explored the alteration of magnetic entropy in ferromagnetic La0.5Ca0.3-xSrxMnO3 (x = 0.120, 0.135, 0.150). They identified that samples with x = 0.120 and 0.150 exhibited typical M-T behavior with Curie temperatures at 300 K and 323 K, respectively. Conversely, for x = 0.135, the composition displayed a two-step dependence with inflection points at 309 K and 320 K, corresponding to the Curie temperatures of orthorhombic and rhombohedral phases. Notably, the highest absolute magnetic entropy values were measured at 1.87 J Kg-1K-1, 1.72 J Kg-1K-1, and 1.7 J Kg-1K-1 for samples with x-values of 0.120, 0.135, and 0.150, respectively (Kim et al., 2007). Phan et al. (2003) performed substitutions of Ba for Ca in La0.7Ca0.3-xBaxMnO3 compounds (x = 0.12, 0.24, and 0.3), observing a substantial change in magnetic entropy above 300 K. With increasing levels of Ba doping, the absolute change in magnetic entropy diminished. For instance, for x = 0.12, the absolute change was 1.85 J Kg-1K-1 at 298 K for a 1 T magnetic field, while for x = 0.24, it was 1.72 J Kg-1K-1 at 230 K, and for x = 0.3, it measured 1.6 J Kg-1K-1 at 336 K. It was recognized that these materials held potential for magnetic refrigeration applications near room temperature (Phan *et al.*, 2003).

Sun *et al.* (2006) analysed the magnetocaloric effect of $La_{2/3}(Ca, Pb)_{1/3}MnO_3$ which had transited from paramagnetic insulator to ferromagnetic metal at 290 K. They recorded an absolute change of magnetic entropy of 7.5 J $Kg^{-1}K^{-1}$ and a change of adiabatic temperature of 5.6 K for a change of magnetic field of 7 T. This was a smaller value than that of $La_{2/3}Ca_{1/3}MnO_3$ for the same change of magnetic field (Laajimi *et al.*, 2019). Phan and Yu also investigated the magnetocaloric effect of $La_{0.6}Ca_{0.3}Pb_{0.1}MnO_3$, $La_{0.7}Ca_{0.2}Pb_{0.1}MnO_3$ and $La_{0.7}Ca_{0.1}Pb_{0.2}MnO_3$ samples and recorded

the largest absolute change of magnetic entropy of 3.72 J $Kg^{-1}K^{-1}$ at 337 K for a change of magnetic field of 1.35 T for $La_{0.7}Ca_{0.1}Pb_{0.2}MnO_3$ (Phan & Yu, 2007). Bejar *et al.* (2007) investigated polycrystalline perovskite samples of $La_{0.7}Ca_{0.3-x}K_xMnO_3$ for (x = 0.05, 0.075, 0.01) and found the largest absolute magnetic entropy values of 3.95, 3.75 and 3.49 J $Kg^{-1}K^{-1}$ at 270, 281 and 272 K respectively for the change of magnetic field of 2T (Bejar *et al.*, 2007).

2.3.2 Most Promising Systems in the Field of Magnetic Refrigeration.

Over the past few years, the field of magnetic refrigeration has been of great interest to researchers all over the world due to its numerous advantages over the conventional vapor compression cooling technique (Gottscahll *et al.*, 2019). The idea of magnetic refrigeration started in 1881 when Warburg discovered the principle of MCE (Zverev & Tshin, 2016). He noticed that under the effect of a magnetic field intensity, iron metal would either heat up or cool down. He concluded that change in internal energy resulted into change in temperature of the iron metal as a result of the influence of magnetic field intensity. In 1905, Langevin showed that the magnetisation changes of a paramagnet resulted into a reversible change of temperature of a sample (Ivanov *et al.,* 2016).

The practical use of magnetic cooling was first tried by two American scientists, Peter Debye (1926) and William Giaque (1927). They did this independently of each other. Their main aim was to achieve temperatures which was below the boiling point of helium. In 1933, Jiok and Mc Dougall demonstrated a basic experiment on magnetic refrigeration. Later de Haas (1933) and Kurt (1934) also did the same experiment. During this experiment, they applied MCE to obtain a sub-Kelvin temperature of 0.25K. To achieve this, a paramagnetic $Gd_2(SO_4)_3$ $8H_2O$ salt was used. This was cooled using liquid helium at a temperature of 1.5K and magnetised in 0.8T magnetic field intensity (Dixey *et al.*, 2020). The demagnetisation and cooling of the Gd- containing salt was achieved by simply removing the magnetic field intensity. Brown constructed a reciprocal magnetic refrigerator to demonstrate the possibility of having a near room temperature magnetic refrigeration. He used a Gd metal to obtain a temperature span of 47K with 50 cycles minus a heat load (Podmiljsak *et al.*, 2015). Though his work was promising, it was not followed up for the next two decades.

The research on MCE and magnetic refrigeration was later revived by Gschneider and Percharsky in 1997 when they reported on the GMCE (giant magnetocaloric effect) in $Gd_5Si_2Ge_2$. The MCE was highly improved in $Gd_5Si_2Ge_2$ as a result of the transformation that accompanied

the magnetic transformation. Gschneidner *et al.* (1999) constructed a rotary magnetic refrigerator that used Gd spheres as a functional cooling material and $Nd_2Fe_{14}B$ permanent magnets to supply 1.5T fields. This had a predicted efficiency improvements of between 20 -30% above the traditional vapour cooling systems. The principle of applying active magnetic regenerator (AMR) in cooling apparatus to enhance heat transfer was introduced by Steyert in 1978 following the earlier work by Huang *et al.* (2019). Steyert evaluated the Stirling cycles for magnetic refrigeration and heat engines. The AMR cycle was further developed by Steyert and Barclays in 1983 and later by Barclays in 1984. In his seminal paper in 1984, Barclays demonstrated that a much larger temperature lift is achievable than just adiabatic temperature rise of the magnetic refrigerant when using an active magnetic component and a regenerator at the same time (Jeong, 2014).

The original magnetic material that was available as a refrigerant was the rare earth metal lanthanide gadolinium (Gd). It was reported that at T_c of 29K, Gd exhibits a second order ferromagnetic to paramagnetic phase transition (Mudryk & Pecharsky, 2020). Many researchers have studied the MCE and heat capacity of Gd. Because of its high thermal conductivity, Gd was first proposed as a candidate for magnetic refrigeration. This was later dropped when it was discovered that it oxidises easily and does not exhibit a strong MCE at room temperature. In order to improve the MCE of Gd, Zhang *et al*. (2022) and Gschneider *et al*. (1999) studied some Gd based compounds. They reported that $Gd_{0.7}4Tb_{0.26}$ and $Gd_{0.5}Dy_{0.5}$ present MCE equivalent to Gd at approximately 280K and 265k respectively. Further, they found out that $(Gd_4 Bi_xSb_{1-x})_3$ has a maximum MCE of about 50% of pure Gd for a 10T field change with the width of the peaks reaching 60 – 100K at half maximum. This enables it to provide a reasonable cooling power over a reasonable temperature range of approximately 240 to 340K (Brown,1976).

Following the initial discovery of the magnetocaloric effect (MCE) in pure iron by Thanh in 2009, research in this field shifted focus towards rare earth metals and their compounds, as highlighted by Cwik et al. in 2021. A pivotal moment arose with the observation of a reversible giant magnetocaloric effect in GdSiGe at Ames Laboratory, as reported by Belo et al. in 2019. Subsequently, a significant sub-room temperature giant MCE was uncovered in Gd5(Ge1-xSix)4. This breakthrough triggered substantial interest from both practical and theoretical perspectives, spurring investigations into these materials' magnetocaloric properties, as noted by Nayak et al. in 2009. A remarkable characteristic of these compounds emerged, marked by their capability to undergo a first-order magnetic and structural phase transition, inducing a substantial change in

entropy upon crossing their ordering temperature. In their comprehensive study, Pecharsky et al. in 2002 detailed the behavior of Gd5(Ge1-xSix)4 at very low temperatures for all values of x. They found that Gd5(Ge1-xSix)4 exhibits an orthorhombic Gd5Si4-type structure with a ferromagnetic ground state. Moreover, they noted that at room temperature, three distinct crystallographic phases exist, contingent upon the specific values of x. Specifically, Gd5Si4 remains stable at certain values of x, transitioning to a Sm5Ge4-type structure with a similar space group but larger volume and slightly varied atomic arrangements at other values. When x reaches a particular point, monoclinic Gd5Si2Ge2 with the space group P1121/a emerges, maintaining stability at temperatures below 570 K. Pecharsky et al. in 1997 highlighted that the unit cell contains four formula units, differing based on how similar building blocks are arranged. These blocks are linked by none, one, or two covalent-like Si-Ge bonds, resulting in successive increases in the unit cell volume.

Oesterreicher *et al.* (1984), while studying the magnetic effect of rare- earth transition metal compounds that have T_c within the room temperature, noted that it was possible to use $Y_2F_{17-x}CO_x$ and $Y_2F_{17-x}Ni_x$ as a room temperature magnetic refrigerant. The investigations done on $Ce_{2x}Dy_xFe_{17}$ alloys found that the absolute change in magnetic entropy within 1.4T magnetic field intensity was approximately 1.67, 1.41 and $1.18 JKg^{-1}K^{-1}$ with x = 0.0, 0.3 and 0.5 with the corresponding temperature being approximately 234K, 267K and 286K respectively. Wang *et al.* (2004) observed that the maximum adiabatic temperature in $Ce_2Fe_{17-x}Co_x$ and $Er_2Fe_{17-x}Ni_x$ (x = 0.3) are 4.75K and 4.51K with corresponding T_c values being 294.2K and 293.5K respectively, which is near Gd metal though much cheaper than that of Gd metal. Hu et al, 2002 observed that the change in magnetic entropy of $Ni_{52.6}Mn_{23.1}Ga_{24.3}$ (a Heusler alloy metal) at 300K is approximately $18.0 JKg^{-1}K^{-1}$ which is close to that of $Gd_5Si_2Ge_2$ and a bit higher than that of Gd near room temperature.

Heusler alloys typically undergo a first-order temperature-induced transition from a martensitic to an austenitic phase. In 1984, Webster et al. made a significant observation regarding the Heusler alloy Ni2MnGa, noting that it underwent a ferromagnetic transition at a critical temperature (Tc) of 376K, with a substantial magnetic moment primarily attributed to Mn atoms connected to Ni atoms (Webster et al., 1984). Krenke et al. (2005) investigated NiMnSn and highlighted a noteworthy magnetocaloric effect (MCE), which they linked to the augmentation of magnetization

36

as the martensitic transition temperature increased. Furthermore, they indicated that substituting Ni with Co led to an elevation in temperature, approaching near-room temperature values.

Sharma et al. (2015) found that substituting Mn with Co yielded an expansion of a non-modulated tetragonal martensitic structure, observable even at room temperature. Correspondingly, Nayak et al. (2009) reported that substituting Ni with Co induced a gradual reduction in the transition temperature proportional to the Co concentration (Webster et al., 1984). Remarkably, in the Heusler alloy NiMnSn, replacing Fe for Mn led to a lowering of Mn-antiferromagnetic interactions, thereby causing a systematic decrement in the martensitic transition temperature (Deltell *et al.*, 2021).

Another interesting material for MR is a rare-earth transition metal compounds of crystallising in the cubic $NaZn_{13}$ type structure (Bruck, 2005). Evdokimenko and Kripyakevich (1963) noted that this structure can be stabilised by adding iron and nickel or by adding at least 10% of Si or Al. Another compound which has been of interest is La (Fe, Si)$_{13}$. This compound has unraveled performance with the Neel temperature, that the temperature above which the transition from anti-ferromagnetic to paramagnetic occurred, being between 200K to 262K with lower iron content. As opposed to $Gd_5Ge_2Si_2$, this phase transition metal does not show any structural change, thus above and below Curie temperature, the material remains cubic. Lately a large MCE was reported in (La, Fe, -Si, Al) system after several investigations by different researchers (Liu *et al.,* 2011). Though the magnetic property of $LaFe_{13-x}Si_x$ had been extensively researched on, it was not until the year 2000 when its magnetocaloric property was discovered by (Hu *et al.*, 2007). They noted that $LaFe_{13-x}si_x$ had an entropy variation which was as high as 20 $JKg^{-1}K^{-1}$ in a field change of 0 - 5T with very low concentration of Si. In their later work, Hu *et al.* (2007) reported that the large change in entropy in $LaFe_{13-x}Si_x$ was related to the metamagnetic behaviour and negative lattice expansion. The extreme value of variation in magnetic entropy of the fields 1T, 2T and 5T are given as 10.5, 14.3 and 19.4 $JKg^{-1}K^{-1}$ respectively. To take care of change in Curie temperature that could significantly affect the change of magnetic entropy, Hu *et al.* (2007) proposed that Fe should be replaced by the correct amount of Co.

In other studies, it was observed that the maximum absolute variation in magnetic entropy value of $LaFe_{11.2}Co_{0.7}Si_{1.1}$ near T_c of 274K within the field change of 0 -5T was 20.3$JKg^{-1}K^{-1}$ which was more than the value recorded for Gd by almost a factor of 2 and almost equivalent to the values of $Gd_5Si_2Ge_2$ and $MnFeP_{0.45}As_{0.55}$ (Zhou *et al.*, 2004). Further Hu *et al.* (2007) observed that in La

$(Fe_{1-x}Co_x)_{11.9}Si_{1.1}$ for (x = 0.04, 0.06 and 0.08), the T_c increased from 243K to 301K with increasing from 0.04 to 0.08. At the same time, the absolute magnetic entropy decreased gradually from 23 to 15.6 $JKg^{-1}K^{-1}$ for the field that changed from 0 – 5T. Shen *et al.* (2009), studied the MCE of $La_{0.5}Pr_{0.5}Fe_{11.5-x}Co_xsi_{1.5}$ for values of ranging from 0 to 1. They found out that when Co is substituted in $La_{0.5}Pr_{0.5}Fe_{11.5}si_{1.5}$, the phase transition at T_c changed from first order to second order when the value of is 0.6. They also noted that magnetic entropy decreased as Co concentration increased and T_c also increased from 181K when to 295K when (Gschneidner & Pecharsky, 2000). It is important noting that when, the maximum values of the absolute change in magnetic entropy at T_c is 295K with specific heat capacity of 6.0 and 11.7 $JKg^{-1}J^{-1}$ for a magnetic field intensity change of 0 - 2 T and 0- 5T respectively. These values are almost 20% higher than that of Gd (Zhong *et al.*, 2018).

Other researchers have studied how replacing Fe with Co affects the MCE in $LaFe_{11.7-x}Co_xSi_{1.3}$ (Shen *et al.,* 2008), $LaFe_{11.9-x}Co_xSi_{1.1}$, $LaFe_{11.8-x}Co_xSi_{1.2}$ (Gamzatov *et al.*, 2007) and $LaFe_{11.4-x}Co_xSi_{1.6}$ (Phan *et al.*, 2005). Shen *et al.* (2005) studied the MCE of $La_{0.7}Pr_{0.3}Fe_{13-x}Si_x$. They showed that the MCE has an increase in Curie temperature and a reduction in absolute change in magnetic entropy when Si is replaced with Fe. The consequence of replacing Mn with Fe on La $(Fe_{1-x}Mn_x)_{11.7}Si_{1.3}$ for $0 \leq x \leq 0.03$ was studied by Wang *et al.* (2004). They reported that T_c was decreasing at the rate of 174K per 1% of Mn. They also noted that there was a large absolute variation in magnetic entropy for a wide range of temperature. There was also a tendency to degenerate as increases with the values given as 17 $JKg^{-1}K^{-1}$ for T_c =130K and 25 $JKg^{-1}K^{-1}$ for T_c = 188K over a field range of 0 – 5T. Anh et al considered the consequence of replacing Nd on MCE. They found that the increase in Curie temperature resulted into a reduction in MCE in $La_{1-x}Nd_xFe_{11.44}Si_{1.56}$ for values given as $0 \leq x \leq 0.4$ .Shen *et al.* (2004) found that when R is substituted with La in $La_{1-x}R_xFe_{11.5}Si_{1.5}$ there was a monotonic decrease in T_c. The absolute change in magnetic entropy for revolution in magnetic field intensity from 0 – 5T also changed from 23.7 $JKg^{-1}K^{-1}$ for to 32.4 $JKg^{-1}K^{-1}$ when for $La_{1-x}Pr_xFe_{11.5}Si_{1.5}$ and 32.0 $JKg^{-1}K^{-1}$ for $La_{1-x}Nd_xFe_{11.5}Si_{1.5}$ for but remained constant at 24 $JKg^{-1}K^{-1}$ for $La_{1-x}Ce_xFe_{11.5}Si_{1.5}$ for $0 \leq x \leq 0.3$ (Gamzatov *et al.,* 2007).

Fujita *et al.* (2004) and Chen *et al.* (2012) self-sufficiently studied the upshot of hydrogenation on MCE. They observed that when interstitial hydrogen was added to $LaFe_{13-x}Si_x$, Curie temperature moved to higher temperature but large MCE remained. There was also a change of

entropy of 17 $JKg^{-1}K^{-1}$ in $LaFe_{11.5}Si_{1.5}H_{1.3}$ at a temperature of 288K. Fujieda *et al.* (2004) controlled the concentration of interstitial hydrogen by changing the annealing temperature under which they prepared the sample. Wang *et al.* (2004) while studying the MCE of La $(Fe_{1-x}Mn_x)_{11.7}Si_{1.3}Hy$ observed that tuning T_c around room temperature was possible by controlling hydrogen concentration. Chen et al did research on how interstitial carbon affects $LaFe_{13-x}Si_xC_\delta$ carbides. They reported that for $LaFe_{11.6}Si_{1.4}C_\delta$ with $\delta = 0$, 0.2, 0.4 and 0.6, the entropy change was almost constant when δ is below 0.2 but decreased rapidly when δ is greater than 0. The maximum value of the absolute change in magnetic entropy for a magnetic field intensity of range between 0 -5T were given as 24.2 $JKg^{-1}K^{-1}$ for $\delta = 0.2$, 18.8 $JKg^{-1}K^{-1}$ for $\delta = 0.4$ and 12.1 $JKg^{-1}K^{-1}$ for $\delta = 0.6$ Guo *et al.* (1998) investigated the change of entropy and the loss of hysteresis in $Lafe_{11.7}(Si_{1-x}Cu_x)_{1.3}$. They found that when the Cu content increased from 0 to 0.2, the Curie temperature changed from 185 to 200K and the absolute change of magnetic entropy dropped. However, the absolute change in magnetic entropy was approximately 20 $JKg^{-1}K^{-1}$ which was considered to be to be large when the value of was 0.2. They further noted that the introduction of Cu reduced both the thermal and magnetic hysteresis.

The first synthetisation of the distorted perovskite structure of manganites with formula given as $R_{1-x}M_xMnO_3$ was done by Jonker (1950). In the formula, R is the trivalent rare-earth elements like Y, Tb, Ho, Gd, Sm, Pr, Eu etc., and M is the divalent alkaline earth ions like Ba, Pb, Sr or K^{1+}, Ag^{1+} etc. The perovskite A-site are formed from homogeneous solid solution (Daniels *et al.*, 2013). Some advantages of this compound over GdSiGe and Gd alloys are that they are cheap, have good chemical stability, large electrical resistivity and small coercive force. These compounds are highly doping dependent since their Curie temperature could easily be tuned to any needed range by simply adding some special types of metal (Sasaki *et al.*, 2002). These compounds were proposed as candidates for room temperature refrigeration. However, it was later discovered that their absolute change in magnetic entropy would decrease significantly when their doping levels were increased hence making their practical application impossible. For example, the absolute change in entropy of $La_{0.8}Ca_{0.2}MnO_3$ with a magnetic field intensity change of 1.5T reached 5.5 $JKg^{-1}K^{-1}$ which was about 1.5 times that of Gd but with Curie temperature of only 230K.

It was also reported that the Curie temperature increased to 263 K when the ratio of Ca was adjusted to $La_{0.6}Ca_{0.4}MnO_3$ but the absolute magnetic entropy reduced 70% of Gd value at 3.0T (Andrade *et al.*, 2016). The Curie temperature was improved by adding Pb and Sr which increased

it to 327 and 296K respectively but the absolute change in magnetic entropy decreased significantly. The magnetocaloric effect (MCE) of $(La_{1-x}Ca_x)$ MnO_3 is the most extensively researched on compound among the manganite family. Moreli *et al.* (1996) investigated the MCE of $(La_{1-x}M_x)$ MnO_3 with M = (Ca, Sr, Ba). They reported that the values of the absolute change in magnetic entropy were not large. They noted that varying doping concentrations would enable tuning of the MCE peak temperature within the temperature range of 250 to 350K. Guo *et al.* (1997) reported the presence of a large MCE in $(La_{1-x}Ca_x)$ MnO_3 polycrystalline samples with $0.20 \leq x \leq 0.33$. They noted that for a change of magnetic field intensity of 1.5 T, the absolute change in magnetic entropy reached its peaks of 5.5 $JKg^{-1}K^{-1}$ at 230K, 4.7 $JKg^{-1}K^{-1}$ at 224K and 4.3 $JKg^{-1}K^{-1}$ at 260K for the values of 0.2, 0.25 and 0.33 respectively. The reported values were larger than that of Gd which had a change in magnetic entropy of 4.2 $JKg^{-1}K^{-1}$ for the same magnetic field intensity of 1.5T.

Zang *et al.* (1996) later discovered a smaller value of absolute change in magnetic entropy 0.6 $JKg^{-1}K^{-1}$ with a change of magnetic field intensity of 1T having a wider breadth of MCE peak δT_{FWHM} of 62K in $La_{0.67}Ca_{0.33}MnO_3$ for = 0.33 than the one reported by Guo *et al.* (1998). The suggested that the observed discrepancy could have been as a result difference in chemical composition and/or the way the samples were prepared. Szymczak *et al.* (2010) investigated the effect of hydrostatic pressure on the change of entropy, the crucial components and Curie temperature in $La_{0.7}Ca_{0.3}MnO_3$ (Zhang *et al.*, 1996). They observed that when pressure is applied, the magnetic entropy of a solid could change significantly without magnetic variation. They concluded that combined effects of applied hydrostatic pressure and magnetic field intensity on the manganite calorie properties are promising candidates for refrigerators. Among the compositions, $La_{0.67}Ca_{0.33}MnO_3$ had the largest MCE. In fact, Lins *et al.* (1979) took the measurement of MCE of $La_{0.67}Ca_{0.3}MnO_3$ and found the change in adiabatic temperature of 2.4K for a change of magnetic field intensity of 2.02T. This value was less than that of Gd. Xu *et al.* (2001), reported that $La_{0.54}Ca_{0.32}MnO_{3\text{-}\delta}$ had a large absolute change of magnetic entropy of 2.9 $JKg^{-1}K^{-1}$ for a change of magnetic field intensity of 0.9T. The sample Curie temperature was recorded as 272K which was approximately 10K higher than that of $La_{0.67}Ca_{0.33}MnO_3$. This suggested that $La_{0.54}Ca_{0.32}MnO_{3-\delta}$ could possibly be used as a magnetic refrigerant for a sub-room temperature refrigerator.

Hueso *et al*. (2002) showed that the MCE peak temperature could be tuned without suppressing the values of MCE of $La_{0.67}Ca_{0.33}MnO_{3-\delta}$ nanoparticles synthesised using sol-gel technique. They also found out that the change of magnetic entropy was inversely proportional to the size of the grain. Phan *et al*. (2007) while investigating the magnetic and magnetocaloric properties of $(La_{1-x})_{0.8}Ca_{0.2}MnO_3$ with $0.05 \leq x \leq 0.3$ noted that decrease in Lanthanum favored not only MCE but also raised the Curie temperature to a higher temperature which is favorable to magnetic refrigeration at various temperatures. Hou *et al*. (2002) studied the MCE of $La_{0.67-x}Ca_{0.33}MnO_3$ for, 0.02, 0.06 and 0.1. They found that the largest value for change of magnetic entropy was 2.78 $JKg^{-1}K^{-1}$ at 272 K over a change of magnetic field intensity of 1T when. They noted that this was good for a sub-room temperature magnetic refrigeration. Several efforts have been made to fit MCE in the room temperature range by exploring the MCE of $(La_{1-x}Sr_x)$ MnO_3 manganites. For example, Szewczyk *et al*. (2000) reported the MCE of $La_{0.845}Sr_{0.55}MnO_3$ polycrystalline manganites, which had phase transition at 234K. The absolute change in magnetic entropy and the change in adiabatic temperature reached 6.6 $JKg^{-1}K^{-1}$ and 3.3 K respectively for a change of magnetic field intensity of 7T.

Subsequently, they conducted measurements on the magnetocaloric effect (MCE) of $(La_{1-x}Sr_x)MnO_3$ with varying Sr concentrations (x = 0.135, 0.155, 0.185, and 0.200). It was observed that the increase in MCE exhibited a direct correlation with the rise in Sr doping, except for a certain case. Notably, the change in adiabatic temperature attained its highest value at 4.15 K for a magnetic field intensity shift of 7T. This phenomenon was previously observed by Demin *et al*. (2004) in $(La_{1-x}Sr_x)MnO_3$ when Sr was introduced. Specifically, for a magnetic intensity change of 0.82T, they documented adiabatic temperature shifts of 0.2 K at 175 K for one scenario, 0.37 K at 180 K for another, 0.7 K at 160 K for a third, and 0.78 K at 436 K for the fourth. In a separate study, Mira et al. (2002) noted an absolute change in magnetic entropy amounting to 1.5 J Kg-1K-1 at 370 K, achieved through a 1 T adiabatic temperature alteration in the La0.67Sr0.33MnO3 sample. This result was in alignment with the findings recorded by Xu et al. (2001). Phan et al. (2007) reported a significant absolute change in magnetic entropy value, measuring 2.12 J Kg-1K-1 at 305 K for a magnetic intensity change of 1 T in La0.65Sr0.35MnO3. Furthermore, Pekala et al. (2008) undertook measurements on the MCE of La0.8Sr0.2MnO3, synthesized using the carbonate precursor method. They identified an absolute change in magnetic entropy of 1.7 J Kg-1K-1 at 275 K for a 2 T magnetic intensity alteration.

Later, they measured the MCE in nanosized form of $La_{0.8}Sr_{0.2}MnO_3$ prepared using sol-gel process. They recorded a Curie temperature of approximately 295K and 301K respectively. The absolute change of magnetic entropy recorded were 0.5 and 2.2 $JKg^{-1}K^{-1}$ for a change of magnetic intensity of 2T. Pakela *et al*. (2008) again prepared the same manganite in carbonate precipitation and measured. The recorded the absolute change of magnetic entropy value of 2.0 $JKg^{-1}K^{-1}$ at 331K for a change of magnetic intensity of 2T which made the material a potential candidate for magnetic refrigeration. The researchers Phan *et al*. (2005), Zhong *et al*. (2021) and Xu *et al*. (2001) have studied the MCE properties of $La_{1-x}Ba_xMnO_3$. Phan *et al*. (2007) measured the MCE of $La_{0.7}Ba_{0.3}MnO_3$ polycrystalline manganite and found an absolute change of magnetic entropy of 0.6 $JKg^{-1}K^{-1}$ at 336 K for a change of magnetic intensity of 1 T.

A study that looked into how oxygen stoichiometry affects the magnetocaloric and magnetic properties of $La_{0.67}Ba_{0.33}MnO$ was carried out. It was noted that oxygen deficiency is directly proportional to the reduction of MCE in the sample. They also reported that this compound had a large absolute change in magnetic entropy of 2.7 $JKg^{-1}K^{-1}$ at 350 K for a change of magnetic intensity of 1 This was attributed to differences in chemical composition and sample preparation method. Koubaa *et al*. (2009) also did some research on $La_{0.65}Ba_{0.3}M_{0.05}MnO_3$ with M being replaced with Na, Ag and K. They noted that the highest change in the absolute magnetic entropy values were 2.65, 2.82 and 2.66 $JKg^{-1}K^{-1}$ for M = Na, Ag and K at 310, 300 and 290 K respectively. The measurement of MCE of $La_{0.7-x}Eu_xBa_{0.3}MnO_3$ for 0.05, 0.10 and 0.15 was done by Dhahri *et al*. (2009). They reported a highest MCE of 298 K with absolute change of magnetic entropy value of approximately 2.3 $JKg^{-1}K^{-1}$ for a magnetic field intensity of 1 T when. In conclusion, it was noted that $La_{0.67}Ba_{0.33}MnO_3$ materials are generally suitable for a room-temperature magnetic refrigeration (Varshney *et al*., 2014).

Several researchers have also studied the MCE of $(La_{1-x}Pb_x)$ MnO_3 manganites. The magnetocaloric properties of $La_{1-x}Pb_xMnO_3$ manganites with, 0.2, 0.3, 0.4 and 0.5 was studied by Chau *et al*. (2003). They reported that the absolute change in magnetic entropy value was directly proportional to the increase in Pb concentration up to when. Thereafter decreased for a larger Pb doping levels. The highest value of absolute change in magnetic entropy recorded was 1.53 $JKg^{-1}K^{-1}$ at 358 K for a change of a magnetic field of 1.35 T for $La_{0.7}Pb_{0.3}MnO_3$. Min *et al*. (2005) later measured both the changes in the adiabatic temperature and magnetic field intensity of $La_{1-x}Pb_xMnO_3$ with, 0.2 and 0.3. They reported that the largest value of absolute change of magnetic

entropy was recorded for this composition (Szewczyk *et al*., 2005). However, for a change of magnetic field intensity of 1.5 T, the change of adiabatic temperature obtained was approximately 0.68 K and 1 K for and at 292 and 349 K respectively. Tozri *et al*. (2010) studied the MCE of $La_{0.8}Pb_{0.1}MnO_3$ and $La_{0.8}Pb_{0.1}Na_{0.1}MnO_3$ and noted that the absolute change of magnetic entropy values was much lower than the ones discussed earlier. The recorded values were 0.43 and 0.68 $JKg^{-1}K^{-1}$ at 201 and 247 K for a change of magnetic field intensity of 1 T. It was therefore concluded that though the absolute change in magnetic entropy value and the adiabatic temperature change could be obtained in the room-temperature range, the values were very small and therefore not suitable for room temperature magnetic refrigeration.

2.3.3 Previous Works on the Fe_2-P Type Systems in Magnetic Refrigeration.

Bruck *et al*. (2004), investigated the magnetic phase diagram of the compounds MnFeP and MnFeAs as the center of the study. They noted these hexagonal Fe_2P based compounds are stable with ferromagnetic order being accompanied by a discontinuous volume change. Adding, they observed that the Curie temperature increased from 150 K to a value above the room temperature while the total magnetic moment was not affected by the changes in the atomic compositions. Duc *et al*. (2019) observed large magnetocaloric effect in $MnFeP_{0.45}As_{0.55}$ at room temperature where they noted that the temperature of 300 K, the absolute change in entropy value were 18 and 28 $JKg^{-1}K^{-1}$ for a change of magnetic field intensity of 1.5 and 5 T respectively. Tegus *et al*. (2008) did some work on how Cr and Co substitution for Fe in $MnFe(P_{1-x}As_x)$ would affect the curie temperature and the absolute change in magnetic entropy value. They reported that in Mn $(Fe_{1-x}Cr_x)$ $P_{0.47}As_{0.53}$ alloy, Cr reduced both its Curie temperature and the absolute magnetic entropy value. it was also observed that there was a phase transition from first order to second order was confirmed by (Johnson & Shull, 2006). It was further reported that when, the Curie temperature was 275 K, the absolute change in magnetic entropy value reduced by 25%. At a Curie temperature of 190 K, the absolute change of magnetic entropy reduced by 65%.

For Mn $(Fe_{1-x}Co_x)$ $P_{0.5}As_{0.5}$, substituting 10% of Co for Fe reduced the Curie temperature from 282 to 260 K and the absolute magnetic entropy value by 55% (Xiao *et al.,* 2019). Liu *et al*. (2021) studied the MCE of $Mn_{1.1}Fe_{0.9}(P_{0.8}Ge_{0.2})$ and noted that this compound had the same shape for both decreasing and increasing fields with the highest change of entropy of 74 and 78 $JKg^{-1}K^{-1}$ for increasing and decreasing fields respectively. For change of magnetic field intensity of 5 T at about 257 K. Trung *et al*. (2009) showed that the critical state of phase transition could be controlled by

altering the annealing the conditions or the composition of the material while retaining large MCE over a large range of temperature.

These materials but not all can be modified to reduce hysteresis loss around the phase change which is paramount to its low and cyclic magnetic field (below IT) process. Attempts are currently being carried out to improve how these materials perform. This is done by doping and alloying the Fe_2P type materials with other atoms with the aim of improving among others, their transition order, transition temperature, mechanical properties, thermal hysteresis structural properties and dynamical properties. Changing the ratios of the Mn: Fe or Si: P (Dung *et al*., 2011; Yan *et al*., 2013) and applying different doping elements like Ni, Cu, Co, B and Cr are just among the methods being used to tune these material properties for magnetic refrigeration application (Brück *et al*., 2012; Ou, 2013). In light of this, this study was aimed to determine whether substituting the atom present at site A in $FeMnP_{1-x}A_x$ (A = Si, x = 0.33) with Sn, In and Se would effectively alter their elastic, structural and vibrational properties. This would further help establish if these materials were stable for application as magnetocaloric refrigerants.

2.4. Structural Properties and their Relation to Stability of Materials.

The structural properties obtained from DFT calculations are very fundamental concepts for understanding the behaviour of materials at the atomic and molecular level. They play an important role in materials design, property optimisation, and predicting materials responses when exposed to different conditions. These properties form the foundation for further exploration of a material's mechanical, thermal, electronic, and optical behaviour. A set of characteristics that are used to describe the geometry and arrangement of atoms or molecules in a material are what is referred to as the material's structural properties. These properties play a vital role in understanding the physical stability, mechanical behaviour, and other physical properties of the material. Comprehending the structural properties of a material helps in forecasting and managing its behaviour in certain applications. Some common examples of a materials structural properties include Lattice constants, coordination number, Crystal structure, grain size, Crystallographic orientation, defects, morphology, packing density and crystal symmetry (Le *et al*., 2012).

The crystal structure gives information about the periodic arrangement of atoms in a crystalline material. Typical measurements that are used to characterise the crystal structure are the unit cell

dimensions, lattice parameters, and the positions of atoms within the unit cell. In Density functional theory, Lattice Parameter are used to define the size and shape of the unit cell in a crystal. These parameters are very crucial for understanding the crystal structure and crystal symmetry. Atomic Positions determines the equilibrium positions of atoms within the unit cell, the accuracy of which influences the predicted properties, such as bond lengths and bond angles. DFT studies defects and imperfections such as vacancies and interstitials to shed more light on their impact to a material's structural stability and electronic properties. Bond Lengths and bond angles within molecules and solids are essential for giving more information on the chemical bonding and reactivity of materials under investigation. In summary the crystal structure, crystal symmetry, and defects influence properties such as mechanical strength, electrical conductivity, thermal properties, and even the response to external stimuli like light and pressure (Newnham, 2012). Materials scientists and engineers use this knowledge to design materials with specific properties and optimise their performance for numerous technological and industrial applications.

2.5 Elastic Properties and their Relation to the Stability of Materials.

Elastic constants are often used to characterise the capacity of a material to resist deformation to an externally applied force. The elastic properties for the polycrystalline magnetocaloric materials are important because of their relation to the mechanical stability of the system (Music & Schneider, 2006; Pugh, 1954). Some of the key elastic properties of a material include; elastic modulus (young's modulus), Shear modulus (modulus of rigidity), bulk modulus, modulus of resilience and toughness, Pugh's ratio, Poisson's ratio, stiffness(compliance), ductility, brittleness, elastic anisotropy, tensile strength, yield strength and elastic limit among others. During the same time magnetic and elastic change at T_C, the polycrystalline structure remains stable if it exhibits a minimum change in its crystal-structure parameters and possesses higher elastic constants. A deeper comprehension of the link between the structural stability with the elastic constants for the magnetocaloric material, as well as, the influence of suitable alloying material on the elastic properties is therefore necessary in the study of compounds suitable for magnetic refrigeration.

The bulk modulus is commonly regarded as a measure of a material's resistance to deformation when subjected to applied pressure. A higher bulk modulus signifies a heightened capacity to withstand deformation under pressure. Similarly, the shear modulus assesses the ability to

withstand reversible deformation caused by shear stress. An elevated shear modulus indicates a greater resistance to shear deformation (Music *et al*., 2007; Pugh, 1954; Vito's *et al*., 2007). Poisson's ratio gauges a crystal's stability against shear and spans from -1 to 0.5 (Nye, 1985). A larger Poisson's ratio implies a material's ability to endure plastic deformation. Young's modulus, defined as the ratio of stress to strain, serves as a measure of a solid material's stiffness. A higher Young's modulus corresponds to a stiffer material (Lines, 1979; Nye, 1985). The ratio of shear modulus to bulk modulus (G/B) in polycrystalline phases is employed to predict the brittle or ductile behavior of materials (Vitos *et al.,* 2007). A higher G/B value is indicative of brittleness, while a lower G/B value is associated with ductility. The critical value that distinguishes brittleness from ductility is approximately 0.57. Furthermore, the value of (C_{12} - C_{44}) can also define the ductility or brittleness of a crystal. A positive value suggests ductility in polycrystalline phases, whereas a negative value signifies brittleness (Fu *et al*., 1999).

Since FeMnP$_{1-x}$ A$_x$ alloys have a hexagonal crystal structure, there are five autonomous elastic constants that make up the full elastic-constant matrix. These independent elastic constants are: C_{11}, C_{12}, C_{13}, C_{33} and C_{44}. According to Nye (1985) the corresponding Bon stability conditions for the hexagonal system are: $C_{11} > 0$; C_{11} - $C_{12} > 0$; $C_{44} > 0$; (C_{11}+C_{12}) C_{33}-2$C_{13}^2 > 0$. The bulk moduli B and shear moduli G are deduced in equations 1 and 2 (Hanh *et al.,* 2019)

$$B = \frac{1}{3}\left(C_{11} + 2C_{12}\right) \tag{2.1}$$

$$G = \frac{1}{5}\left(3C_{44} + C_{11} - C_{12}\right) \tag{2.2}$$

Alternatively, the bulk moduli and shear moduli can also be estimated by Voigt-Reuss-Hill (VRH) approximation (Hanh *et al.,* 2019), where the Voigt bounds of B and G are shown in equations 3 and 4

$$B_V = \frac{2}{9}\left(C_{11} + C_{12} + \frac{1}{2}C_{33} + 2C_{33}\right) \tag{2.3}$$

$$G_V = \frac{1}{30}\left(7C_{11} - 5C_{12} + 12C_{44} + 2C_{33} - 4C_{13}\right) \tag{2.4}$$

And the Reuss bounds are given by equations 5 and 6

$$B_R = \frac{(C_{11}+C_{12})C_{33}-2C_{13}^2}{C_{11}+C_{12}+2C_{33}-4C_{13}} \qquad (2.5)$$

$$G_R = \frac{5}{2}\left\{\frac{\left[(C_{11}+C_{12})C_{33}-2C_{13}^2\right]C_{44}C_{66}}{3B_V C_{44}+\left[(C_{11}+C_{12})C_{33}-2C_{13}^2\right](C_{44}+C_{66})}\right\} \qquad (2.6)$$

The expressions for B and G using VGH approximations can finally be written as shown in equations 7 and 8

$$B = \frac{1}{2}(B_V + B_R) \qquad (2.7)$$

$$G = \frac{1}{2}(G_V + G_R) \qquad (2.8)$$

Where the subscripts R and V represent the Reuss and the Voigt forms respectively. Further, poisson's ratio v, young's moduli E, and anisotropic coefficient A are obtained according to the outlined equations 2.9, 2.10 and 2.11 (Hanh *et al.,* 2019)

$$E = \frac{9BG}{3B+G} \qquad (2.9)$$

$$v = \frac{3B-2G}{2(3B+G)} \qquad (2.10)$$

$$A = \frac{2C_{44}}{C_{11}-C_{12}} \qquad (2.11)$$

The energy of a solid under strain is evaluated by applying the following equation

$$\delta E = E_{tot} - E_0 = \frac{V}{2}\sum_{i=0}^{6}\sum_{j=0}^{6}C_{ij}e_i e_j \qquad (2.12)$$

where V is the volume of the unstrained lattice cell,

δE is the change in energy when strain is applied on the lattice cell,

e_i and e_j are the strain vectors

C_{ij} is the elastic constant matrix ($C_{11}, C_{12}, C_{13}, C_{33}$ and C_{44} in the case of a hexagonal system)

2.6 Vibrational Properties and their Relation to Stability of Materials

Vibrational properties refer to the collective behaviour of atoms or molecules in a material as they undergo vibrational motion around their equilibrium positions. These properties play a crucial role in determining the dynamic stability of materials, especially at the atomic and molecular levels. Understanding and controlling these properties are essential for designing and engineering stable materials for various industrial and technological applications. These properties are related to the motion of atoms or molecules within a material around their equilibrium positions. In solids and molecules, the atoms are not static but rather vibrate around their equilibrium positions due to the presence of thermal energy. These vibrational motions are quantised and are described by vibrational modes, each of which is associated with a specific frequency and amplitude of motion. In the context of materials science and quantum mechanics, the vibrational properties of a material are often studied using techniques like density functional theory or molecular dynamics simulations (Srivastava, 2022).

Some important vibrational properties include; phonons dispersion, phonon density of states, thermal properties such as vibrational energies, vibrational entropy, thermal expansion, phase transition specific heat capacity and Debye temperature. Thermal conductivity, lattice anharmonicity, polarisation, material defects, material dislocations, chemical bonds and eigen vectors are other common vibrational properties that influence the stability of materials. While harmonic oscillators are assumed in simple models, the vibrations in real materials can exhibit anharmonic behaviour due to more complex interactions between atoms. Lattice anharmonicity influences the thermal conductivity, specific heat, and phase transitions of any given material. Phonon excitations largely influence the vibrational contributions to the specific heat capacity of a material arise from phonon excitations. In addition, the density of states plays an important role in determining the specific heat capacity of a material at different temperatures. Investigating the vibrational properties of solids is necessary as it helps predict and engineer its behaviour in various applications, ranging from materials design in electronics to understanding thermal transport in

solids. These properties provide crucial insights into the material's response to external perturbations and its overall physical properties (Qiu *et al.*, 2020).

2.6.1 Phonons

A phonon is a matter wave and is defined as a unit of vibrational energy that arises from the oscillating atoms within a crystal lattice. It is essentially classified as a quasiparticle meaning it is not a real particle but it behaves like one. A phonon does not satisfy the Pauli exclusion principle in that it does not carry any spin but can exist in a vacuum. The two types of phonons in real solids are acoustic phonons and optical phonons. The acoustic phonons are associated with long wavelength vibrations and an in-phase oscillation of the neighbouring particles. They have quite low frequencies in the GHz region and are generated by heat and sound (Srivastava, 2022). Optical phonons on the other hand, are associated with short wavelength vibration and an out of phase movement of atoms in the crystal lattice. Phonons are very valuable in accountancy for diversity of properties and dynamical behaviour of crystalline materials, such as thermal conductivity, electrical conductivity, mechanical properties, phase transition, neutron scattering and superconductivity (Alfè, 2009). A crystal is dynamically stable if its potential energy always upsurges against any blends of atomic displacements. In the harmonic approximation, this is equivalent to the condition that all phonons have real and positive frequencies (Togo & Tanaka, 2015). The phonon density of state is defined by equation 2.13.

$$g(\omega) = \frac{1}{N} \sum_{qj} \delta(\omega - \omega_{qj}),$$
(2.13)

Where ω is the phonon frequency and N is the number of unit cells in the crystal. Once phonon frequencies over Brillouin zone are known, from the canonical distribution in statistical mechanics for phonons under the harmonic approximation, the energy E of phonon system is given in equation 2.14.

$$E = \sum_{qj} \hbar \omega_{qj} \left[\frac{1}{2} + \frac{1}{\exp(\hbar \omega_{qj} / k_B T) - 1} \right]$$
(2.14)

where $T; k_B$ and $\hbar$ are the temperature, the Boltzmann constant, and the reduced Planck constant, respectively.

2.6.2 Thermodynamic properties

Thermodynamics stands as a branch of physics devoted to comprehending the interactions involving heat, temperature, work, and their interconnectedness with energy, radiation, and the intrinsic characteristics of matter. It delves into scenarios where energy exchanges lead to shifts in a system's temperature or state (solid, liquid, gas). As this study will unveil, thermodynamics proves to be an exceptionally efficacious tool for elucidating the collective properties of matter, as well as the intricate connections between these properties and the intricate mechanics governing atoms and molecules (Lemmon & Span, 2015). Beyond its theoretical aspects, thermodynamics also extends its reach to address pragmatic questions. These include unraveling the mechanics behind a refrigerator's ability to cool its contents, deciphering the transformations transpiring within a power plant or an automobile engine, and elucidating the fate of the kinetic energy of a moving object as it comes to a halt. By utilizing the laws of thermodynamics, explanations can be derived for these and myriad other real-life phenomena (Qiu *et al.,* 2020). There are many properties of the thermodynamic system that are measurable, and these properties are useful in describing the present physical state of the system. These include volume, temperature, pressure, specific heat capacity, latent heat, internal energy, entropy, enthalpy, Gibbs free energy, Helmholtz free energy, Landau free energy among others (Thol *et al*., 2016). The thermodynamic state of a material dictates the availability and distribution of energy among its atoms or molecules, which, in turn, affects a materials dynamic behaviour.

Using the thermodynamic relations, a number of thermal properties, such as constant volume heat capacity C_V, Helmholtz free energy F and entropy S, can be computed as functions of temperature as shown in equations 2.15, 2.16 and 2.17 (Dove, 1993).

$$C_V = \sum_{qj} C_{qj} = \sum_{qj} k_B \left(\frac{\hbar \omega_{qj}}{k_B T} \right)^2 \frac{\exp\left(\hbar \omega_{qj}/k_B T \right)}{\left[\exp\left(\hbar \omega_{qj}/k_B T \right) - 1 \right]^2} \tag{2.15}$$

$$F = \frac{1}{2} \sum_{qj} \hbar \omega_{qj} + k_B T \sum_{qj} \ln\left[1 - \exp\left(-\hbar \omega_{qj}/k_B T \right) \right] \tag{2.16}$$

$$S = \frac{1}{2T} \sum_{qj} \hbar \omega_{qj} \coth\left[\hbar \omega_{qj}/2k_B T \right] - k_B \sum_{qj} \ln\left[2\sinh\left(\hbar \omega_{qj}/2k_B T \right) \right] \tag{2.17}$$

Gibbs free energy $G(T, p)$ at given temperature T and pressure p is obtained from Helmholtz

free energy $F(T;V)$ through the transformation

$$G(T,p) = \underset{V}{Min}\left[F(T;V) + pV\right]$$ (2.18)

where the right hand side of equation 17 means finding a minimum value in the square bracket by changing volume V.

$F_{ph}(T;V)$ is approximated by the sum of the electronic internal energy $U_{el}(V)$ and phonon helmholtz free energy $F_{ph}(T;V)$ as shown in equation 18,

$$F(T;V) \square U_{el}(V) + F_{ph}(T;V),$$ (2.19)

where $U_{el}(V)$ is the total energy of the electronic structure obtained from first principle calculation and $F_{ph}(T;V)$ is obtained from the first principle phonon calculation at T and V (Togo & Tanaka, 2015).

In thermodynamics, heat capacity at constant pressure is given by

$$C_P(T,p) = C_v\left(T,V(T,p)\right) + T\frac{\partial V(T,p)}{\partial T^2}\frac{\partial S(T;V)}{\partial V}\bigg|_{V-V(T,p)}$$ (2.20)

The second term of equation (2.20) contributes to the heat capacity from the thermal expansion.

2.7 Theory of Computational Physics

Computational physics (CP) is defined as an interdisciplinary field that brings together elements of computer science, physics and mathematical models in order to study and solve physical problems through numerical simulations and computational techniques. It is with its existence that researchers are now able to investigate physical phenomena, analyse complex systems, and make predictions that would be challenging or impossible using traditional analytical methods. Computational physics makes the use of computers and algorithms to model, simulate, and analyse complex physical phenomena hence has become an integral part of modern scientific research and engineering. It complements theoretical physics and experimental physics, the two other common ways of solving problems in physics very well. CP often regarded as "computer experiments"

involves computer simulation to provide solutions to linear and nonlinear systems of equations, ordinary and partial differential equations, Fourier transforms, stochastic processes, and Monte Carlo methods. CP uses programming languages such as FORTRAN, C, C++, and Python.

Computational physics acts as a complement to experimental and theoretical fields of scientific investigation traditionally. It has earned successful applications in fields such as the design of an electric circuit, molecular modelling, design and testing of aerodynamics, material science, protein folding and atmospheric science. Computational physics works by the creation of mathematical models as well as solutions by use of computers and also programming techniques. Most mathematical models created by physicists mostly have something to do with vast loads of information that can only be processed by powerful computers. There is often a debate about the exact computational physics categorisation in the general field of physics. Some claims are that it is a theoretical physics branch simply due to its involvement in deep theoretical sections of physics and insufficient strong experimental support. Other views are that it lies more on the experimental side simply because the data applied is mainly drawn from experiments. However, scientists unanimously agree that computational physics lies in between experimental and theoretical components.

Modern physics to a large extent depends on computers to solve many of the complicated mathematical components of theories and experiments. Fields of physics like fluid mechanics, accelerator physics and astrophysics both rely on computation and programming. In the section of accelerator physics, for instance, computers have to make an analysis after monitoring and recording large amounts of information each and every moment particles get involved in a collision in an accelerator. Computational physics of the solid state tries to explore the connection between the atomic characteristics of solids and their extensive features by making an analysis of large quantities of data relating to the molecular level of solids. Other tasks that can be worked out employing computational methods are solving integral and differential equations or extremely large matrices that are employed to create calculations related to physical systems.

2.7.1 Density Functional Theory

In elucidating the characteristics and behaviors of multi-electron systems within the domains of solid-state physics, chemistry, and material sciences, quantum mechanics has emerged as a pivotal player. This significance has been facilitated by employing approximate theoretical approaches, such as first-principle calculations. One widely employed theoretical framework in quantum mechanics and condensed matter

physics is density functional theory (DFT), a valuable tool for exploring the electronic structure and properties of atoms, molecules, and solids. DFT revolves around utilizing the concept of electron density, as opposed to the more intricate wave functions of individual electrons, to accurately describe the intricate many-body interactions within a system. DFT effectively determines the electronic properties of a system's ground state by identifying the electron density that minimizes the total energy of the system. This is accomplished by solving the Kohn-Sham equations, which constitute a set of self-consistent field equations capturing the behavior of non-interacting electrons within an effective potential. The entire framework of density functional theory took shape in the mid-1960s, grounded in two fundamental mathematical theorems established by Walter Kohn and Pierre Hohenberg, along with the formulation of a set of equations as articulated by Walter Kohn and Lu Jeu Sham (Sholl & Steckel, 2011).

The initial theorem, established by Hohenberg and Kohn, asserts that the ground-state energy derived from Schrödinger's equation is a distinctive functional of the electron density $\rho(r)$ or $n(r)$. Essentially, this theorem establishes an unequivocal connection between the ground-state wave function and the corresponding ground-state electron density. In simpler terms, the ground-state energy E can be represented as a functional energy $E[n(r)]$, with $n(r)$ representing the electron density. Another articulation of this outcome by Hohenberg and Kohn is that the ground-state electron density uniquely dictates all attributes of the ground state, including energy and wave function. Regrettably, while the first Hohenberg–Kohn theorem rigorously confirms the existence of a functional based on electron density and its applicability to solve the Schrödinger equation, it doesn't provide insight into the actual nature of the functional itself (Goling, 1999). The second theorem, also formulated by Hohenberg and Kohn, defines a profoundly significant characteristic of the functional. This theorem posits that the electron density that minimizes the total energy of the functional is indeed the authentic electron density corresponding to the comprehensive solution of the Schrödinger equation (Perdew *et al*., 2005). If the true form of the functional were known, adjusting the electron density until the functional's energy is minimized would pinpoint the relevant electron density. In practice, this variational principle is applied with approximate functional forms. A constructive manner to depict the functional, as defined by the Hohenberg–Kohn theorem, involves single-electron wave functions (Orestes *et al.,* 2007).

2.7.2 The Kohn and Sham Equations.

The Kohn-Sham equations are a set of equations that involve finding the solutions of a set of non-interacting electrons that are moving in an effective potential. The effective potential is comprised of the external potential from the nuclei and the one due to the electron-electron interactions, represented by the exchange-correlation functional. They are the basic equations that are derived from the variational principle and are self-consistently solved to obtain the ground-state electron density n(r), which represents the number of electrons per unit volume at each point in space (Shi & Wasserman, 2021). The functional of the energy can be written as,

$$E\left[\{\psi_i\}\right] = E_{known}\left[\{\psi_i\}\right] + E_{XC}\left[\{\psi_i\}\right] \tag{2.21}$$

The "known" terms of equation 2.21 include four contributions

$$E_{known}\left[\{\psi_i\}\right] = \frac{h^2}{m}\sum_i \int \psi_i^* \nabla^2 \psi_i d^3r + \int V(r)n(r)d^3r + \frac{e^2}{2}\iint \frac{n(r)n(r')}{|r-r'|}d^3rd^3r' + E_{ion} \tag{2.22}$$

The terms on the right-hand side of equation 2.22 are the electron kinetic energies, the Coulomb interactions between the electrons and the nuclei, the Coulomb interactions between pairs of electrons, and the Coulomb interactions between pairs of nuclei respectively. The other term $E_{XC}\left[\{\psi_i\}\right]$, of equation 2.21 is the exchange–correlation functional, and it is defined to include all the quantum mechanical effects that are not included in the "known" terms. The Kohn–Sham equations now have the form

$$\left[\frac{h^2}{2m}\nabla^2 + V(r) + V_H(r) + V_{XC}(r)\right]\psi_i(r) = \varepsilon_i\psi_i(r) \tag{2.23}$$

On the left-hand side of equation 22, there are three potentials, V, V_H, and V_{xc}. The first of these defines the interaction between an electron and the collection of atomic nuclei. The second is called the Hartree potential and is defined by equation 2.24 as:

$$V_H(r) = e^2\int \frac{n(r')}{|r-r'|}d^3r' \tag{2.24}$$

This potential describes the Coulomb repulsion between the electron being considered in one of the Kohn–Sham equations and the total electron density defined by all electrons in the problem.

The Hartree potential includes a Coulomb interaction between the electron and itself. V_{XC} can formally be defined as a "functional derivative" of the exchange-correlation energy as expressed in equation 2.25

$$V_{XC}(r) = \frac{\delta E_{XC}(r)}{\delta n(r)} \tag{2.25}$$

The functional derivative is written using δ rather than d to emphasize that it is not quite identical to a normal derivative (Paier *et al.*, 2006). The solution of the Kohn-Sham equations is found iteratively in a self-consistent manner as described in section 2.73.

2.7.3 The Procedure Self-Consistent Field.

According to Shi and Wasserman (2021), the self-consistent field (SCF) procedure is a fundamental iterative method applied mostly in density functional theory to find the solution to the Kohn and Sham equations. As earlier on mentioned these equations are used to describe the behaviour of non-interacting electrons in an effective potential, which includes the external potential from the nuclei, the electron-electron Hartree fock potential and the exchange-correlation potential. A summary of the SCF calculation is well outlined in figure 2.2.

Self-Consistent loop
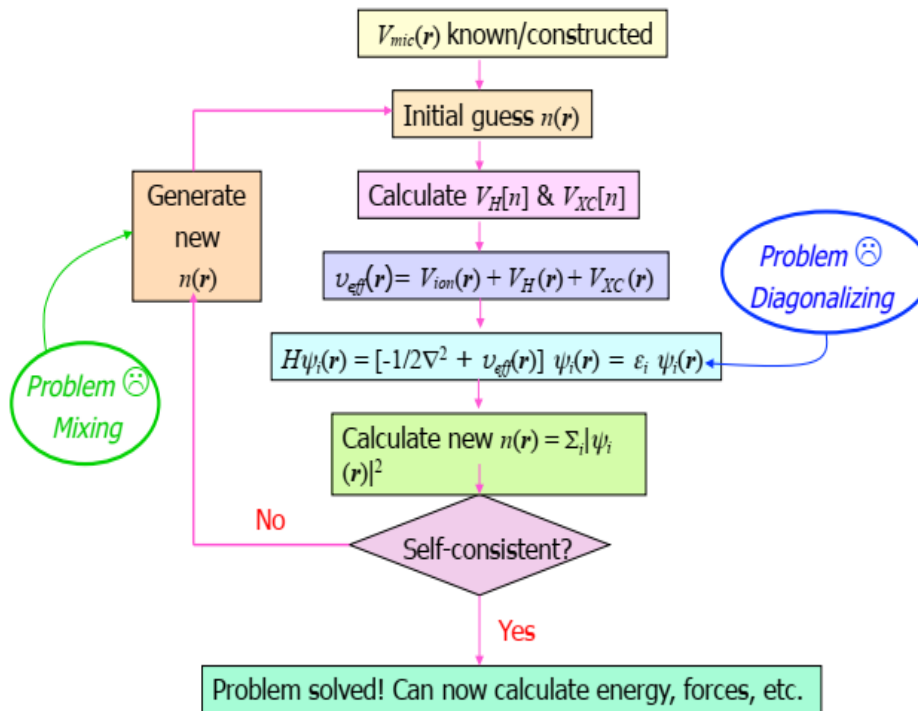
Figure 2. 2: Schematic diagram of the self-consistent field calculation

Source: Shobana (2019).

The self-consistent field calculation involves the following steps:

a) Initialisation

This is where the initial guesses for the electron density n(r) and the Kohn- Sham wave functions ψ(r) are set up

b) The effective potential construction

Here, the potentials $V_H(n)$ and $V_{XC}(n)$ that are dependent on n(r) are first calculated. After this, the effective potential V_{eff} is constructed according to the equation 2.

$$V_{eff}(r) = V_{ion}(r) + V_H(r) + V_{XC}(r) \tag{2.26}$$

c) Solving the Kohn -Sham equation

This is achieved using the constructed effective potential, and gives rise to the Kohn-Sham wave functions Ψ(r) and energies ε. The Kohn sham equation being solved in this step is essentially the Schrödinger-like equation with the effective potential acting on the wave function.

$$H\psi_i(r) = \left[-\frac{1}{2}\nabla^2 + V_{eff}(r) \right] \psi_i(r) = \varepsilon_i \psi_i(r) \tag{2.27}$$

d) Updating the electron density

In this step, the output electron density n(r) is calculated from the square of the absolute values of the updated Kohn-Sham wave functions $|\Psi(r)|^2$.

e) Convergence check

This step involves checking the convergence of the electron density n(r) and the Kohn-Sham wave functions Ψ(r) by comparing the updated electron density with the previous one. This can also be done by observing other convergence criteria, like the change in total energy of the system or the density root-mean-square deviation. If convergence has not been achieved the iterative process is repeated again until the electron density and wave functions converge to a self-consistent solution. Once convergence criteria have been met then we proceed with calculations of the useful physical properties of interest.

2.7.4 The Choice of the Basis Set

The choice of the basis set in density functional theory calculations is a very important factor to consider because it can significantly affect the accuracy and efficiency of the results. The basis set represents a series of mathematical functions that used to get an approximation of the wave functions of electrons present in any given system. Plane wave basis set and Brillouin zone sampling are the most common choice for DFT calculations. Plane waves are mathematical functional that give easy treatment mapping use as a fundamental description of the electronic plane wave functions of periodic systems. While Bloch's theorem stated that, in a body of the periodic system, each electronic plane wave function can be written as a multiplication of a periodic function. Therefore, the periodicity of a unit cell of atoms in three directions is modelled

based on the periodic boundary conditions (PBC). The modelling of a stable system is achieved through the convergence of the total forces and energy. The plane wave basis sets are used to execute and express electronic density. According to Payne *et al.* (1992), the Bloch's theorem is written as in equation 2.28

$$\psi_k(R+T) = e^{ik.r}\psi_k(R) \tag{2.28}$$

A finite solid mostly contains continuous quantum numbers. The finite solid, a kinetic cut-off energy is used to limit the set to a sphere in the reciprocal space in use as shown in the equation below

$$E_{cut-off} > \frac{h^2|K+T|^2}{2} \tag{2.29}$$

The Brillouin zone which contains an infinite number of k-points is usually expressed in terms of Bloch's functions. Numerous techniques have been developed to offer well-optimized selections of k-points for calculations. One such method is the enhanced tetrahedron approach (Blöchl et al., 1994), which partitions the reciprocal space unit cell into tetrahedra. Additionally, the Monkhorst-Pack method is employed to generate a set of specific points within the Brillouin zone (Monkhorst & Pack, 1976), ensuring a judicious distribution of k-points for accurate calculations. The equation of Bloch function $_{I,R}$ is of great importance in finding the solution of each k-point. The band energy is usually integrated over each k point in order to obtain total energy which can be written as in the equation below.

$$E = \sum E_{ik}\, g_i(k)dk \tag{2.30}$$

The volume of the Brillouin zone is given by BZ and the electronic occupation being represented as g_i of the state i at point k.

2.7.5 Pseudopotentials

Pseudopotentials (PPs) are often used to replace the highly localised core electrons with effective potentials. This in turn permits the application of a smaller basis set which decreases computational cost and at the same time, preserving accuracy. Depending on the elements involved in a certain calculation, various pseudopotentials can be used. Calculations in the Quantum Espresso software are performed using the plane wave basis set. The basis set takes care of free electrons in a system intending to reproduce local features of a particular material in terms of

regions and bonds where there are rapid wavefunction oscillations for example around the nuclei. The substitution of real potential with pseudopotentials which gives easy treatment and introduction of a frozen core which is composed of core and valence electrons. The wavefunction is imitated by a soft wiggle pseudo-wavefunction with the same charge as the all-electron wavefunction within this region (Hamann *et al.*, 1979). Therefore, the valence electrons determine most properties of materials such as electronic, structural and mechanical properties. *Ab initio* approximation pseudopotentials are most preferred to the full approximation potential method since it considers solemnly mobile valence electrons leaving the deep inner core states and also the sturdy potential binding them to the nuclei creating the calculation comparatively easier. The ion cores usually play a minimal role in a material system, nevertheless, their good integration into pseudo potentials plays a crucial role in the plane wave basis sets in electronic structures calculation. The real potential and pseudo-wave function both converge at a similar potential at the point called a certain cut-off radius, r_c (Hans Hellmann, 1934).

In the Schrödinger equation, Coulomb's potential is taken care of by an effective potential term, to cater for problem created by motions of ion core, it is by use of Pseudopotentials. The Pseudopotentials function is to imitate the character of an atom ion core. This results in the elimination of core states with pseudo-wave function with less peaks describing the valence electrons. (Blöchl, 1994). Studies show that Projector augmented wave (PAW) pseudo-potential (PP) is a way for reformulating standard Kohn-Sham formalism with numerically inconvenient behaviour into more computationally digested type, that involves a unique Kohn-Sham formalism problem with certain correction. The projector augmented wave (PAW) pseudo-potential (PP), the core electrons are considered frozen at the atomic solutions therefore regarded as the full all-electron wavefunction (Cottenier *et al.*, 2005). It is a distinctive method of determining the electron structure of alloy and materials since it describes well the nodal peak behaviour of valence electrons plane wave function and at identical time allowing the inclusion of the higher core states into the self-consistent interaction procedures.

Studies by Andersen (1975) reports that Projector augmented wave (PAW) pseudo-potential (PP) derives concepts from the all-electron linear augmented plane wave (LAPW) methodology. It is a generalisation of those PP and LAPW methods, and allows for DFT calculations to be conducted with greater computational efficiency. During this study, norm conserving pseudo-potentials are used to mimic the inner core electrons and also the nuclei. In the USPP methodology,

the charge of the core electrons is allowed to change, whose variation is compensated with the introduction of localised atom centered augmentation charges (Vanderbilt, 1990).

2.7.6 Exchange Correlation Functionals

The exchange-correlation functional usually exists as approximation of the many body effects due to absence of self-energy contribution in DFT. The exchange-correlation functionals is described as median of the electron-electron interaction (Toulouse, 2005). The explicit treatment of the interactions between individual particle would lead to a degree of an impractical system of equations. Self-energy is a contribution of a small part of energy of a particle in a system that relies on mutual interaction of particles present in the whole system. This method gives us the advantage of working on properties of a material under study with maximum utilisation of computational resources with precision on accuracy and cost, hence anomalous results can be avoided. The Hartree Fock method gives calculation on self-energy for the ground state properties. Despite the fact that this method utilises greater computational cost, it gives higher accurate precision of different effects. Therefore, we can say that *ab initio* studies of properties of a material provides for solution of a quantum many bodies system involving electron coordinates and atomic interaction problem (Hafner, 2008).

2.7.7 Convergence Criteria in DFT

The convergence criteria are the limits that informs when a density functional theory calculation is likely to have sufficiently attained the most accurate and stable result, following a number of various iterative processes such as the Self consistent field calculation, geometry optimisation, phonon calculation among others charges (Vanderbilt, 1990). Some of the pointers that can be used to check this process include examining the energy convergence to ascertain that the total energy of a system is minimised to a stable value which should be below a certain threshold. The density convergence gives a threshold for the maximum allowed change in the electron density between iterations. A calculation is termed as converged if the change in electron density falls below this specific threshold. Kohn-Sham Orbital Convergence plays a major role in the determination of accurate electronic properties.

In geometry optimisation calculations, forces on atoms are calculated to check their convergence by adjusting the atomic positions are adjusted to reach a minimum energy configuration. Force convergence gives a limit for the maximum allowed force components on

atom so that the geometry optimisation is considered converged if the forces fall below this limit. The convergence criteria should therefore be in such a way as to strike a balance between computational efficiency and the accuracy of the results. A strict convergence criterion will result to more accurate outputs but will require more computational resources and time. On the contrary, the relaxed the convergence criteria, the less the computational costs and the less reliable the results. In practice, it is good to often test and adjust the convergence criteria so as to make sure that the calculations provide physically meaningful results for the specific system under investigations (Sun *et al.*, 2017).

2.7.8 Limitations of Density Functional Theory.

In as much as a number of advantages of DFT calculations on matters versatility and accuracy over semi-empirical methods, some limitations have also been reported and they are as follows:

i.   Band gap underestimation in semiconductors and insulators, leading to incorrect predictions of their optical and electronic properties.

ii.   Exchange-Correlation functional approximations which often lead to errors in band gaps, reaction energies, and dispersion interactions.

iii. DFT oversimplifies the true many-body electron-electron interactions by treating electrons as non-interacting. These approximations will result to inaccuracies in some calculations.

iv.   For large systems or systems with a large number of atoms, DFT calculations become computationally demanding. This limits its application in solving some real-world problems, e.g., large biological system and complex nanomaterials.

v.   At high temperatures DFT will not accurately capture thermal and vibrational effects of materials while computing these properties.

vi.   DFT may fail to provide accurate descriptions of disordered systems and defective systems with accuracy. This is because computing disorder can be calls for creation of larger supercell whose calculations are challenging and computationally demanding.

vii. s generally not well-suited for studying strongly correlated systems, DFT is not efficient in investigating correlated systems with strong electron-electron interactions such as high-temperature superconductors or Mott insulators (Cohen *et al.*, 2008).

2.8 Coefficient of Performance (COP) of a Refrigerator

A refrigerator is a cyclic device that transfers heat from low temperature medium (to a high temperature medium. It operates based on the principle of the Clausius statement also known as the refrigerator statement of the second law of thermodynamics which states that; "it is impossible to cause heat to flow from a cold body to a hot body without doing external work on the working substance." This is simply to say that, energy does not transfer spontaneously by heat from a cold object to a hot object, work input is required to run a refrigerator (Sözen *et al.*, 2012). A working substance in this sense is usually a gas or a liquid that can absorb heat from the source convert some of it into work and reject the remaining heat into the sink. The working of a refrigerator, is the same as that of a heat pump where, the engine takes in energy Qc from a cold reservoir and expels energy Qh to a hot reservoir which can be accomplished only if work is done on the engine. See figure 2.3.
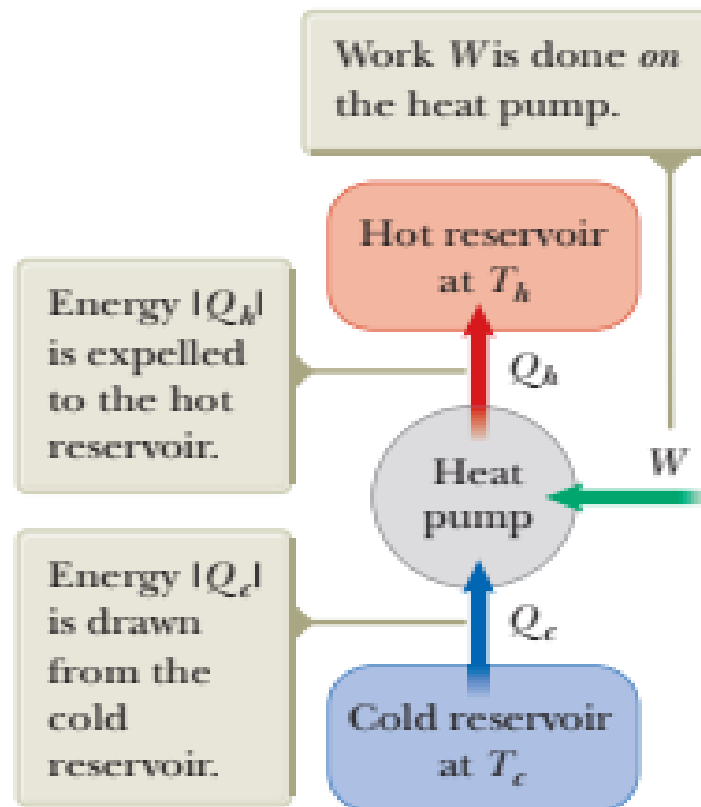
Figure 2. 3: A Schematic representation of a heat pump and a refrigerator

Source: Hermes *et al.* (2009)

The effectiveness or efficiency of a refrigerator is described in terms of a number called the coefficient of performance (COP). The COP is similar to the thermal efficiency for a heat engine in that it is a ratio of the useful (desired) energy transferred to or from a reservoir to the total (required) energy input. For a refrigerator or a heat pump operating in the cooling mode, the useful energy is energy removed from the cold reservoir Qc and the total energy input is the work W done on the system. The most effective refrigerator or air conditioner is one that removes the greatest amount of energy from the cold reservoir in exchange for the least amount of work (Albertini *et al.*, 2017). Therefore, for the devices operating in the cooling mode, the COP in terms of the energy transferred at low temperature Qc and the work done on the refrigerator W is defined as:

$$COP = \frac{Qc}{W}$$
(2.31).

The desired energy output Qc, which is the amount of heat extracted from the cold reservoir inside the refrigerator can be calculated using the following formula:

$$Qc = m \times c \times \theta$$
(2.32)

Where: m is the mass of the substance being cooled which usually comprises of the food and items stored in the refrigerator. c is the specific heat capacity of the working substance being cooled. θ is the difference in temperature between the cold medium and the surrounding outside the refrigerator, that is the difference between the temperature of the cold reservoir and the temperature of the outside environment.

The required energy input W, which is the difference between the energy expelled to the hot reservoir and the energy drawn from the cold reservoir can also be expressed as:

$$W = Qh - Qc = P \times t$$
(2.33)

Where P is defined as the power rating in Watts of the refrigerator's compressor system and t is the time in seconds that the compressor operates to transfer the heat.

The coefficient of Performance of a refrigerator is affected by a number of factors such as its design, its insulation, and the compressor efficiency. Moreover, it is also influenced by the operating conditions and the total load inside of the refrigerator. It is important to also note that

the higher COP value the more efficient refrigerator in its performance, since more heat is transferred for any given amount of work done (Albertini *et al*., 2017). In terms of the hot reservoir temperature Th and the cold temperature reservoir Tc, the COP can also be expressed as:

$$COP = \frac{Tc}{Th - Tc}$$

(2.34)

CHAPTER THREE
MATERIALS AND METHODS

3.1 Computational Methodology

The various resources, tools and procedures that were used to achieve all the objectives stated in section 1 subsection 1.3 are discussed under this chapter. This work was carried out within a period of two years as follows. To start with, structural optimisation, elastic and vibrational properties calculations of the host crystal $FeMnP_{1-x}Si_x$ (x = 0.33) were carried out. It was after this that replacement of the Si_x sites with elements of interest (Se, Sn and In) alternately was done. This was followed by calculations of structural, elastic and vibrational properties for each of the three compounds $FeMnP_{1-x}Se_x$, $FeMnP_{1-x}Sn_x$ and $FeMnP_{1-x}In_x$ (x = 0.33) respectively. The schematic representation of the host crystal showing all the atomic positions is presented in figure 3.1.
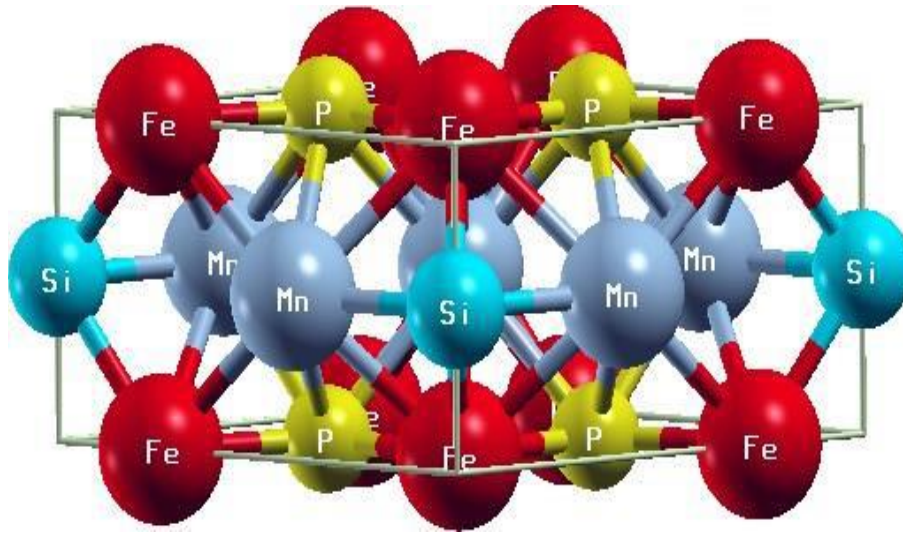
Figure 3. 1: Crystal structure of unit cell of $FeMnP_{0.66}Si_{0.33}$ (Source; XCrySDen software)

First principle DFT formalism was used in this study. All the computations were performed using the Quantum Espresso - Quantum-opEn-Source Package for Research in Electronics, Simulations and Optimisation computer code (Giannozzi *et al*., 2009). Quantum espresso is a multi-use software for first principles or *ab initio* calculations of disordered and periodic condensed matter systems. The Vanderbilt's ultra-soft pseudo potentials was used to define the electron-ion potential (Vanderbilt, 1990) since it made sure that rapid convergence in the total

calculated energy of the systems was achieved. The Perdew, Burke, and Ernzerhof form of the Generalised Gradient Approximation (GGA) pseudo potential was used to treat the exchange and correlation energies in structural properties calculations (Giannozzi *et al*., 2009). XcrysDen, software which is compatible with Linux operating system was used to visualise the system. GNU plot and xmgrace were the tools used to plot the graphs of interest.

The conjugates gradient method (Fletcher & Reeves, 1964) was employed to optimised electronic minimisation cycles in unit cell structure. The smearing width of 0.05 eV (Grimme *et al*., 2011) was employed for the Gaussian smearing function. The Broyden, Fletcher, Goldfarb and Shannon (BFGS) were carried out to relax the cell structure. The calculations for the energy volume curves were achieved by employing PAW exchange correlation functional (Blöchl, 1994; Kresse & Joubert, 1999), where the internal atomic positions were relaxed while fixing the unit cell structure. The significance of internal structure optimisation was to generate energy volume constant derivative such as the pressure and the bulk modulus. The conjugate gradient method (Fletcher & Reeves, 1964) which is a standard numerical minimisation approach was employed to minimise the volume in the unit cell structure (Grimme *et al*., 2011). The k point grids and kinetic energy cut off threshold were tested to ensure all optimised energies parameters converged in the unit cell structure (Payne *et al*., 1990). The data analysis and presentation were carried out using the xmgrace, XcrysDen, and GNU plot in the QE computer code.

3.2 The Structural Properties Calculation

The input file preparation was done by first, creating a text file with an extension .in to input the calculation parameters. The system's crystal structure, such as the lattice type, lattice constants, atomic positions, and the number of atoms per unit cell were then specified. Following this, the calculation settings, including the type of calculation pseudopotentials, and convergence criteria were defined. Quantum ESPRESSO was executed with the input files using the appropriate command and this generated several output files containing the results of the calculation. Convergence of the results with respect to various parameters, such as k-point sampling, energy cutoff, and cell size was checked. The output files were analysed to extract the desired structural properties of the materials which included the lattice parameters, atomic positions, bond lengths

and bond angles. XcrysDen was used to visualise the crystal structure and the obtained results, this was important in verifying the exactness of the calculation.

3.2.1 Structural Optimisation and Relaxation

For all the proposed materials under the study, structural relaxation and optimisation was done using Broyden, Fletcher, Goldfarb and Shannon approach (Srivastava, 1984) considering three magnetic arrangements namely ferromagnetic (FM), paramagnetic (PM) and anti-ferromagnetic (AFM)) to obtain the most energetic stable states. Thereafter, energy-volume calculations were implemented and the data obtained fitted to the third-order Birch-Murnaghan equation of state to extract the structural parameters for all the respective systems. Structural parameters optimisation for $FeMnP_{1-x}A_x$ (A_x= Si, Se, In, and Sn) alloys was achieved through relaxing the atoms in *x*, *y* and *z* dimensions until the systems attained the lowest energy positions as per the set criterion for convergence. The atomic dimension in the relaxed positions was used to ensure both the k-point grid and the plane wave kinetic energy cut off optimisation are achieved. The lowest energy of the system formed the basis of total minimise energy as a function of the cell volume. The lowest energy was due to the k-points and plane wave kinetic cut-off energy having optimised values. The variable cell relaxation algorithm was employed for obtaining the minimised total energy value by using ultra soft pseudopotentials (USPP) and Perdew-Burke-Ernzerhof (PBE) exchange-correlation functions. For each step the ionic positions and the lattice parameters were optimised with energy and force convergence criteria of 10^{-5} eV/atom and 0.005 eV/A respectively.

3.2.2 k-point Optimisation

The K-points optimisation was done to accurately sample the Brillouin zones for the systems under investigation in order to provide reliable and meaningful results. The experimental value lattice parameter was used in this calculation with a relatively coarse k-point grid and a minimal k-point sampling to speed up the process. After the initial calculation was complete, the total energy from the output file was extracted and recorded as a reference for convergence. The energy unit for kinetic Energy cut-off was set in Rydberg for $FeMnP_{1-x}A_x$ (A_x= Si, Se, In, and Sn) alloys. The generation of special k-mesh points was achieved using the Monkhorst-pack scheme which enabled the integration parts of the irreducible Brillouin zone (IBZ) mesh from a small size to a dense large size since $FeMnP_{1-x}A_x$ (A_x= Si, Se, In, and Sn) alloys are heavy grid.

3.2.3 Optimisation of Plane Wave Kinetic Cut-off Energy (ecutwfc)

The cut-off energy determined the number of plane waves used to expand the wavefunctions and electronic charge density and its proper optimisation was essential in ensuring that accurate and reliable results were obtained without wasting computational resources. The k-point grid convergence is accustomed to calculating the plane wave cutoff energies. During the study on plane wave cut-off energy, the lattice parameters and k-points mesh were set at their optimised values in the entire calculations. For every step, the kinetic cut-off energy was varied under constant k-points, lattice parameters and force convergence criteria of 10^{-5} eV/atom until optimisation was achieved.

3.3 Elastic Properties Calculation

Broyden, Fletcher, Goldfarb and Shannon algorithms were used to optimise the atomic positions (Wang & Ye, 2003). Calculations of elastic constants, Debye temperature, poisson ratios, young's modulus, bulk modulus and shear Modulus (all in Voigt-Reuss-Hill approximations), average Debye sound velocity and solid density were all calculated using Thermo_pw computer code interfaced with Quantum Espresso (Corso, 2018). The calculations of the self-consistent field (SCF) were first performed to obtain the equilibrium structure of the crystal using pw.x. Next, the obtained structure was used as input for a geometry optimisation calculation to relax the atomic positions and bring the system to its minimum energy configuration. A series of strained crystal structures was created by application of small deformations to the optimised structures. This was for example, achieved by changing the lattice parameters along each direction (x, y, z) independently by a small percentage. For each of the strained structures, a geometry optimisation was once again performed using pw.x to relax the atomic positions and find their minimum energy configuration. For each relaxed strained structure, the stress tensor was obtained from the change in the total energy with respect to the applied strain.

The elastic constants of the compounds were computed using stress-strain data that was obtained from the previous step. These elastic constants provided knowledge about the materials mechanical properties and also gave information about how the all the materials under investigation responded to the applied stress. After that the stress-strain data was fitted to the appropriate equations that relate the stress to the strain components and this process helped

determine the elastic constants. The calculated elastic constants were finally used to obtain the various elastic properties of the materials which included the bulk modulus, the shear modulus, the Young's modulus, the Pugh's ratio and Poisson's ratio. These properties were analysed to provide valuable information about the material's mechanical behaviour, mechanical stability and the anisotropy of the crystals. For the ferromagnetic phase, the wave functions (W.F) Kinetic Energy cut-off points were all set at 90 Ry and the charge density cutoff was set at 1080 Ry. A smearing width of 0.05 Ry and convergence threshold of 10^{-6} Ry with a mixing beta of 0.7 was applied. The K points separation of 3 x 3 x 5 was used for all the compounds. For the antiferromagnetic phase and paramagnetic phase, the wave functions Kinetic Energy cut-off points were all set at 80 Ry and the charge density cutoff was set at 960 Ry. A convergence threshold of 10^{-3} Ry with a mixing beta of 0.4 were applied. The K points separation of 3 x 3 x 2 was used for all the compounds.

3.4 Vibrational Properties Calculation

The Frozen phonon approach was used to compute the vibrational properties. A representative phonon calculation on the grid of $FeMnP_{1-x}A_x$ (A= Si, Se, Sn and In, x = 0.33) was performed using the phonopy code which was interfaced with quantum espresso (QE) (Giannozzi *et al*., 2009). The plane-wave basis projector augmented wave (PAW) technique (Blöchl, 1994) was applied in the context of density functional theory (DFT) inside the generalised gradient approximation (GGA) in the Perdew–Burke–Ernzerhof (PBE) form (Dal Corso, 2014) as employed in the phonopy-QE code. A plane-wave energy cutoff of 90 Ry and an energy convergence criterion of the order of 10^{-10} eV were used for all the calculations. For the unit cell, a k-point sampling mesh of 14 ×14 ×16 was used and the equivalent density mesh was used for the supercells in addition to a 0.05 Ry smearing width. A 1×1×2 super cell of the conventional unit cell and a predetermined atomic displacement of 0.01 Å approach was utilised in these calculations. The scope of the phonon calculation used was 3N = 27×q linear-response calculations. Interatomic force constants, phonon modes, phonon frequencies, phonon density of states, phonon energy and phonon thermal properties were evaluated according to the set of appropriate fundamental equations that relate to these quantities.

.

3.4.1 Phonon Properties Calculation

Firstly, a self-consistent field (SCF) Calculation was set up and a standard density calculation for all the material was run using Quantum ESPRESSO software. This was done in order to provide the electronic ground state information necessary for phonon calculations. The dynamical matrix was then obtained using the matdyn.x command in Q espresso code to calculate the dynamical matrix at specific wave vectors called the q-points. The dynamical matrix represents the force constants between atoms and is a core requirement for phonon calculations. After that, the input files required by phonopy were set up the input files required so as to analyse the phonon properties. These input files were prepared to include the information that was earlier on obtained from the Quantum ESPRESSO calculations, such as the crystal structure and dynamical matrix. The next step involved running the phonopy code to perform phonon calculations. Lastly phonopy was used to analyse the dynamical matrix, phonon dispersion and calculate phonon frequencies and modes at different q-points in the Brillouin zone. The analysis of the phonon dispersion gave rise to the phonon dispersion relations, which represented the phonon frequencies as a function of wave vector in the Brillouin zone. This information helped understand the phonon properties of the material, such as acoustic phonon modes and optical phonon modes, phonon frequencies and phonon density of states (PDOS).

3.4.2 Thermal Properties calculation

For the thermal properties calculation an SCF calculation using Quantum ESPRESSO was first performed to obtain the ground state electronic structure. Quantum ESPRESSO's matdyn.x code was then applied to calculate the dynamical matrix of the solids at specific q-points. This required the setting up of an appropriate input file for matdyn.x that specified the q-points and other parameters for all the materials under study. Next the input files required by Phonopy were prepared and they his typically included the creation of a POSCAR file that contained the crystal structure and a FORCE_CONSTANTS file containing the dynamical matrix that had been earlier obtained from the Quantum ESPRESSO calculations. After that phonopy calculations using the input files prepared in the previous step were run alternately for each material. It was at this point that the analysis of the dynamical matrix and calculations of the phonon frequencies and modes at various q-points in the Brillouin zone was then carried out. Visualisation and interpretation of the analysed phonon dispersion obtained from the phonopy calculations was second lastly done using the XcrysDen software package. Lastly phonopy was used to calculate thermal properties of the

materials which included properties such as phonon contributions to specific heat capacity at constant volume, vibrational entropy, vibrational free energy and thermal conductivity, based on the phonon dispersion and thermal properties of the materials under investigation.

CHAPTER FOUR
RESULTS AND DISCUSSION

4.1 Structural Properties

The FeMn-based magnetocaloric materials with the formula $FeMnP_{1-x}A_x$ (A= Si, x = 0.33) are alloys that have been defined to have a hexagonal crystal structure of space group P-62m with a group number of 189. The transition metals Fe and Mn occupy the 3f and 3g sites, whereas the metalloids P and A occupy the 2c site and the 1b site respectively. Yibole *et al*. (2018), observed that around room temperature, this group of compounds, exhibit a first order magneto elastic transition resulting to changes in the ratio of the lattice parameters (c/a) without noticeable changes in the volume. It was also observed that in the neighbourhood of the room temperature, this group of materials, experiences first order ferromagnetic (FM) to paramagnetic (PM) phase transition and hence their increased research investigation as possible candidates for practical application in magnetic refrigeration (Guillou *et al.,* 2015). Magnetocaloric materials operate under continuous magnetic and thermal cycles and so require to be structurally stable across phase transition which is one of the needed criteria to vet a good solid-state refrigerant. This study focused on trying to optimise the structural stability of $FeMnP_{1-x}A_x$ (A= Si, x = 0.33) by replacing the atom at the A site with other viable, nontoxic metalloids; Selenium (Se), Tin (Sn) and Indium (In) and studying their effect on the structural properties of the host material. The main aim of substituting the atoms at A site was to imitate the bonding between atoms without possibly changing the structure of the compound.

Lattice parameters, cell dimensions, crystal structure, bond length as well as bond angles are considered to be among the main structural properties of crystal structures. They are inherent characteristics that describe the arrangement and organisation of atoms or molecules in a materials crystal lattice. These properties majorly impact on how a certain material behaves under various conditions. Bond angle are major considerations for the three dimensional set up of atoms that represents a molecule or a solid. It governs various properties of a substance such as reactivity, biological activity, colour, polarity, magnetism and phase of matter among others. The crystal structure defines the long-range order and periodic arrangement of atoms in a material. Some of the common crystal structures include cubic, tetragonal, orthorhombic, hexagonal, rhombohedral, and monoclinic structures (Chung *et al*., 2016).

Bond length is on the other hand, the mean distance between nuclei of 2 fused atoms in a molecule. It determines the bond dissociation energy and the bond strength in that it is inversely related to both. This is to say that when all other features are held constant, a smaller bond distance results into a stronger bond and a dissociation energy that is high. Lattice parameters are a set of numerical values that define the dimensions and angles of the unit cell in a crystal lattice. They are comprised of lattice constants (a, b, c) and the inter-axial angles (α, β, γ) where α is the angle between the b and c axes, β is the angle between the a and c axes, and γ is the angle between the a and b axes (Niu, 2016). It is important to note that the bond length, bond angles, crystal structure and the lattice parameters significantly influence the structural stability of a material by controlling the strength of chemical bonds, determining the arrangement of atoms in a crystal, and influencing the material's elasticity and response to external forces.

4.1.1 The Ferromagnetic (FM) Phase.

The main focus for structural properties of a material is majorly on the dimensions of the unit cell comprising of the cell dimensions known as the lattice parameters. For a hexagonal structure there are three lattice constants a, b and c described by the condition a = b $\neq$ c. From this description, the geometry of the optimised structures for this phase, was characterised by the primitive lattice vectors ak, bk and ck, whose lengths were 5.811, 5.811 and 3.529 Angstrom respectively. The values of the lattice constants a, b and c presented in the table 4.1 were then calculated as follows, a = b = (alat/ak) and that of c was given by c = (alat/ck). The angle γ between the lattice vectors a and b is $120°$, angle α between lattice constants b and c is $90°$, angle β between lattice constants a and c is $90°$. Each unit cell for all the materials in the ferromagnetic phase contained 4 formula units and 9 atoms. table 4.1 presents the calculated values of the lattice constants of $FeMnP_{1-x}A_x$ (A= Si, Se, Sn and In, x = 0.33) together with the reported experimental and theoretical values as reported by (Hoglin *et al*., 2015) and (Shuang *et al*., 2017).

The Lattice Constants of The Selected Materials in the FM Phase.

It can be seen from table 4.1 that for the base material $FeMnP_{0.66}Si_{0.33}$, the percentage difference of the structural parameters a, b, c and V from experimental results reported by Hoglin *et al*. (2017) were 0.892%, 0.486% and 3.054% respectively which were generally low and acceptable. This is a general trend inherent to GGA calculations which tend to underestimate some properties of materials. This shows that the calculated lattice parameters are in good agreement with the reported

experimental data. The percentage deviations for $FeMnP_{1-x}A_x$ (Se, Sn and In, x = 0.33) were not reported due to the unavailability of experimental data for these materials. Similarly, no theoretical studies are available in literature for these materials for comparison.

Table 4. 1: Lattice constants of the selected materials for the FM phase by use of GGA_PBE functionals.

Material	Lattice constants	This work	Exp Values	Other DFT Values	% Deviation from Exp Values
$FeMnP_{0.66}Si_{0.33}$	a =b (Å)	6.111	6.166	6.128	0.892
	c (Å)	3.274	3.290	3.072	0.486
	Volume (Å^3)	105.917	109.254	106.375	3.054
$FeMnP_{0.66}Se_{0.33}$	a =b (Å)	5.921			
	c (Å)	3.536			
	Volume (Å^3)	107.358			
$FeMnP_{0.66}In_{0.33}$	a =b (Å)	5.929			
	c (Å)	3.894			
	Volume (Å^3)	118.548			
$FeMnP_{0.66}Sn_{0.33}$	a =b (Å)	5.975			
	c (Å)	3.821			
	Volume (Å^3)	118.189			

The Bond Lengths for the Selected Materials in the FM Phase.

Bond length is a key property that plays a very essential role in understanding the bonding mechanism of compounds. The values of bond lengths for the selected materials in the ferromagnetic phase are presented in table 4.2. It is evident from table 4. 2 that the percentage deviations of the present theoretical results from existing experimental values reported by Hoglin *et al*. (2015) and Shuang *et al*. (2017) for $FeMnP_{0.66}Si_{0.33}$ and as outlined in column 5 are between 0.4% and 2%. This

is error is small and acceptable and it can be it attributed to the well-known fact that the generalised gradient approximation tends to underestimates some properties of solids such as the cohesive energies between the bonded atoms due to approximation made in exchange-correlation functionals (Perdew *et al*., 1998). The percentage deviations of the present theoretical results from the base material $FeMnP_{0.66}Si_{0.33}$ outlined in column 6 of table 4.2 are roughly between 0.3% and 2%. This deviation is further attributed to the inherent properties of DFT that underestimates the parameters of the materials. This is yet another clear indication that substituting the A site of $FeMnP_{0.66}Si_{0.33}$ with Se, In and Sn does not significantly affect the structure of the compounds in the ferromagnetic state. This is important since any significant deviations would indicate that the dopant is distorting the structure significantly and this is not a desired result.

Table 4. 2*: Bond lengths in Angstroms for the selected materials in the FM phase by use of GGA_PBE functionals.

Material	Bond lengths	This work	Exp Values	% Deviation from Exp. values	% Deviation from $FeMnP_{0.66}Si_{0.33}$ values
$FeMnP_{0.66}Si_{0.33}$	Fe-Mn	2.631	2.685	2.011	
	Fe-P	2.296	2.314	0.778	
	Fe-Si	2.307	2.318	0.474	
$FeMnP_{0.66}Se_{0.33}$	Fe-Mn	2.669			1.444
	Fe-P	2.258			1.655
	Fe-Se	2.343			1.560
$FeMnP_{0.66}In_{0.33}$	Fe-Mn	2.683			1.976
	Fe-P	2.304			0.348
	Fe-In	2.354			2.037
$FeMnP_{0.66}Sn_{0.33}$	Fe-Mn	2.683			1.976
	Fe-P	2.304			0.348
	Fe-Sn	2.324			0.736

A longer bond length implies weaker bonds, and the material may be more prone to breaking or undergoing chemical reactions. On the other hand, shorter bond lengths indicate stronger bonds and increased stability against bond dissociation. Deviations from ideal bond lengths can also influence bond angles and torsional angles, affecting the molecular or crystal geometry and stability. Focusing on the bond lengths between the Fe atom and the replacing atoms at the A site, it is clear that length Fe - Si is the smallest of all the four materials presented. It can also be seen that the length Fe - In is the largest giving a percent deviation of 2.037% from the same site of the host crystal. This could possibly imply that of the four compounds, $FeMnP_{0.66}In_{0.33}$ has the least stability against bond dissociation. $FeMnP_{0.66}Sn_{0.33}$ recorded the smallest deviation of 0.736 % percentage of the bond length between Fe - Sn from the same site of the host crystal which indicates stronger bond.

The Murnaghan Equation of State Fits for the Selected Materials in the FM Phase.

To attain a well relaxed structure, variable cell optimisation computation and relaxation of the cutoff energy, k-points and lattice parameters were competed. Graphs of the computed total energies of all the proposed compounds as functions of volume in the FM phase are presented in figures 4.1, 4.2, 4.3 and 4.4. These energies were then fitted to the Birch-Murnaghan equation of state to obtain the equilibrium lattice constants and bulk modulus. The Murnaghan equation of state is given by the interplay between the pressure and volume acting on the object (Murnaghan, 1944). This equation usually depicts itself when modelling the behaviour of matter under the condition of high pressure as clearly shown in earth sciences.

Calculations of the bulk elastic and the bulk structure properties are crucial parameters to be determined in the condensed matter and solid-state physics. The bulk calculations enabled the Visualisation, comprehension, characterisation and prediction of the properties of the alloys. The structural, mechanical and electronic properties of materials and alloys under intense research can give an explanation for extreme conditions for an alloy and possibly recommend if the material is suitable for a given industrial application or not. The Murnaghan equation of state is based on derivation assumption emanating from the equation of continuum mechanics. The modulus of incompressibility B_0 and its first order derivative with respect to the pressure, B_0', are both measured at ambient pressure. The coefficients such as volume (V) at zero pressure, volume derivative, bulk modulus, first and second order derivative of bulk modulus with pressure were

76

obtained after fitting the data to the respective equations of state. Therefore, the bulk modulus and the pressure derivative of the bulk modulus were established and reported.

The plot shows Energy (Ry) versus Volume $(a.u)^3$ with annotations:

$E_{min} = -1424.47583$ Ry
$V_{min} = 468.54$ $a.u^3$
$B_o = 25569$ kbars
$B'_o = 1.00$
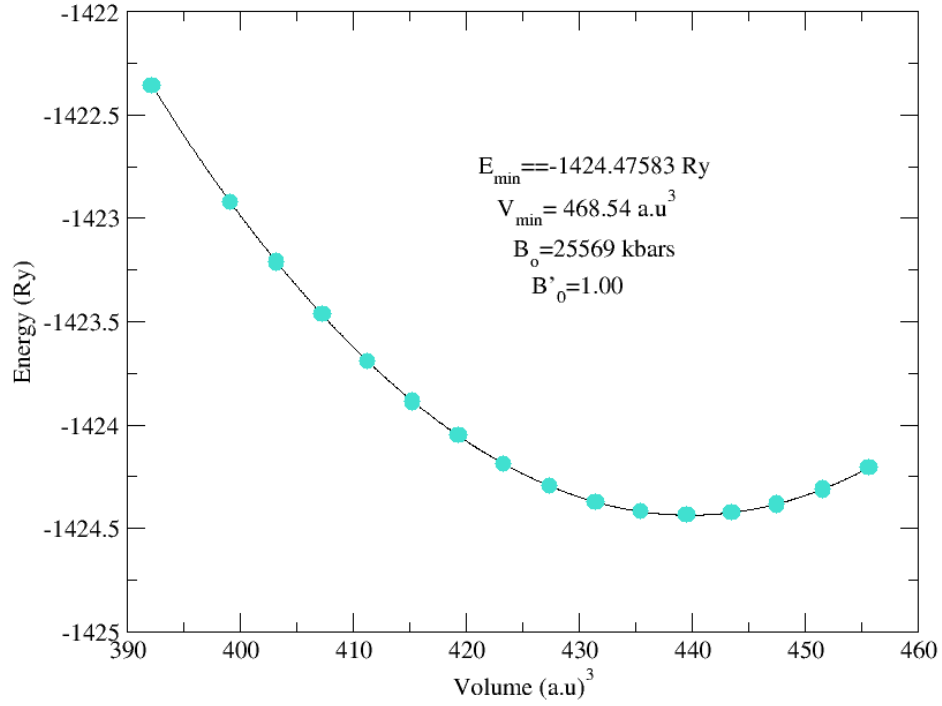
Figure 4. 1: Murnaghan equation of state fit for the FM phase of $FeMnP_{0.66}Si_{0.33}$.
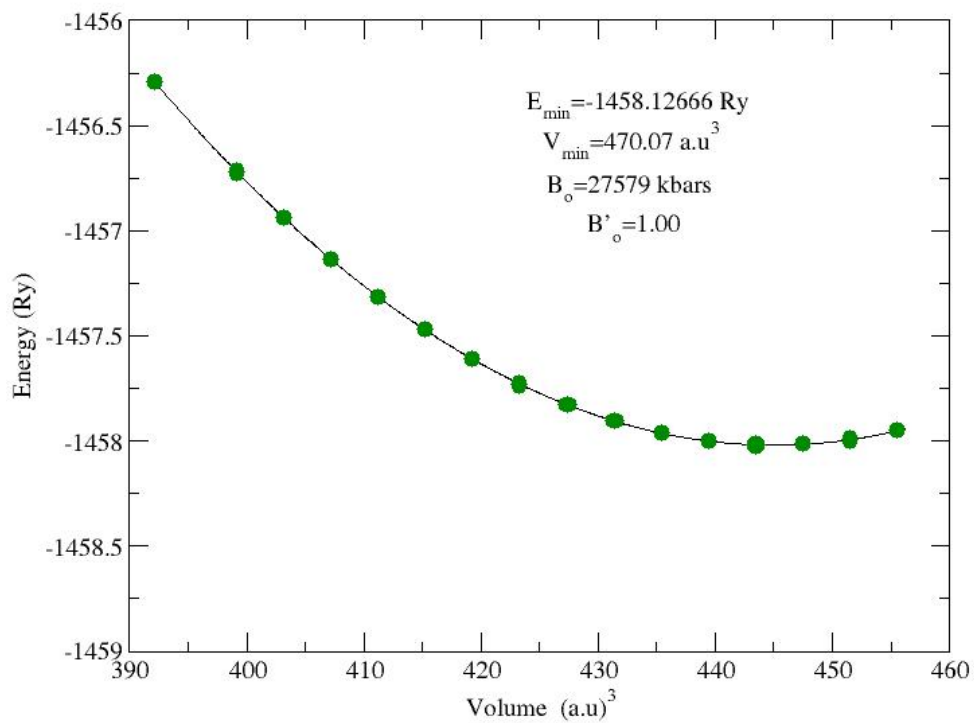
Figure 4. 2: Murnaghan equation of state fit for the FM phase of FeMnP$_{.66}$Se$_{0.33}$
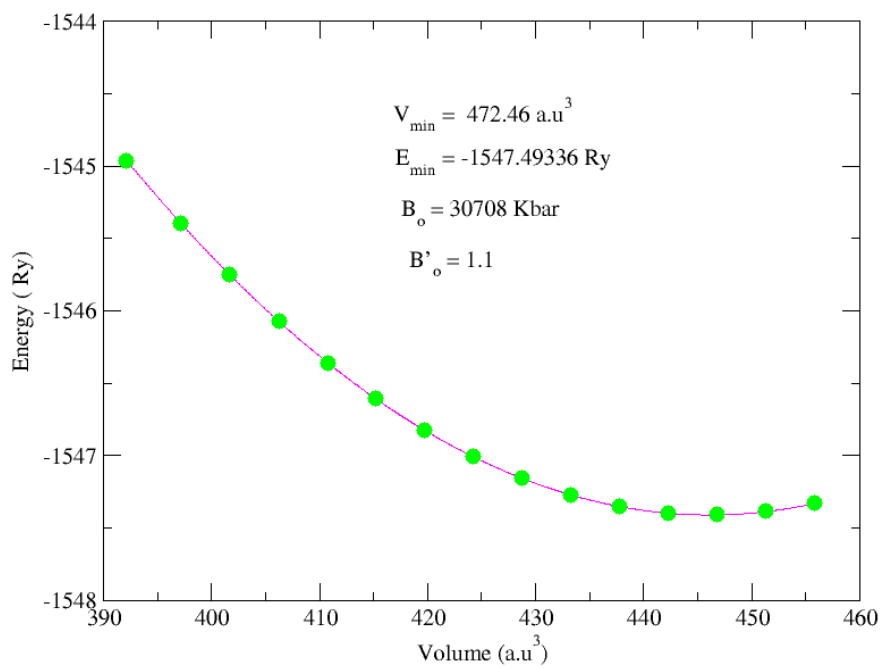
Figure 4. 3: Murnaghan equation of state fit for the FM phase of FeMnP$_{0.66}$Sn$_{0.33}$
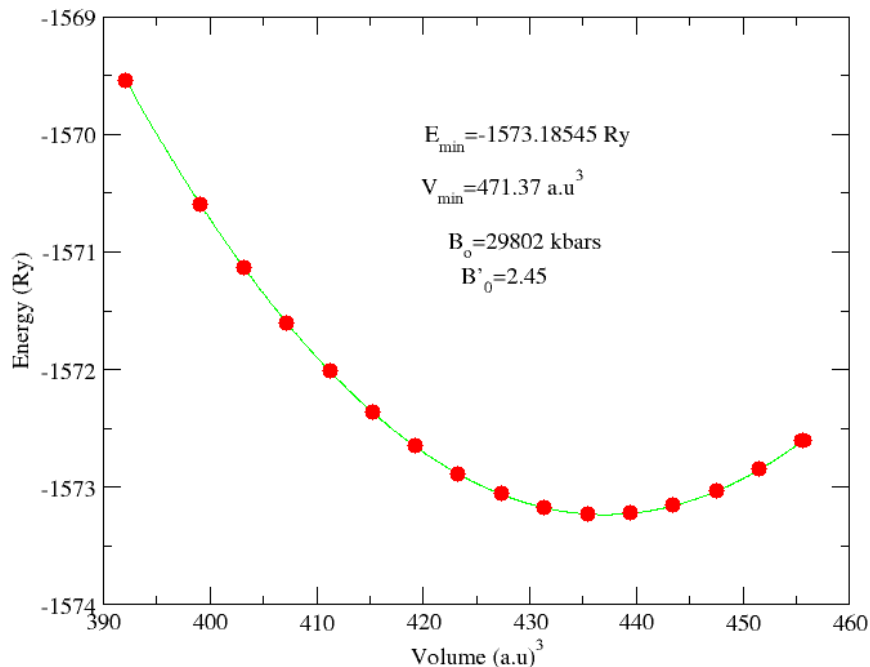
Figure 4. 4: Murnaghan equation of state fit for the FM phase of $FeMnP_{0.66}In_{0.33}$

From the figures 4.1, 4.2, 4. 3 and 4.4 it is observed that the expected shape of the energy-volume curves was established, in particular they all had similar shapes but different minima. This is a clear indication that there was no significant strain introduced to these structures on replacing the A site of the host material with other metalloids. This led to the conclusion that, replacing the A site of the base material with other atoms did not noticeably change the structure of these compounds. Additionally, the derivatives of pressure and the bulk modulus for $FeMnP_{0.66}Si_{0.33,}$ $FeMnP_{0.66}Se_{0.33},$ $FeMnP_{0.66}Sn_{0.33}$ $FeMnP_{0.66}In_{0.33}$ were calculated to be 1.00, 1.00, 1.10 and 2.45, respectively. These results suggest that $FeMnP_{0.66}In_{0.33}$ is the stiffest and hence less disposed to compressive distortion owing to its large value of the bulk modulus.

4.1.2 The Antiferromagnetic (AFM) Phase

In the antiferromagnetic state, the unit cells for all the materials under study contained 6 formula units and 18 atoms each. For this phase, the hexagonal structure was also characterized by optimised primitive lattice vectors ak, bk, ck, whose lengths are 5.811, 5.811, 3.529 Angstrom respectively. The values of the lattice constants a, b and c presented in table 4.3 were then calculated as follows, a = b = (alat/ak) and that of c was given by c = (alat/ck). The angle γ between

79

the lattice vectors a and b is $120°$, angle α between lattice vectors a and c is $90°$, angle β between lattice vectors b and c is $90°$.

The Lattice Constants of the Selected Materials in the AFM Phase.

Table 4.3 presents the computed values of the lattice constants of $FeMnP_{1-x}A_x$ (A= Si, Se, Sn and In, x = 0.33) together with the previously reported experimental and theoretical values as outlined by Shuang *et al*. (2017) and Hoglin *et al*. (2015). It can be seen from table 4.3 that for the host material $FeMnP_{0.66}Si_{0.33}$, the percentage deviation of the lattice constants a = b, c and the volume V of the hexagonal structures from the corresponding experimental results were 3.10%, 4.00% and 5.61% respectively. These are relatively large deviations and could possibly indicate that along the magnetic phase transition from the ferromagnetic to the antiferromagnetic state the base compound was structurally unstable.

Table 4. 3: Lattice constants of the selected materials in the AFM phase by use of GGA_PBE functionals.

Material	Lattice constants	This work	Exp Values	Other DFT Values	Deviation from Exp Values
$FeMnP_{0.66}Si_{0.33}$	a =b (Å)	5.829	6.018	5.941	3.10
	c (Å)	3.531	3.342	3.426	4.00
	Volume (Å³)	103.931	108.346	106.579	5.61
$FeMnP_{0.66}Se_{0.33}$	a =b (Å)	5.899			
	c (Å)	3.569			
	Volume (Å³)	107.572			
$FeMnP_{0.66}In_{0.33}$	a =b (Å)	5.932			
	c (Å)	3.891			
	Volume (Å³)	118.382			
$FeMnP_{0.66}Sn_{0.33}$	a =b (Å)	5.971			
	c (Å)	3.819			
	Volume (Å³)	117.940			

The large deviations could also be as a result of computational error from the generalised gradient approximation functionals which overestimates fundamental gaps in lattice parameters calculations. The percentage deviations from experimental for $FeMnP_{0.66}Se_{0.33,}$ $FeMnP_{0.66}In_{0.33,}$ and $FeMnP_{0.66}Sn_{0.33}$ were not reported due to the unavailability of related experimental data for these materials.

The Bond Lengths for the Selected Materials in the AFM Phase.

As mentioned earlier, the bond length is a crucial property that plays a very indispensable role in understanding the bonding mechanism of compounds. The values of bond lengths for the selected materials are presented in table 4.4 for the antiferromagnetic phase. It is evident from this that the percentage deviations (column 5) of the present theoretical results from existing experimental values (column 4) as reported by Hoglin *et al.* (2015) for $FeMnP_{0.66}Si_{0.33}$ are 3%, 4.9% and 0.07%. This is further attributed to the approximations made in the unknown exchange correlation functionals used in DFT calculations (Perdew *et al*., 1998).

A well-known fact also is that the generalised gradient approximation tends to underestimates cohesive energies between the bonded atoms resulting to a greater tendency of contraction than elongation in the bonds as seen in these results This low and acceptable deviation of 0.07% between the Fe -Si atoms could also be attribute to atomic sizes and the arrangements of the atoms in these compounds. This is yet another clear indication that the calculated density functional theory data of the bond length for $FeMnP_{0.66}Si_{0.33}$ in this work was in good agreement with the experimental data reported by Hoglin *et al*. (2017). The percentage deviations from experimental for $FeMnP_{0.66}Se_{0.33,}$ $FeMnP_{0.66}In_{0.33,}$ and $FeMnP_{0.66}Sn_{0.33}$ were not reported due to the unavailability of experimental data for these materials.

Table 4. 4*: Bond lengths in Angstroms for the selected materials AFM phase by use of GGA_PBE functionals.

Material	Bond lengths	This work	Exp Values	Deviation from Exp. values
$FeMnP_{0.66}Si_{0.33}$	Fe-Mn	2.601	2.685	3.00
	Fe-P	2.199	2.314	4.90
	Fe-Si	2.316	2.318	0.07
$FeMnP_{0.66}Se_{0.33}$	Fe-Mn	2.598		
	Fe-P	2.197		
	Fe-Se	2.371		
$FeMnP_{0.66}In_{0.33}$	Fe-Mn	2.531		
	Fe-P	2.165		
	Fe-In	2.543		
$FeMnP_{0.66}Sn_{0.33}$	Fe-Mn	2.531		
	Fe-P	2.177		
	Fe-Sn	2.527		

Still from table 4.4 and focusing on the bond lengths between the Fe atom and the replacing atoms at the A site, it is clear that bond length Fe - Si is the smallest of all the four materials studied and has a value of 2.316 Angstroms. It can also be seen that the length Fe - In with a calculated value of 2.543 Angstroms is the largest of the four materials. This could possibly imply that of the four compounds, $FeMnP_{0.66}In_{0.33}$ has a higher thermal conductivity which is a property linked to higher bond lengths. This is because a big bond length provides more room for atoms to move and vibrate, allowing good heat conduction due to greater flexibility and freedom of motion of the molecules. Additionally, a longer bond length between atoms indicates lower strain or tension within the molecule. This is an advantage in the design of desirable materials for practical applications in industries because reducing strain can make the molecule more stable and less reactive.

4.1.3 The Paramagnetic (PM) Phase.

The unit cells for all the materials under study in the paramagnetic state also contained 6 formula units and 18 atoms each. For this phase which was also a hexagonal structure, the three lattice constants a, b and c were described by the condition $a = b \neq c$. From this description, the geometry of the optimised structures for this phase, was characterised by the primitive lattice vectors ak, bk and ck, whose lengths were also given by the dimensions 5.811, 5.811 and 3.529 Angstrom respectively. The values of the lattice constants a, b and c presented in the table 4.5 were then calculated as follows, a = b = (alat/ak) and that of c was given by c = (alat/ck). The angle γ between the lattice vectors a and b was 120°, angle α between lattice vectors a and c was 90° and the angle β between lattice vectors b and c was also 90°.

The Lattice Constants of the Selected Materials in the PM Phase.

Table 4. 5: Lattice parameters of the selected materials for the PM phase by use of GGA_PBE functionals.

Material	Lattice constants	This work
$FeMnP_{0.66}Si_{0.33}$	a =b (Å)	5.684
	c (Å)	3.570
	Volume (Å^3)	99.911
$FeMnP_{0.66}Se_{0.33}$	a =b (Å)	5.742
	c (Å)	3.596
	Volume (Å^3)	102.675
$FeMnP_{0.66}In_{0.33}$	a =b (Å)	5.822
	c (Å)	3.825
	Volume (Å^3)	106.223
$FeMnP_{0.66}Sn_{0.33}$	a =b (Å)	5.833
	c (Å)	3.790
	Volume (Å^3)	111.774

The calculated values of the lattice constants for $FeMnP_{0.66}Si_{0.33}$, $FeMnP_{0.66}Se_{0.33}$, $FeMnP_{0.66}In_{0.33}$, $FeMnP_{0.66}Sn_{0.33}$ are presented in table 4.5. There was no existing experimental and theoretical data to compare with the current results for the paramagnetic phase. However, looking at this work's results on the structural properties of the selected materials for the ferromagnetic and anti-ferromagnetic state, it can be noted that these results are more similar in trend to the results obtained in the anti-ferromagnetic phase. The bond angle as well as the bond length are considered to be among the most important structural properties of materials. Bond angle determines the three-dimensional set up of atoms which characterizes a molecule. It guides a number of vital properties of a material which includes factors such as colour, biological activity, magnetism, phase of matter, reactivity and polarity (Chung *et al.*, 2016).

The Bond Lengths of the Selected Materials in the PM Phase.

Table 4. 6: Bond lengths in Angstroms for the selected materials for the PM phase by use of GGA_PBE functionals

Material	Bond Lengths	This work
$FeMnP_{0.66}Si_{0.33}$	Fe-Mn	2.740
	Fe-P	2.149
	Fe-Si	2.302
$FeMnP_{0.66}Se_{0.33}$	Fe-Mn	2.589
	Fe-P	2.142
	Fe-Se	2.348
$FeMnP_{0.66}In_{0.33}$	Fe-Mn	2.458
	Fe-P	2.122
	Fe-In	2.583
$FeMnP_{0.66}Sn_{0.33}$	Fe-Mn	2.482
	Fe-P	2.129
	Fe-Sn	2.491

From table 4.6 and focusing on the bond lengths between the Fe atom and the replacing atoms at the A site, it is clear that bond length Fe - Si is the smallest of all the four materials studied and

has a value of 2.302 Angstroms. It can also be seen that the length Fe - In with a calculated value of 2.583 Angstroms is the largest of the four materials. This again is a clear indication that of the four compounds, $FeMnP_{0.66}In_{0.33}$ has a higher thermal conductivity which is a property that is linked to higher bond lengths. This is because a big bond length provides more room for atoms to move and vibrate. This results to greater flexibility and freedom of motion of the molecules thus allowing good heat conduction. Again, the longer the bond length between atoms the lower the strain or tension within the molecule. This is an advantage in the design of desirable materials for practical applications in industries because reducing strain can make the molecule more stable and less reactive. Just like for the lattice parameters, there were no experimental or theoretical data to compare with however the bond lengths are much closer to those of the AFM phase than the FM phase with alternate elongation and contraction.

4.1.4 Discussion of Structural Properties

In summary, as alluded in earlier discussions, the average length between nuclei of two bonded atoms in a molecule is gives the bond length of a material which governs the bond strength and bond dissociation energy in that it is inversely proportional to both. This is in other words to say that when all other factors are held constant, a shorter bond distance results into a stronger bond and a higher dissociation energy (Niu, 2016). As evident from columns 6 of table 4.1, and column 6 of table 4.2, the percentage deviations of the present theoretical results from the available experimental results for the host alloy are between 0.3% and 2.0%. This shows that the calculations for the structural properties of $FeMnP_{0.66}Si_{0.33}$ in the FM phase are in very good agreement with experimental results and hence are fairly accurate and stable structurally.

There are slightly noticeable percentage deviations greater than 2% for the calculations of lattice constants and the bond lengths of the host crystal from the reported experimental data in the AFM phase. This is shown in columns 6 of figure 4.3 and column 5 of figure 4.4 and this could be attributed to the use of generalised gradient approximation (GGA) functional in this study as it tends to underestimate cohesive energies and overestimate fundamental gaps. It could also mean that the host material was structurally unstable across phase transition from ferromagnetic antiferromagnetic phase. There were no structural parameter percentage deviations reported for the paramagnetic phase of the materials under study due to lack existing experimental and theoretical data in this state. Again, looking closely at tables 4.1, 4.2, 4.3, 4.4, 4.5 and 4. 6, it can be seen that for both the lattice constants and bond lengths, the values for $FeMnP_{0.66}Si_{0.33}$ and

FeMnP$_{0.66}$Se$_{0.33}$ are very close and slightly different from those of FeMnP$_{0.66}$Sn$_{0.33}$ and FeMnP$_{0.66}$In$_{0.33}$ which are also very close. This could be attributed to the to the closeness of the atomic radii of the atoms at the A site of the compounds.

The atomic radius of Si is1.55 Å and is close to that of Se which is 1.58 Å whereas for the other pair the atomic radii of Sn and In are 1.88 Å and 1.95 Å respectively (Vincent *et al.,* 2021). In this work, relaxed structures for all the compounds were obtained using variable cell relaxation normally abbreviated as vc relax calculations. Following this optimisation of the -points, cutoff energy and lattice parameters were done to obtain to most stable structures with the minimum energies. Graphs of the computed total energies of the proposed alloys as functions of volume in the FM phase were presented in figures 4.1, 4.2, 4.3, and 4.4. These energies were then fitted to the Birch-Murnaghan equation of state to obtain the equilibrium lattice constants and bulk modulus. From these figures, it can be observed that there was a clear likeness in the energy-volume curves, which exhibited similar shapes but different minima. This observation supports the structural stability of these alloys in the ferromagnetic phase. The implication of this result is that replacing the A site of the host crystal with the selected metalloids did not significantly alter the structure of the compounds.

It is important to also note that, the lattice constant affects the mechanical properties of materials, which includes but not limited to their hardness, elasticity, and strength. A larger lattice constant may result in weaker interatomic or interionic bonds, leading to lower mechanical strength. In addition, the lattice constant is related to the thermal expansion coefficient of a material. This means that heating a material causes the lattice constant typically increases, consequently resulting to the expansion of a material. The electrical and thermal Conductivity of a material are also influenced by the lattice constants by affecting the spacing between atoms or ions. Different lattice constants can impact the mobility of charge carriers or the propagation of phonons or vibrational energy through the crystal lattice. With this information it can be concluded that FeMnP$_{0.66}$In$_{0.33}$ bonds has lower interatomic owing to its slightly large lattice constants in all the 3 magnetic phases.

The bond length between atoms in a material can significantly affect the stability of a material's structure which is determined by the balance between attractive and repulsive forces between atoms or ions. In a stable material, the atoms or ions are arranged in a manner that minimises the total energy of the system. At a specific bond length called the optimal bond length which represent

the most stable configuration for any given material, the attractive forces; covalent bonds, metallic bonds, or ionic bonds between atoms are maximised, whereas the repulsive forces; those due to electron-electron or ion-ion interactions are minimised. A materials bond strength is directly related to the bond length in that a shorter bond lengths results to a stronger bond and vice versa. From the calculated results, small bond lengths are reported in the host crystal FeMnP$_{0.66}$Si$_{0.33}$ in all the 3 magnetic arrangements making it the most stable material structurally. This is because owing to its smaller values of the bond lengths, it forms stronger bonds which hold the atoms or ions tightly together, making the material more resistant to deformation or structural changes.

4.2 Elastic Properties.

4.2.1 The Ferromagnetic (FM) Phase.

The elastic constants of the selected materials in FM phase.

The mechanical stability of a hexagonal polycrystalline structure is established using the elastic potential free energy equation

$$\phi = \frac{1}{2} C_{ij} \varepsilon_i \varepsilon_j \qquad , \text{where } \phi \geq 0 .$$
(4.1)

When $\phi = 0$, there is an equilibrium state and when $\phi > 0$, we have a state of mechanical deformation. This, therefore, calls for the principal minors of the matrix C_{ij} as given by equation (4.2) to all be positive-definite.

$$
C_{ij} =
\begin{bmatrix}
C_{11} & C_{12} & C_{13} & 0 & 0 & 0 \\
 & C_{11} & C_{13} & 0 & 0 & 0 \\
 & & C_{33} & 0 & 0 & 0 \\
 & & & C_{44} & 0 & 0 \\
 & & & & C_{44} & 0 \\
 & & & & & X
\end{bmatrix}
, \text{where } X = \frac{1}{2}\left(C_{11} - C_{12}\right)
$$
(4.2)

The matrix in equation (4.2) is symmetrical about its leading diagonal, that is $C_{ij} = C_{ji}$ (Ledbetter, 1977). Crystals of hexagonal class have 5 independent elastic constants but due to added relation in the matrix, C_{ij} we get the element X which now defines a tetragonal crystal (Liu

et al., 2017).   The calculated eigenvalues of the stiffness matrix from equation (4.2) lead to the following four basic conditions known as the Born stability conditions for mechanical stability of a hexagonal crystal shown in equation 4.3:

$$C_{11} > 0; \quad C_{11} > C_{12}; \quad C_{44} > 0; \quad (C_{11}+C_{12}) \, C_{33} > 2C_{13}^2. \tag{4.3}$$

Table 4. 7: The elastic constants in Kbars for the selected materials in the FM phase.

Material	C_{11}	C_{12}	C_{13}	C_{33}	C_{44}	C_{11}/C_{12}	$C_{11}C_{33}/C_{13}^2$
$FeMnP_{0.66}Si_{0.33}$	2517.630	839.529	1350.224	2365.614	1042.143	2.999	3.267
$FeMnP_{0.66}Se_{0.33}$	2563.944	983.805	1117.622	2480.59406	850.099	2.606	5.092
$FeMnP_{0.66}In_{0.33}$	1487.394	759.847	1241.799	1521.194	583.788	1.957	1.467
$FeMnP_{0.66}Sn_{0.33}$	1824.1889	875.537	1260.287	1785.204	660.004	2.084	2.050

Table 4.7 presents the elastic constants in Kbars for the studied materials in the FM phase. From this table, it can be noted that the values of elastic constants were calculated to satisfy the four Born stability conditions that are stated in equation 4.3 for hexagonal structures. This, therefore, shows that all the four structures studied in this work were stable elastically. Stability ratios as shown in the last two columns 6 and 7 of table 4.7 are all positive definite from which it can be further concluded that all the four components exhibit mechanical stability in the ferromagnetic phase. Further, when $C_{33} > C_{11}$, the compounds are more incompressible along the C-direction than along the A-direction. From 4.7, it is also noted that only $FeMnP_{0.66}In_{0.33}$ that satisfies this condition.

The elastic Anisotropy of the selected materials in the FM phase.

A polycrystalline structure is said to be anisotropic if it shows characteristics with unlike values when dimensions are taken along axes in dissimilar orientations. It can be easily noticed that in

compounds or single crystals of solid elements where atoms, ions or molecules are arranged in systematic lattices. The elastic anisotropy, represented by the symbol A, is used to explain how elastic properties of solids act towards the direction of the stress (Sun *et al*., 2004). Hexagonal crystals have three shear-type anisotropy ratios defined in terms of the elastic constants by equations (4.4), (4.5) and (4.6).

$$A_1 = \frac{\frac{1}{6}\left(C_{11} + C_{12} + 2C_{33} - 4C_{13}\right)}{C_{44}}. \tag{4.4}$$

$$A_2 = \frac{2C_{44}}{\left(C_{11} - C_{12}\right)}. \tag{4.5}$$

And

$$A_3 = A_1 A_2 = \frac{\frac{1}{3}\left(C_{11} + C_{12} + 2C_{33} - 4C_{13}\right)}{C_{11} - C_{12}}. \tag{4.6}$$

The shear-type anisotropy ratios derived from C_{ij} values in table 4.7 for the selected materials using the three equations stated in expressions 4.4, 4.5 and 4.6 are given in the table 4.8.

Table 4. 8: Shear type anisotropic ratios for the selected materials in the FM phase.

Material	A1	A2	A3
FeMnP$_{0.66}$Si$_{0.33}$	0.430	1.242	0.534
FeMnP$_{0.66}$Se$_{0.33}$	0.792	1.076	0.852
FeMnP$_{0.66}$In$_{0.33}$	0.092	1.605	0.148
FeMnP$_{0.66}$Sn$_{0.33}$	0.310	1.391	0.432

An elastic anisotropy ratio of 1, shows that a crystal is isotropic. Otherwise, values of A which are less than or more than 1 suggest anisotropy. The computed shear anisotropic factors for the

studied materials are listed in table 4.8. from which can be easily seen that all the materials under consideration are elastically anisotropic. This is because the anisotropic values of both A_1 and A_3 are all less than 1 and those of A_2 are all greater than 1. In terms of stability, an anisotropic ratio not equal to one could imply a more uniform response of a given material to external forces, potentially contributing to better overall stability. It should be however noted that the stability of a material is influenced by a combination of factors beyond just the anisotropic ratio.

Calculations of, young modulus 'E', poisson ratios 'v' bulk modulus 'B' and shear Modulus 'G' all under Voigt and Reuss approximations as well as Voigt-Reuss-Hill average of the two approximations are presented in appendix II and figures 4.5, 4.6, 4.7, 4.8 and 4.9.

The bulk Modulus of the selected materials in the FM phase.
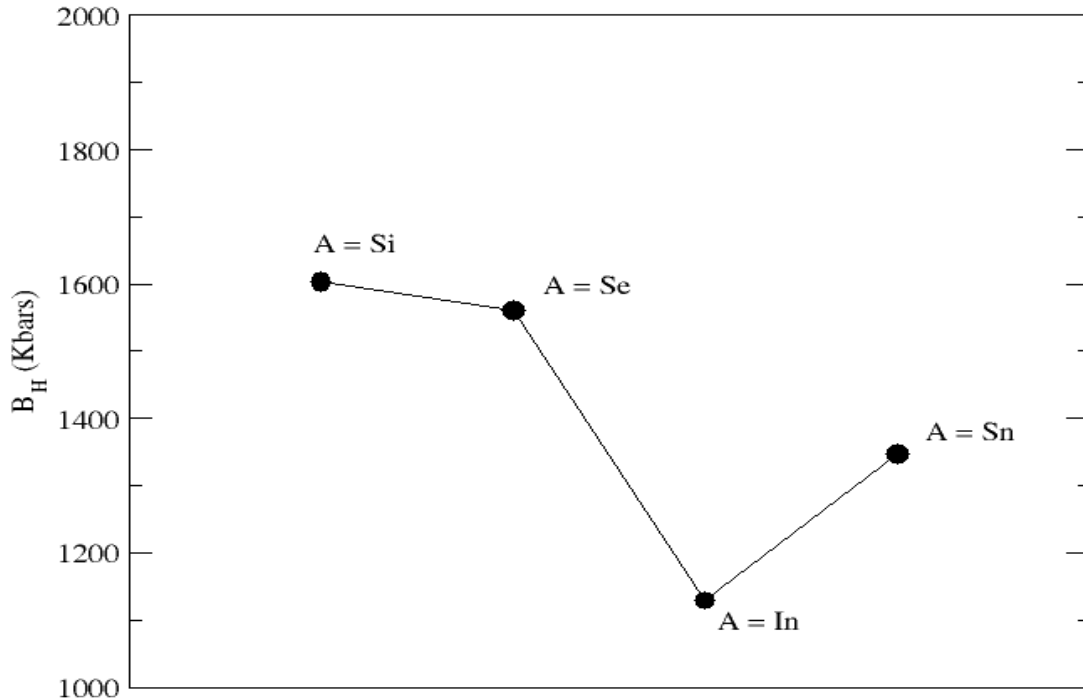
Figure 4. 5: The Voigt-Reuss-Hill average bulk Modulus (B_H) for the FM phase of $FeMnP_{1-x}A_x$ (A= Si, Se, In and Sn: x = 0.33)

Bulk modulus which indicates the incompressibility of a material, is the degree of how a substance endures variations in volume when compressed from all sides. The capacity of a material to resist distortion is directly related to its bulk modulus. That is, the higher the bulk modulus, the stronger its ability to overcome deformation. From Figure 4.5 it is observed that $FeMnP_{0.66}Si_{0.33}$

90

has the highest value of bulk modulus while $FeMnP_{0.66}In_{0.33}$ has the lowest value of bulk modulus. The results clearly demonstrate that, of the four materials investigated in this work, $FeMnP_{0.66}Si_{0.33}$ has the highest capacity to resist deformation.

The shear Modulus of the selected materials in the FM phase.

This is a scientific value that determines the capacity of a material to resist transverse buckle. Mathematically, it is the ratio of shear stress to shear strain. A greater value of shear modulus shows that the structure is very rigid and may require greater force to be bent.
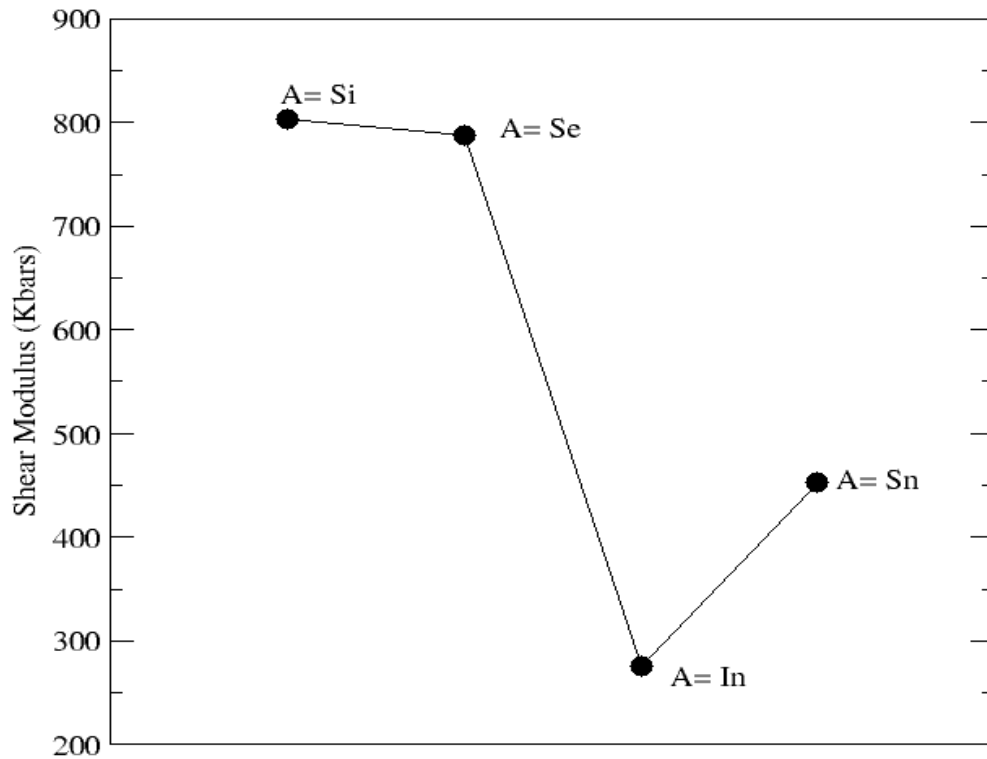
Figure 4. 6: The Voigt-Reuss-Hill average shear modulus (G_H) for the FM phase of $FeMnP_{1-x}A_x$ (A= Si, Se, In and Sn: x = 0.33)

A lesser value of shear modulus demonstrates that the material is either soft or elastic and little force is required to warp it. Note that fluids have null shear modulus and therefore no strength is required to deform them (Chepkoech *et al.,* 2020). The calculated results of shear modulus for the selected materials are presented figure 4.6. Of the 4 compounds studied, $FeMnP_{0.66}Si_{0.33}$ has the highest value of modulus of rigidity hence, a robust capacity to resist plastic distortion.

The Young's modulus (E) of the selected materials in the FM phase.

This is a percentage that measures the tensile springiness of a material. That is, an indicator of the capability of a material to withstand differences in length when exposed to compression or lengthwise tension. It is found when longitudinal stress is divided by the longitudinal strain, and specifies how stiff a solid is. The higher the young's modulus, the firmer the material (Naumov *et al.*, 2020). From figure 4.7, it is observed that the E values decrease in the order: $FeMnP_{0.66} Si_{0.33}$ > $FeMnP_{0.66} Se_{0.33}$ > $FeMnP_{0.66} Sn_{0.33}$ > $FeMnP_{0.66} In_{0.33}$. From this, it can be deduced that $FeMnP_{0.66} Si_{0.33}$ is the stiffest among all the four materials that were studied.
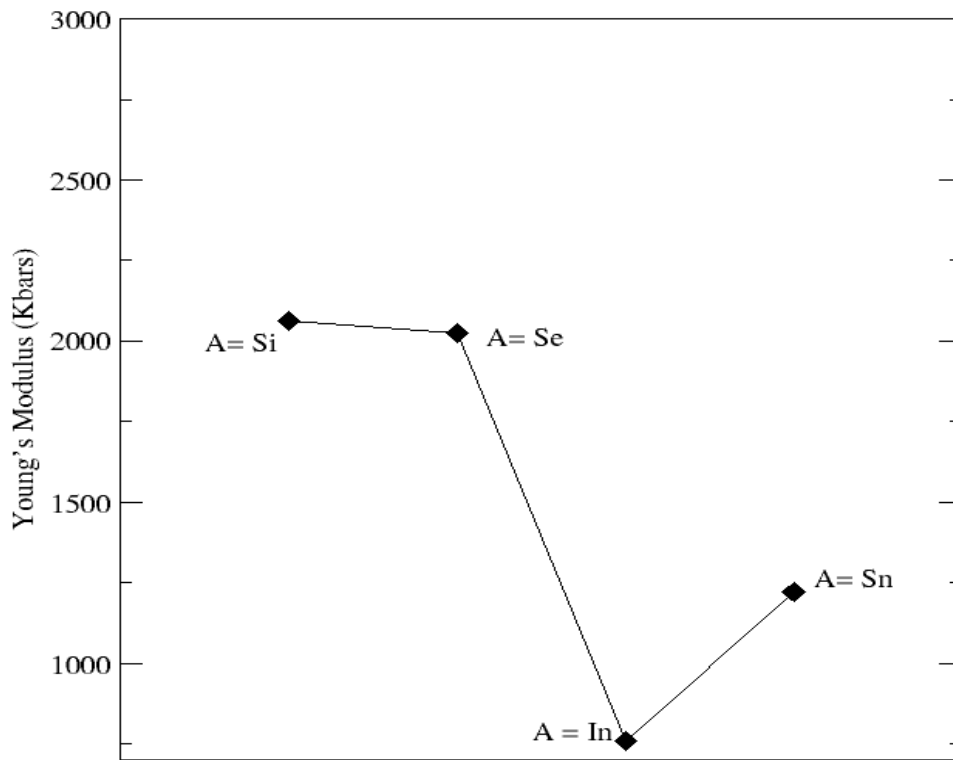
Figure 4. 7: The Young's Modulus (E) for the FM phase of $FeMnP_{1-x} A_x$ (A= Si, Se, In and Sn: x = 0.33)

The Pugh's ratios (B_H/G_H) of the selected materials in the FM phase.

Pugh's ratio indicates of how brittle or ductile a material is. The critical value for this ratio is given as 1.75 which separates these two conditions. A value below 1.75 signifies brittleness and a value above 1.75 points to ductility (Born & Lax, 1955). Considering this, the results in figure 4.8 show that the Pugh's ratios for all the four materials investigated are above the critical value. This,

therefore, implies that they are all ductile though FeMnP$_{0.66}$ In$_{0.33}$ has the highest value of the Pugh's ratio hence the most ductile of the four.
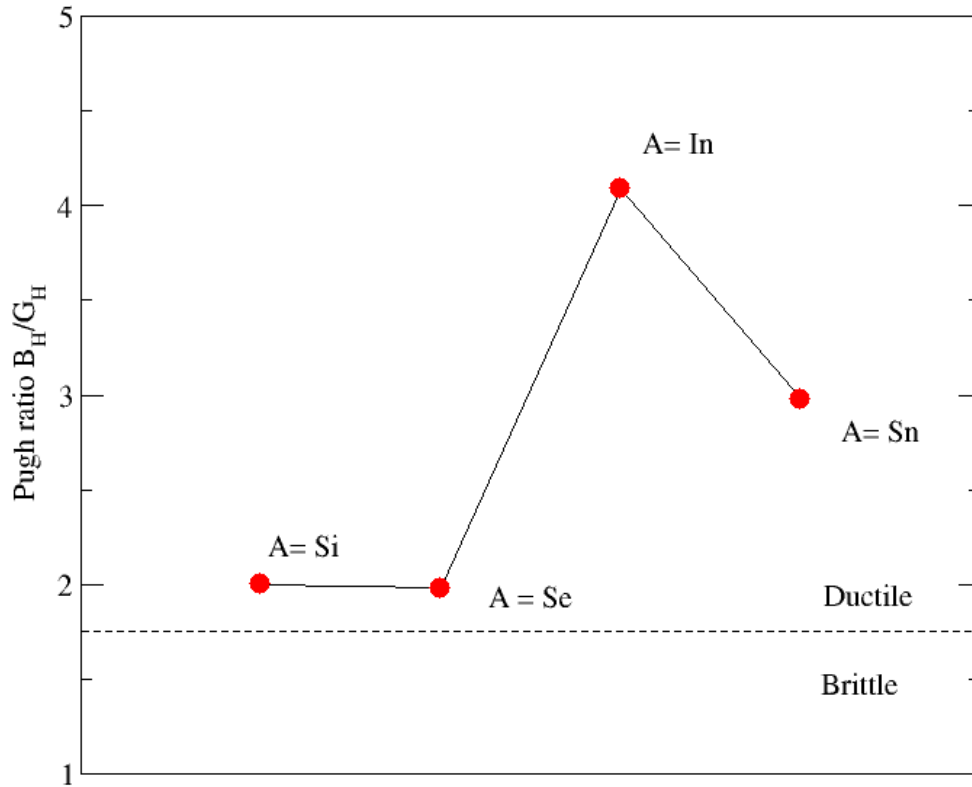
Figure 4. 8: The Voigt-Reuss-Hill average Pugh's ratio (BH/GH) for the FM phase of FeMnP$_{1-x}$A$_x$ (A= Si, Se, In and Sn: x = 0.33)

The Poisson's ratio *(v)* of the selected materials in the FM phase.

This is the most significant factor to be considered when choosing any material for stability sensitive applications in engineering. Poisson's ratio impacts on the dynamic stability of materials, affecting their ability to absorb and dissipate energy during vibrations. It is simply given by working out the ratio of the lateral strain to that of the longitudinal strain in the direction of the stretching force. The Poisson's ratio usually varies between 0 and 0.5 and has a critical value of 0.26 which also splits a ductile from a brittle material. From the data presented in figure 4.9, it can once again be concluded for FeMnP$_{0.66}$ In$_{0.33}$ that has the highest Poisson's ratio and is the most ductile of the four materials under study. An incompressible material is one that does not change volume as it is deforms when subjected to stress. A poisson ratio of 0.5 indicates a material that is perfectly incompressible. Again, from figure 4.9, it can be seen that of all the four materials the

Poisson's ration for FeMnP$_{0.66}$ In$_{0.33}$ is the closest to the value 0.5 which defines incompressibility of a material. This could indicate that its volume does not get deformed easily when subjected to stress.
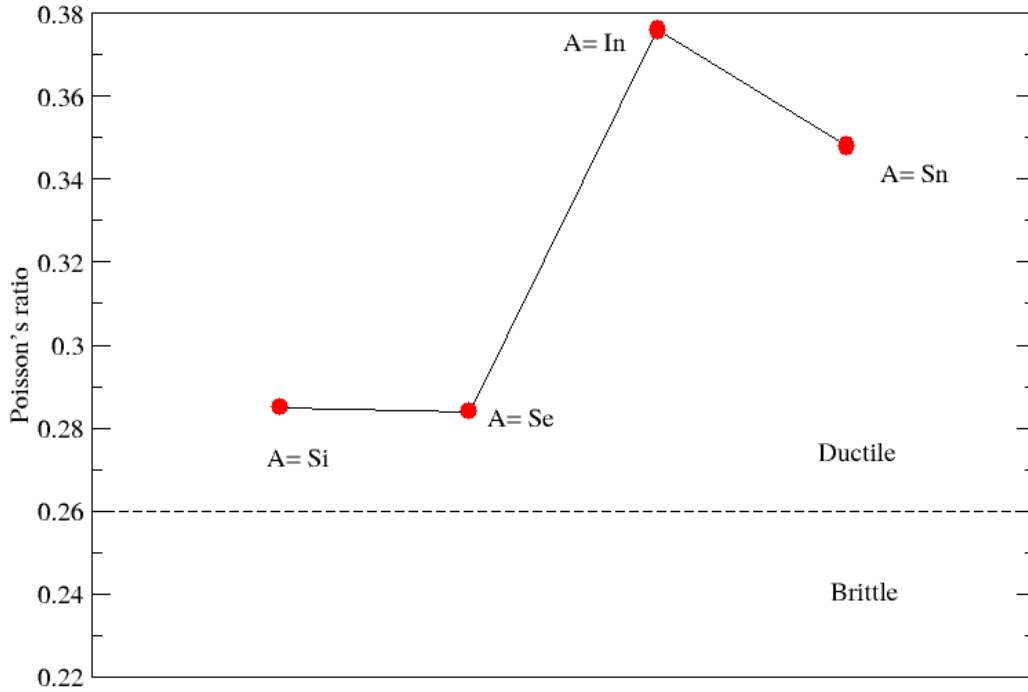
Figure 4. 9: The Poisson's ratio (ν) for the FM phase of FeMnP$_{1-x}$A$_x$ (A= Si, Se, In and Sn: x = 0.33)

To be noted also is that machinability, which is an important property depending on both the elastic constants and bulk modulus indicates how easily a material can be cut, is a critical factor to be considered when defining the usability of a material in practical devices. It is defined as the ratio of B_H to C$_{44}$ (Eraslan *et al*., 2021; Vitos, 2003). The machinability of the four compounds studied, that is, FeMnP$_{0.66}$ Si$_{0.33}$, FeMnP$_{0.66}$ Se$_{0.33}$, FeMnP$_{0.66}$ In0.$_{33}$ and FeMnP$_{0.66}$ Sn$_{0.33}$ are calculated to be 1.539, 1.836, 2.042 and 1.933 respectively. These results, therefore, show that of these four, FeMnP$_{0.66}$ In0.$_{33}$ has the highest value of this physical quantity hence the most usable.

Debye Temperature for the selected materials in FM phase.

This is a significant physical property of objects, being a consequent of the atomic thermal vibration of solids. It is not only characterised by the force of binding between atoms but also replicates the level of dynamic alteration of crystal lattice (Jiang *et al.*, 2019). It is closely connected to a number of physical properties of solids like thermal conductivity, enthalpy, entropy, specific heat, thermal expansion coefficient, elasticity, lattice stability, hardness and melting point. It is used to assemble elastic properties of materials with their thermodynamic properties and differentiate the regions of solids with low temperature from those with high temperatures. The elastic Debye temperature is directly proportionate to the average elastic velocity as shown in equation 4.7.

$$\theta_D = Kv_m \tag{4.7}$$

where

$$K = \frac{h}{k}\left(\frac{3}{4\pi V_a}\right)^{1/3} \tag{4.8}$$

and

$$v_m^{-3} = \frac{1}{3}\left(v_l^{-3} + 2v_t^{-3}\right) \tag{4.9}$$

From Equations (4.7), (4.8) and (4.9), h is the Planck's constant, k is the Boltzmann's constant, V_a is the atomic volume, v_m is the mean acoustic wave velocity, v_t is transverse sound velocity and v_l is the longitudinal sound velocity.

Table 4. 9: Compressional (V_P), bulk (V_B), shear (V_G), average Debye (V_D) sound velocities in m/s, solid density (ρ) in g/cm^3 and Debye temperature (θ_D) in Kelvin for the selected materials in the FM phase calculated by Voigt-Reuss-Hill average approximation.

Material	V_P	V_B	V_G	V_D (m/s)	ρ (g/cm^3)	θ_D (K)
FeMnP$_{0.66}$Si$_{0.33}$	6311.720	4887.980	3458.192	3842.893	6.722	505.262
FeMnP$_{0.66}$Se$_{0.33}$	5973.243	4618.011	3281.038	3655.369	7.241	476.259
FeMnP$_{0.66}$In$_{0.33}$	4592.462	3988.099	1972.139	2316.660	6.936	291.571
FeMnP$_{0.66}$Sn$_{0.33}$	5207.719	4328.740	2507.341	2810.643	6.989	354.424

The Debye temperatures for the following materials FeMnP$_{0.66}$ Si$_{0.33}$, FeMnP$_{0.66}$ Se$_{0.33}$, FeMnP$_{0.66}$ In$_{0.33}$ and FeMnP$_{0.66}$ Sn$_{0.33}$ were found to be 505.262K, 476.259K, 291.571K and 354.424K respectively as indicated in table 4.9. This study was unable to compare these results with any other since none was existing. Nonetheless, it can be easily seen that FeMnP$_{0.66}$ In$_{0.33}$ has the lowest Debye temperature while FeMnP$_{0.66}$ Si$_{0.33}$ has the highest Debye temperature implying that it has the highest interatomic bonding. This can be concluded from reported data of the Fe - A bond lengths on table 4.2, where A is the replacing atom. A careful analysis of the relationship between bond lengths and Debye temperature shows that a smaller bond length which corresponds to a higher interatomic bonding result to a higher Debye temperature and vice versa.

4.2.2 The Paramagnetic (PM) Phase.

The elastic constants of the selected materials in the PM phase.

The elastic stability of a hexagonal crystal structure is determined using the following elastic potential free energy equation,

$$\phi = \frac{1}{2}C_{ij}\varepsilon_i\varepsilon_j \qquad , \text{ where } \phi \geq 0 \tag{4.10}$$

Table 4. 10: Elastic constants in Kbar of the selected materials in the paramagnetic phase.

Material	C_{11}	C_{12}	C_{13}	C_{33}	C_{44}	C_{11}/C_{12}	$C_{11}C_{33}/C_{13}{}^2$
$FeMnP_{0.66}Si_{0.33}$	3231.103	1267.135	1077.012	3663.197	1193.429	2.549	10.204
$FeMnP_{0.66}Se_{0.33}$	3292.870	1544.886	1298.610	3715.531	1072.078	2.131	7.255
$FeMnP_{0.66}In_{0.33}$	1050.171	284.035	54.069	3165.190	248.747	3.697	11.370
$FeMnP_{0.66}Sn_{0.33}$	2310.627	1357.059	1152.515	2336.866	456.295	1.703	4.065

When $\phi = 0$, there is an equilibrium state and when $\phi > 0$, there is a state of mechanical deformation. This, therefore, requires that the principal minors of C_{ij} the matrix given by equation (4.10) must all be positive-definite. Table 4.10 presents results of elastic constants in Kbars for all the materials that had been investigated. Stability ratios shown in the last two columns of table 4.10 are all positive definite, from which it can be concluded that all the four components are elastically stable. Paramagnetic crystals of hexagonal class have 5 independent elastic constants namely C_{11}, C_{12}, C_{13}, C_{33}, and C_{44}. The calculated eigenvalues of the stiffness matrix from equation 4.10, lead to the following four basic conditions called the Born stability conditions for elastic stability of a hexagonal crystal: $C_{11} > 0$; $C_{11} > C_{12}$; $C_{44} > 0$; $(C_{11}+C_{12}) C_{33} > 2C_{13}{}^2$. From this table it can be noted that the values of elastic constants calculated satisfy the four conditions stated above. This therefore shows that four compounds investigated in this work are elastically stable in their paramagnetic state.

The elastic anisotropy of the selected materials in the PM phase.

The elastic anisotropy, denoted by the symbol A, is a property, easily seen in compounds or single crystals of solid elements where atoms, ions or molecules are arranged in regular lattice. This physical property is used to determine how the elastic properties of materials behave towards the direction of the force acting on a unit area of the said material (Sun *et al.*, 2004). For a material to be anisotropic, it displays properties with different values when measurements are taken along axes in different directions. Hexagonal crystals in their paramagnetic phase also have three shear-type anisotropy ratios defined in terms of the elastic constants by equations (4.4), (4.5) and (4.6).

The shear-type anisotropy ratios derived from C_{ij} values in table 4.10 using the three equations are given in the table 4.11.

Table 4. 11: Shear type anisotropic ratios for the selected materials in the paramagnetic phase.

Material	A₁	A₂	A₃
$FeMnP_{0.66}Si_{0.33}$	0.538	1.215	0.654
$FeMnP_{0.66}Se_{0.33}$	0.522	1.227	0.640
$FeMnP_{0.66}In_{0.33}$	2.870	0.649	1.863
$FeMnP_{0.66}Sn_{0.33}$	0.509	0.957	0.487

A crystal is said to be isotropic. When the elastic anisotropy ratio A=1, Otherwise, values of A which are less than or greater than 1 indicate anisotropy. The calculated shear anisotropic factors for the studied compounds in the paramagnetic phase are listed in table 4.11. From these values it can be easily observed that all the materials under consideration are elastically anisotropic since the anisotropic values A_1, A_2 and A_3 are all not equal to 1. In terms of stability, an anisotropic ratio not equal to one could imply a more uniform response of a given material to external forces, potentially contributing to better overall stability of the said material. It should be however noted that the elastic stability of a material is influenced by a combination of factors beyond just the anisotropic ratio and so this result alone cannot fully confirm the elastic stability of the compounds that were investigated. Further, when $C_{33} > C_{11}$, the compounds are more incompressible along the C-direction than along the A-direction. The results on table 4.10, confirm this condition for all the materials studies indicating that they are all incompressible along the C-direction than the A-direction.

Figures 4.10, 4.11, 4.12, 4.13 and 4.14 and appendix II present the results for the calculations of, Bulk modulus 'B' and Shear Modulus 'G' Young modulus 'E', Pugh's ratio 'B_H/G_H' and the Poisson ratios 'ν' under Voigt and Reuss approximations as well as Voigt-Reuss-Hill average of the two approximations.

The Bulk modulus (incompressibility) of the selected materials in the PM Phase.

The bulk modulus is a key parameter that helps determine how a material responds to compressive forces and how stable it is under different conditions. Materials with higher bulk moduli are generally more stable and resistant to volume changes and structural shifts, making this property crucial in various scientific, engineering, and industrial applications. From figure 4.10, it is observed that $FeMnP_{0.66}In_{0.33}$ has the highest value of bulk modulus while $FeMnP_{0.66}Sn_{0.33}$ has the lowest value of bulk modulus. The results clearly demonstrate that, of the four materials investigated in this work, $FeMnP_{0.66}In_{0.33}$ is the stiffest and more resistant to changes in volume when subjected to compressional forces. This means that it is mechanically more stable and will most likely maintain its shape and structure when subjected to external pressure.
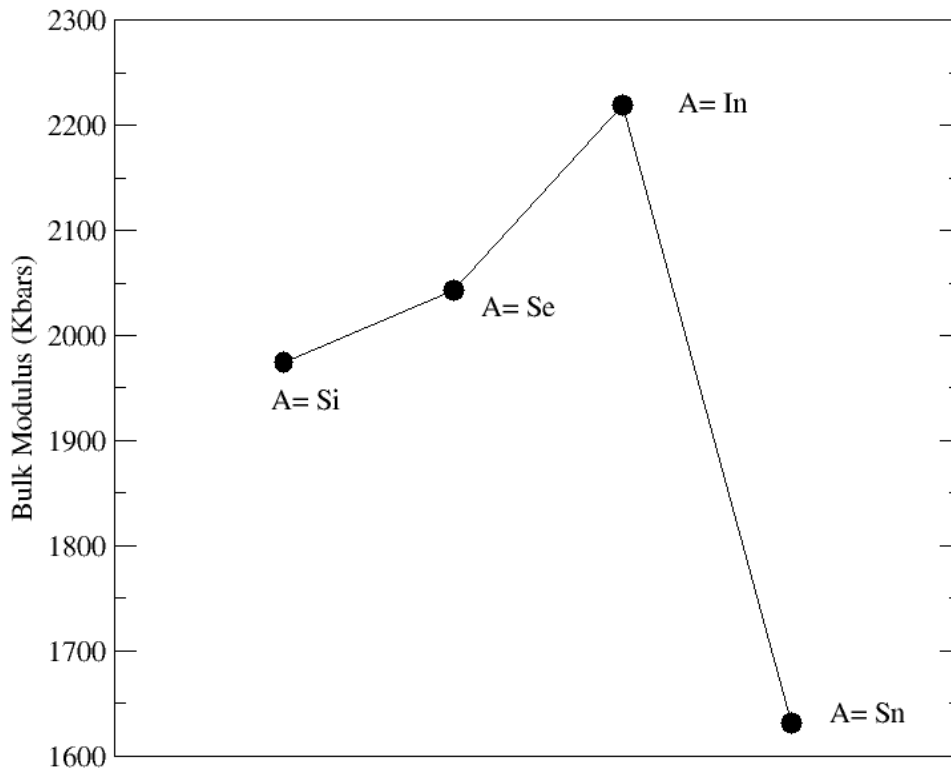
Figure 4. 10: The Bulk Modulus (B_H) for the PM phase of $FeMnP_{1-x}A_x$ (A= Si, Se, Sn, In, x = 0.33).

The Shear Modulus of the selected materials in the PM phase.

Understanding the shear modulus is important for analysing a material's response to forces applied perpendicular to its longitudinal axis, such as when cutting, bending, or twisting a material.

The shear modulus, also known as the modulus of rigidity or elastic modulus, is a material property that describes how a material responds to shear deformation. Shear deformation involves the sliding of adjacent layers of a material parallel to each other. This physical property plays a very significant role in helping scientists and researchers understand the stability of materials, particularly in situations involving shear forces.

The calculated results of shear modulus are presented in figure 4.11. Of the 4 compounds studied, $FeMnP_{0.66} In_{0.33}$ has the largest value of the modulus of rigidity hence, the strongest capacity to resist plastic deformation. Materials with higher shear moduli are generally more stable and less prone to shear-related deformations, making them suitable for applications requiring structural integrity and resistance to shearing forces.
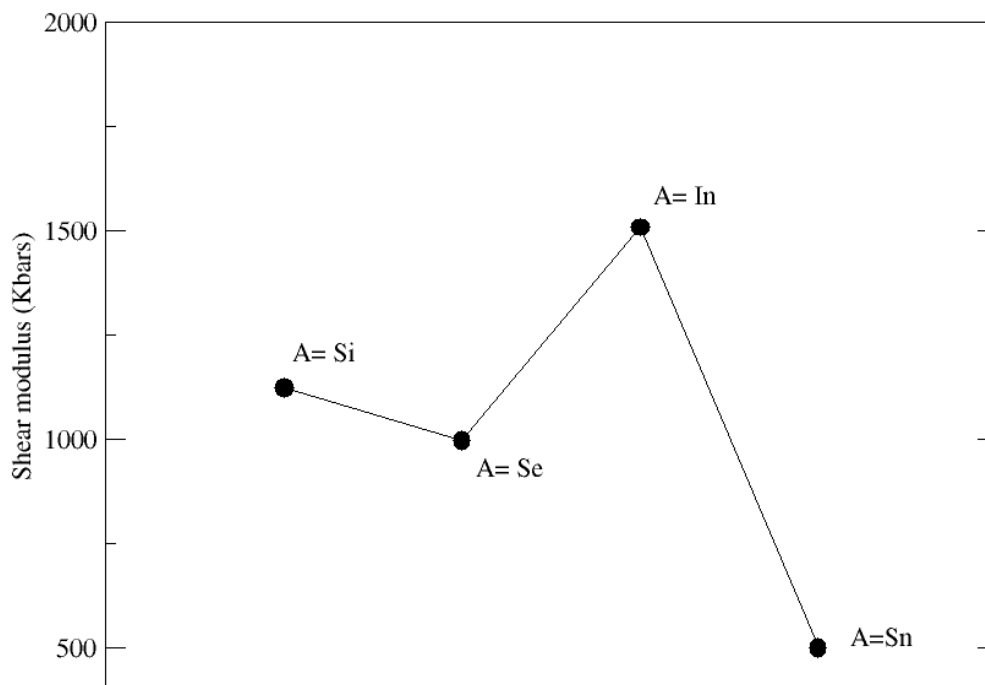
Figure 4. 11: Shear Modulus (GH) for the PM phase of $FeMnP_{1-x} A_x$ (A= Si, Se, Sn, In, x = 0.33).

The Young's modulus (E) of the selected materials in PM Phase.

Young's modulus is a measure of a material's stiffness or rigidity. It describes how much a material will deform under a given load and provides insights into its ability to recover its original shape after the load is removed. Understanding Young's modulus is important for predicting how materials will behave under tensile or compressive forces and for ensuring the stability of

structures and components. It is obtained when longitudinal stress is divided by strain, and the larger the ratio, the stiffer the material (Naumov *et al.,* 2020). From Figure 4.12, it is observed that the E values decrease in order: $FeMnP_{0.66} In_{0.33} > FeMnP_{0.66} Si_{0.33} > FeMnP_{0.66} Se_{0.33} > FeMnP_{0.66} Sn_{0.33}$. It can be deduced that $FeMnP_{0.66} In_{0.33}$ is the stiffest of all the four materials studied. Materials with higher Young's moduli are generally more stable, exhibit less deformation under applied loads, and are better suited for applications requiring structural stability and resistance to deformation.
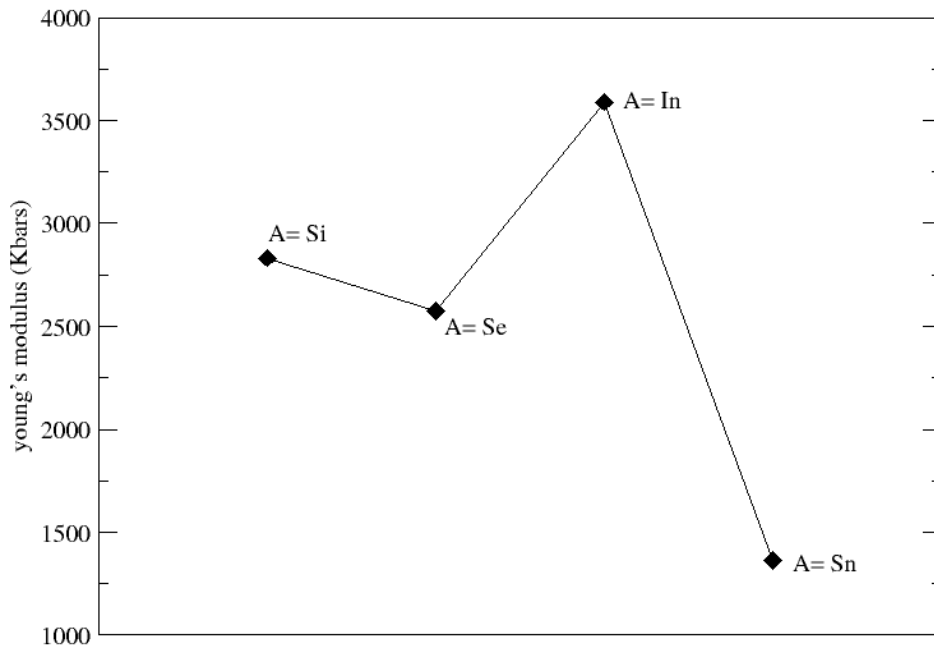
Figure 4. 12*:* Young's Modulus (E) for the PM phase of $FeMnP_{1-x} A_x$ (A= Si, Se, Sn, In, x = 0.33)

The Pugh's ratio of the selected materials in the PM phase.

Pugh's ratio is a powerful tool for assessing stability, especially when multiple candidate materials are being evaluated for a given application. It is also known as the "Material Index" or "Pugh's Criterion," and is a method used to compare and select materials for specific engineering applications based on their physical and mechanical properties. This ratio measures how ductile or brittle a material is and has critical value of 1.75 which separates the two conditions. A value of less than 1.75 represents brittleness and a value above 1.75 indicates ductility (Born & Lax, 1955).

Considering this, the results in figure 4.13 shows that the Pugh's ratios for the three of the four materials studied are above the critical value. This therefore implies that they are ductile. However, for $FeMnP_{0.66}In_{0.33}$ the material index falls below the critical value hence its brittle. Machinability, which is an important property depending on both the elastic constants and bulk modulus indicates how easily a material can be cut. It is the ratio of B_H to C_{44} (Eraslan *et al.*, 2021; Vitos, 2003). The machinability of the four compounds studied, that is, $FeMnP_{0.66}Si_{0.33}$, $FeMnP_{0.66}Se_{0.33}$, $FeMnP_{0.66}In0_{.33}$ and $FeMnP_{0.66}Sn_{0.33}$ are 1.655, 1.906, 8.923 and 3.574 respectively.

The results therefore show that $FeMnP_{0.66}Si_{0.33}$ has the least machinability and $FeMnP_{0.66}In_{0.33}$ has the highest value of machinability hence the best to use in practical magnetocaloric devices applications.
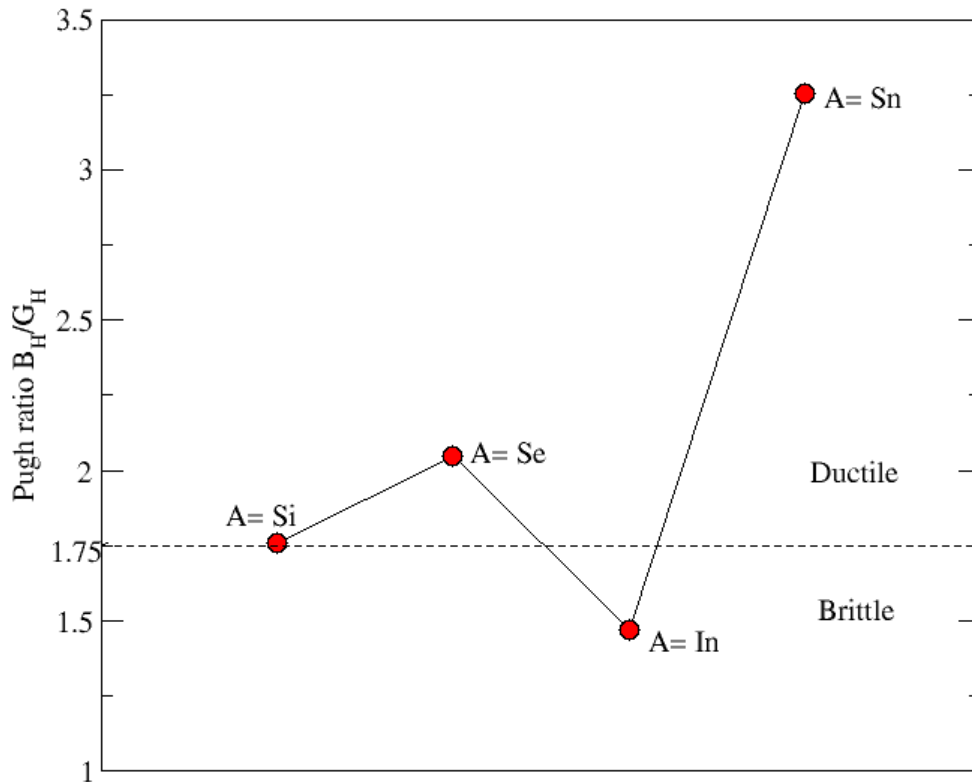
Figure 4. 13: Pugh's ratio (B_H/G_H) for PM phase of $FeMnP_{1-x}A_x$ (A= Si, Se, Sn, In, x = 0.33).

The Poisson's ratio of the selected materials in the PM phase.

This is the most important factor to be considered when selecting any material for use in stability sensitive devices. Materials with low Poisson's ratios are less likely to undergo large volume changes, contributing to stability in applications where volume conservation is important.

It is calculated by getting the ratio of the lateral strain to that of the longitudinal strain in the direction of the stretching force. The ratio usually varies between 0 and 0.5. A material that has a Poisson ratio of 0.5 is perfectly incompressible in that it does not change volume as it is deforms when subjected to stress. Figure 4.14 presents the results of this ratio for the selected materials under study. It can be noted that three of these materials are ductile. The Poisson's ratio for FeMnP$_{0.66}$ In$_{0.33}$ is below the critical value of 0.26 also implying that it is less likely to undergo large volume changes in the PM phase and the best in magnetocaloric applications since volume conservation is important.
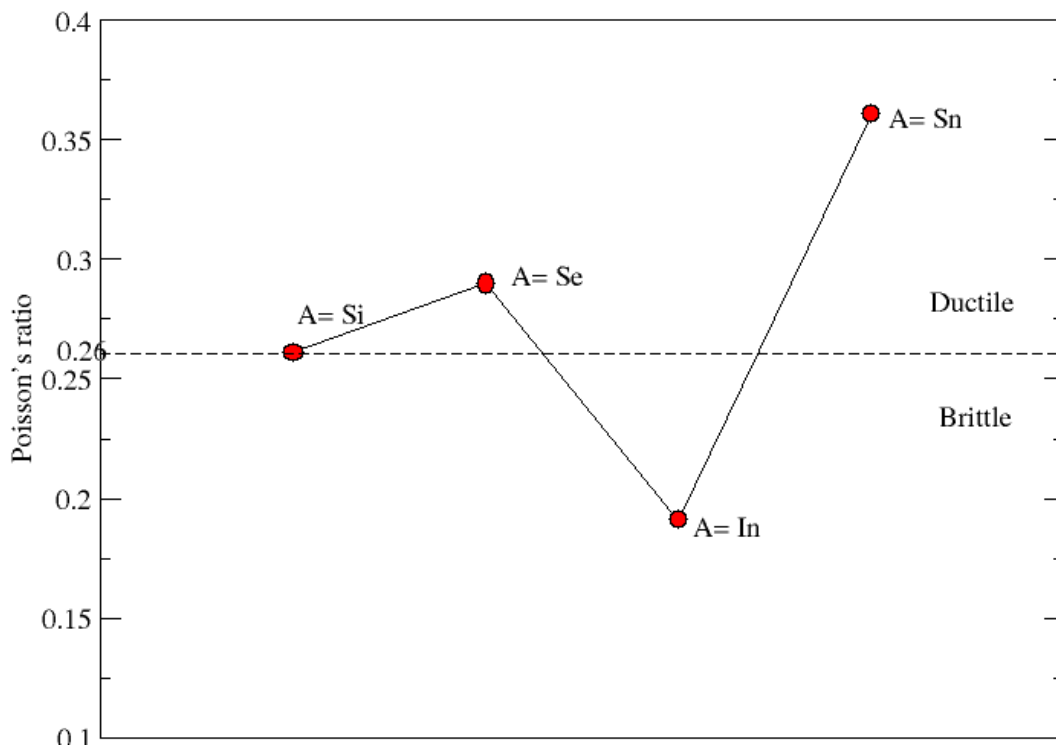
Figure 4. 14: Poisson's ratio (ν) for the PM phase of FeMnP$_{1-x}$ A$_x$ (A= Si, Se, Sn, In, x = 0.33)

The Debye Temperature of the selected materials in the PM phase.

Debye temperature is a key parameter that characterises the vibrational behaviour of atoms in a crystalline material. It provides insights into the stability, thermal properties, and phase behaviour of materials, especially at low temperatures. Materials with higher Debye temperatures may exhibit different stability and behaviour compared to those with lower Debye temperatures, influencing their suitability for various applications (Jiang *et al.*, 2019). It is also closely linked to a number of other physical properties of solids like expansion coefficient, elasticity, hardness,

specific heat and melting point. It is used to differentiate the regions of solids with low temperatures from those with high temperature and is directly proportional to the average elastic mean acoustic wave velocity. The Debye temperature has important implications on the stability and behaviour of materials, especially at low temperatures. At temperatures much lower than the Debye temperature, the lattice vibrations or phonons are frozen out, and the material is said to be more stable thermally. This is because the thermal energy is insufficient to excite higher vibrational modes. The Debye temperatures for the following materials $FeMnP_{0.66}Si_{0.33}$, $FeMnP_{0.66}Se_{0.33}$, $FeMnP_{0.66}In_{0.33}$ and $FeMnP_{0.66}Sn_{0.33}$ were found to be 592.936 K, 531.577K, 129.864K and 370.878K respectively as indicated in table 4.12. This study was unable to compare these results with any other since none was existing. Nonetheless, it can be easily seen that $FeMnP_{0.66}In_{0.33}$ has the lowest Debye temperature while $FeMnP_{0.66}Si_{0.33}$ has the highest Debye temperature implying that it has the highest interatomic bonding. This can be concluded from reported data of the Fe - A bond lengths on table 4.6, where A is the replacing atom. A careful analysis of the relationship between bond lengths and Debye temperature shows that a smaller bond length which corresponds to a higher interatomic bonding result to a higher Debye temperature and vice versa. The Debye temperature can also affect the thermal conductivity of materials, especially at low temperatures. Higher Debye temperatures are generally associated with higher thermal conductivities.

Table 4. 12: Compressional (V_P), bulk (V_B), shear (V_G), average Debye (VD) sound velocities in m/s, solid density (ρ) in g/cm3 and Debye temperature (θD) in Kelvin calculated by Voigt-Reuss-Hill average of the selected materials in the AFM phase.

Material	V_P	V_B	V_G	V_D	ρ (g/cm^3)	θ_D
$FeMnP_{0.66}Si_{0.33}$	7032.425	5303.524	3999.466	4442.769	7.020	592.936
$FeMnP_{0.66}Se_{0.33}$	6636.614	5165.235	3608.842	4018.553	7.654	531.577
$FeMnP_{0.66}In_{0.33}$	7494.356	5429.140	4474.076	1011.613	7.533	129.864
$FeMnP_{0.66}Sn_{0.33}$	5494.501	4627.775	2565.137	2885.626	7.622	370.878

4.2.3 The Antiferromagnetic (AFM) Phase

The elastic constants of the selected materials in the AFM Phase.

Elastic constants play a significant role in determining the material's stability and mechanical behaviour for hexagonal crystal structures, such as those found in many metals. These are parameters that quantify how a material deforms in response to external forces or stresses. As already stated earlier, crystals of hexagonal class have 5 independent elastic constants namely C_{11}, C_{12}, C_{13}, C_{33}, and C_{44}. C_{11} and C_{22} are classified as longitudinal Moduli because they describe a material's response to axial or longitudinal stress. They represent the stiffness of the crystal lattice along its primary symmetry axis usually the c-axis in hexagonal structures. C_{33} also called the transverse Modulus is a constant that describes constant the material's response to transverse or lateral stress applied perpendicular to the c-axis. It characterises the stiffness of the crystal lattice in directions perpendicular to the primary symmetry axis. C_{44} also known as the Shear modulus represents the material's response to shear stress. It shows the resistance of the crystal lattice to shearing forces applied in a plane parallel to the basal plane of the hexagonal lattice.

Table 4. 13: The elastic constants in kbar for the selected materials in the AFM phase.

Material	C_{11}	C_{12}	C_{13}	C_{33}	C_{44}	C_{11}/C_{12}	$C_{11}C_{33}/C_{13}^2$
$FeMnP_{0.66}Si_{0.33}$	2477.565	543.896	873.266	2881.824	1091.107	4.555	9.363
$FeMnP_{0.66}Se_{0.33}$	2408.314	692.159	851.398	2304.452	913.212	3.479	7.656
$FeMnP_{0.66}In_{0.33}$	1676.609	1058.386	1064.599	1908.160	436.386	1.584	2.823
$FeMnP_{0.66}Sn_{0.33}$	2018.745	1064.013	1143.492	2092.920	566.362	1.897	3.231

The calculated eigenvalues of the stiffness matrix from equation 4.10, lead to the four basic conditions called the Born stability conditions for elastic stability of a hexagonal crystal in the antiferromagnetic phase. These are described in equations 4.3. Table 4.13 presents the results for elastic constants of the selected materials in the AFM phase. From this table it can be seen that the values of elastic constants calculated satisfy these four conditions for elastic stability. This therefore shows that four compounds investigated in this work are also elastically stable in this

state. The last two columns of these table also confirm the elastic stability of these materials owing to the fact that these stability ratios are greater than one for all the materials.

The elastic anisotropy of the selected materials in the AFM phase.

Elastic anisotropy refers to the property of a material where its mechanical properties, such as stiffness or Young's modulus, vary significantly with direction within the material's crystal structure. In other words, the material's response to applied stress differs depending on the direction of the stress relative to the crystallographic axes. Elastic anisotropy has important implications for the stability and behaviour of materials. This is because it affects how a material responds to external loads and influences its mechanical performance in different directions (Sun *et al*., 2004). Equations 4.4, 4.5 and 4.6 define the shear type anisotropy ratios for the hexagonal crystals.

The shear-type anisotropy ratios derived from these 3 equations for the antiferromagnetic phase of the investigated materials are given in table 4.14.

Table 4. 14*: Shear type anisotropic ratios for the selected materials in AFM phase.*

Material	A_1	A_2	A_3
$FeMnP_{0.66}Si_{0.33}$	0.368	1.128	0.415
$FeMnP_{0.66}Se_{0.33}$	0.383	1.064	0.408
$FeMnP_{0.66}In_{0.33}$	0.147	1.412	0.208
$FeMnP_{0.66}Sn_{0.33}$	0.177	1.186	0.210

The calculated shear anisotropic factors for the studied compounds in the antiferromagnetic phase are listed in table 4.14. From these values it can be easily observed that all the materials under consideration are elastically anisotropic since the anisotropic values A_1, A_2 and A_3 are all not equal to 1. In terms of stability, an anisotropic ratio not equal to one could imply a more uniform response of a given material to external forces, potentially contributing to better overall stability of the said material. It should be however noted that the elastic stability of a material is

influenced by a combination of factors beyond just the anisotropic ratio and so this result alone cannot fully confirm the elastic stability of the compounds that were investigated. Further, when $C_{33} > C_{11}$, the compounds are more incompressible along the C-direction than along the A-direction. The results on table 4.13, confirm this condition for $FeMnP_{0.66}Si_{0.33}$, $FeMnP_{0.66}In_{0.33}$ and $FeMnP_{0.66}Sn_{0.33}$ indicating that these 3 are incompressible along the C-direction than the A-direction.

Results of the calculations of the bulk modulus 'B' and shear Modulus 'G' Young modulus 'E', Pugh's ratio 'B_H/G_H' and the Poisson ratios 'v' under Voigt and Reuss approximations as well as Voigt-Reuss-Hill average of the two approximations are presented in appendix II, figures 4.15, figure 4.16, figure 4.17, figure 4.18 and figure 4.19.

The bulk modulus of the selected materials in the AFM phase.

Figure 4.15 presents the results of the bulk modulus of $FeMnP_{0.66}Si_{0.33}$, $FeMnP_{0.66}Se_{0.33}$, $FeMnP_{0.66}In_{0.33}$ and $FeMnP_{0.66}Sn_{0.33}$. From this figure it can be observed that $FeMnP_{0.66}Si_{0.33}$ has the highest value of bulk modulus while $FeMnP_{0.66}In_{0.33}$ has the lowest value of bulk modulus.
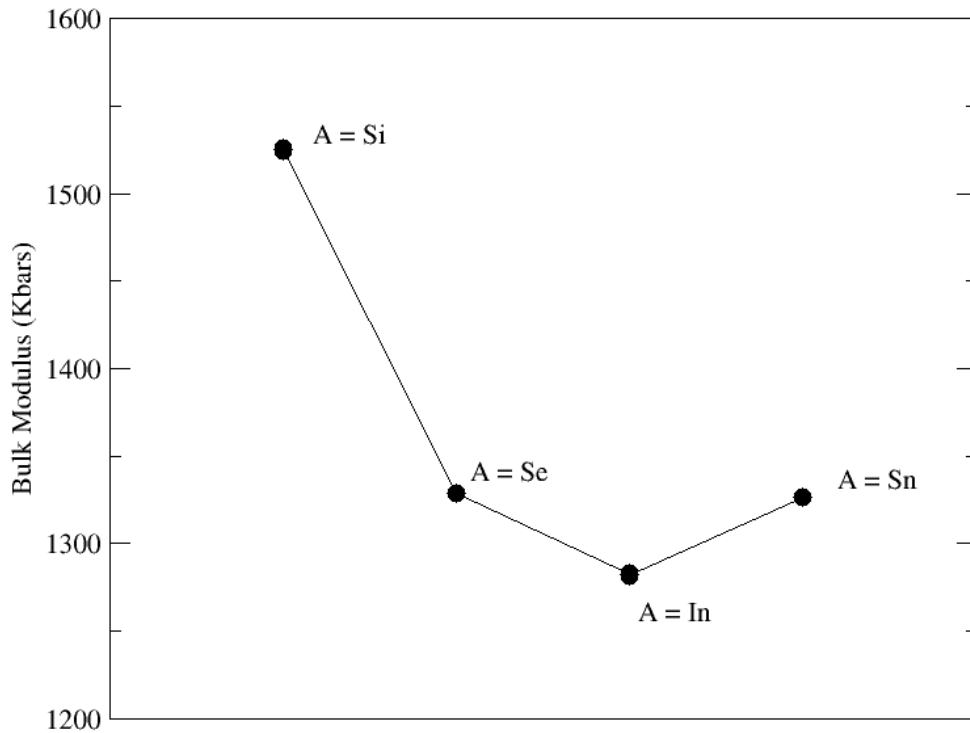
Figure 4. 15: Bulk Modulus (B_H) for the AFM phase of $FeMnP_{1-x}A_x$ (A= Si, Se, Sn, In, x = 0.33)

The bulk modulus is a key parameter that helps determine how a material responds to compressive forces and how stable it is under different conditions. Materials with higher bulk moduli are generally more stable and resistant to volume changes and structural shifts, making this property crucial in various scientific, engineering, and industrial applications. From figure 4.10, it is observed that $FeMnP_{0.66}Si_{0.33}$ has the highest value of bulk modulus while $FeMnP_{0.66}In_{0.33}$ has the lowest value of bulk modulus. The results clearly demonstrate that in the antiferromagnetic phase, of the four materials investigated in this work, $FeMnP_{0.66}Si_{0.33}$ is the stiffest and more resistant to changes in volume when subjected to compressional forces. This means that it is mechanically more stable and will most likely maintain its shape and structure when subjected to external pressure. $FeMnP_{0.66}Se_{0.33}$ and $FeMnP_{0.66}Sn_{0.33}$ have almost similar values of the bulk modulus and this can be attributed to their bonding characteristics being similar.

The Shear Modulus of the selected materials in the AFM phase.

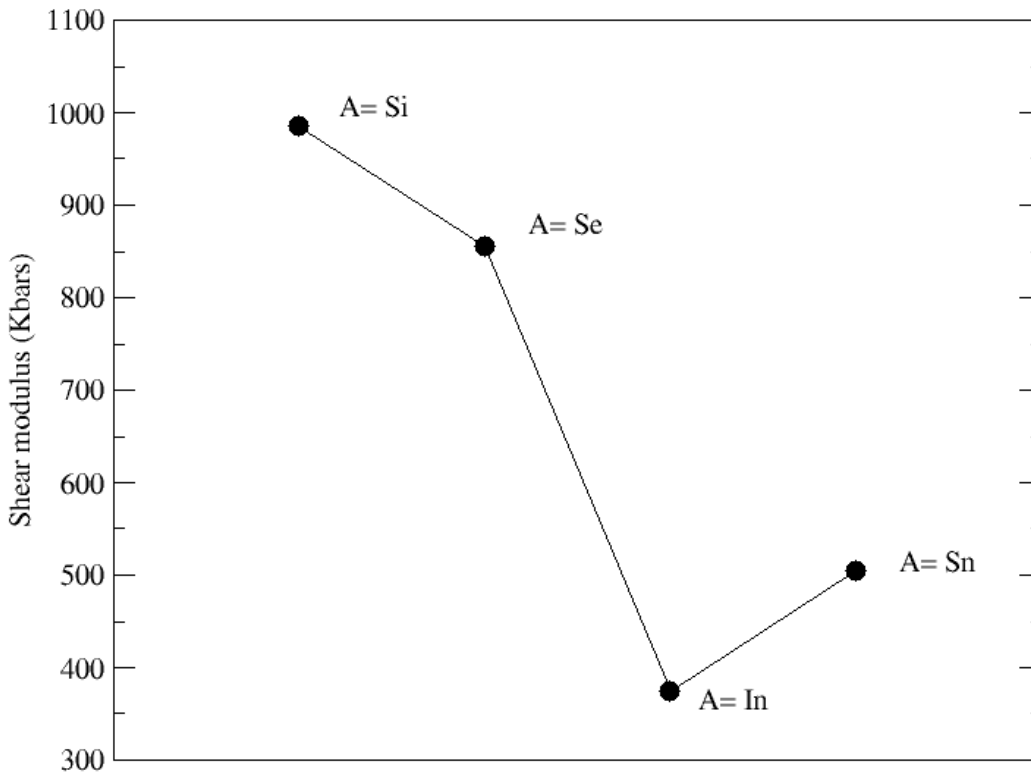**Figure 4.16:** Shear Modulus (G_H) for the AFM phase of $FeMnP_{1-x}A_x$ (A= Si, Se, Sn, In, x = 0.33)

The calculated results of shear modulus of the selected materials in the antiferromagnetic phase are presented in figure 4.16. Of the 4 compounds studied, $FeMnP_{0.66}In_{0.33}$ has the smallest value

of the modulus of rigidity hence, a lower capacity to resist plastic deformation in this phase. Materials with higher shear moduli are generally more stable and less prone to shear-related deformations, making them more suitable for applications requiring structural integrity and resistance to shearing forces.

Understanding the shear modulus is important for analysing a material's response to forces applied perpendicular to its longitudinal axis, such as when cutting, bending, or twisting a material. The shear modulus, also known as the modulus of rigidity or elastic modulus, is a material property that describes how a material responds to shear deformation. Shear deformation involves the sliding of adjacent layers of a material parallel to each other. This physical property plays a very significant role in helping scientists and researchers understand the stability of materials, particularly in situations involving shear forces. From these results, it can be further noted that in applications requiring twisting and turning, $FeMnP_{0.66}In0._{33}$ would be the most favourable.

The Young's modulus (E) of the selected materials in the AFM phase.

The results of the calculations of the Youngs modulus of the investigated materials in the antiferromagnetic face are presented in figure 4.17. This is a ratio that measures the tensile elasticity of a material. That is, a measure of the ability of a material to withstand variations in length when subjected to compression or lengthwise tension. To obtain this ratio, the longitudinal stress is divided by the longitudinal strain and it is used to indicate how stiff a material is. The larger the ratio, the stiffer the material and vice versa (Naumov *et al.,* 2020).

From Figure 4.17, it can be observed that the E values decrease in order: $FeMnP_{0.66}Si_{0.33} >$ $FeMnP_{0.66}Se_{0.33} > FeMnP_{0.66}Sn_{0.33} > FeMnP_{0.66}In_{0.33}$. This observation shows in the antiferromagnetic phase, $FeMnP_{0.66}Si_{0.33}$ is the stiffest of all the four materials studied. Materials with higher Young's moduli are generally more stable, exhibit less deformation under applied loads, and are better suited for practical applications in devices requiring structural stability and resistance to deformation. This suggests that the presence of indium atom in the solid makes it easy to deform the solid when tensile stress is applied. It is further noted that indium is the largest atom out of the four and thus its size could be a contributing factor to this observation.
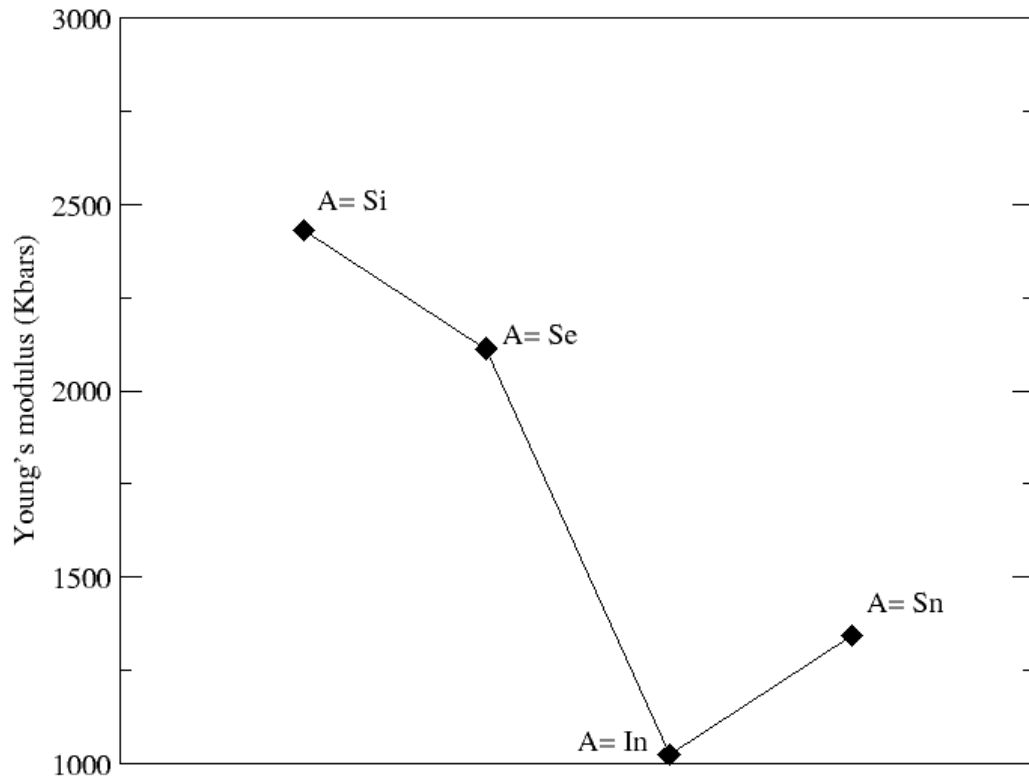
Figure 4. 17: Young Modulus (E) for the AFM phase of $FeMnP_{1-x} A_x$ (A= Si, Se, Sn, In, x = 0.33)

The Pugh's ratio of the selected materials in the AFM phase.

Figure 4.18 presents the results of the DFT calculations of the Pugh's ratio. This ratio is a powerful tool for assessing stability, especially when multiple candidate materials are being evaluated for a given application. It is a method used to compare and select materials for specific engineering applications based on their physical and mechanical properties. This ratio also measures how ductile or brittle a material is and has critical value of 1.75 which separates the two conditions. A value of less than 1.75 represents brittleness and a value above 1.75 indicates ductility (Born & Lax, 1955). Considering this, the results in figure 4.18 shows that the Pugh's ratios for $FeMnP_{0.66} Sn_{0.33}$ and $FeMnP_{0.66} In_{0.33}$ are above this critical value. This therefore implies that they are ductile. However, for $FeMnP_{0.66} Si_{0.33}$ $FeMnP_{0.66} Se_{0.33}$, the material index falls below the critical value and hence they are brittle.
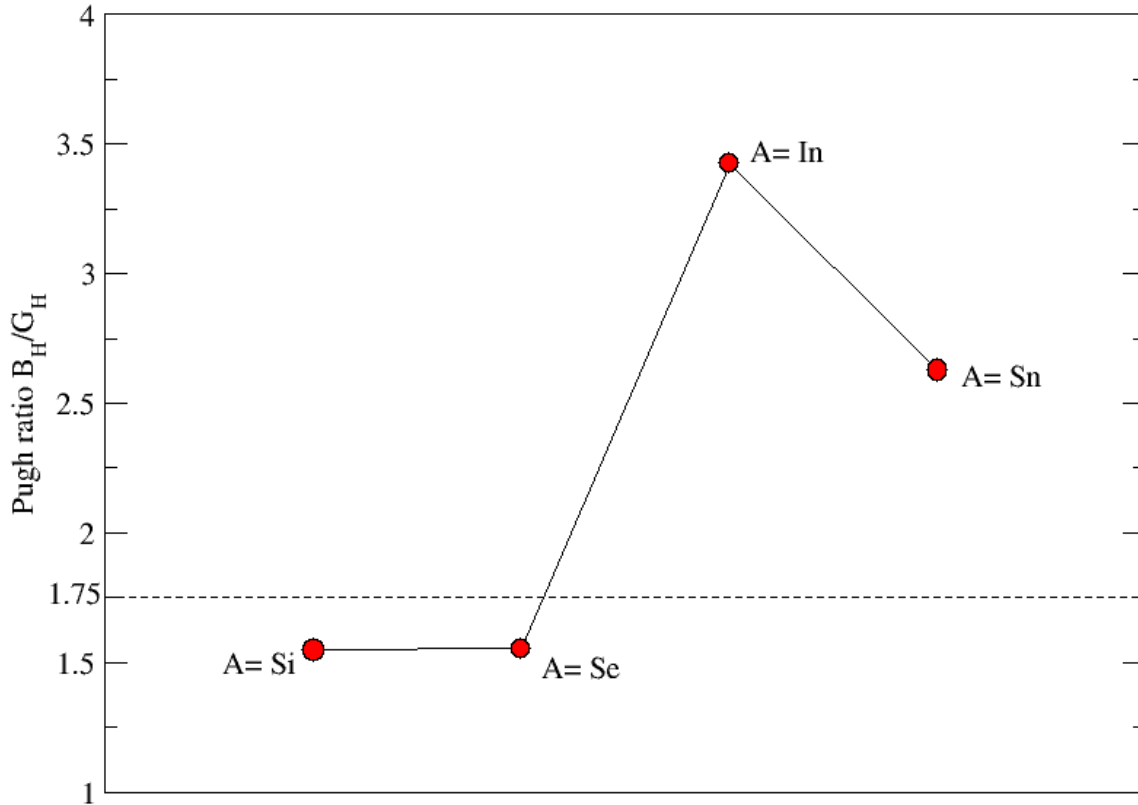
Figure 4. 18: Pugh's ratio (B_H/G_H) for the AFM phase of FeMnP$_{1-x}$A$_x$ (A= Si, Se, Sn, In, x = 0.33)

Machinability, which is an important property depending on both the elastic constants and bulk modulus indicates how easily a material can be cut. It is the ratio of B_H to C_{44} (Eraslan *et al.*, 2021; Vitos, 2003). The machinability of the four compounds studied, that is, FeMnP$_{0.66}$Si$_{0.33}$, FeMnP$_{0.66}$Se$_{0.33}$, FeMnP$_{0.66}$In0$_{.33}$ and FeMnP$_{0.66}$Sn$_{0.33}$ are 1.398, 1.455, 2.938 and 2.342 respectively. The results, therefore, show that both FeMnP$_{0.66}$In0$_{.33}$ and FeMnP$_{0.66}$Sn$_{0.33}$ have good machinability in the antiferromagnetic phase compared to the other two.

The Poisson's ratio of the selected materials in the AFM phase.
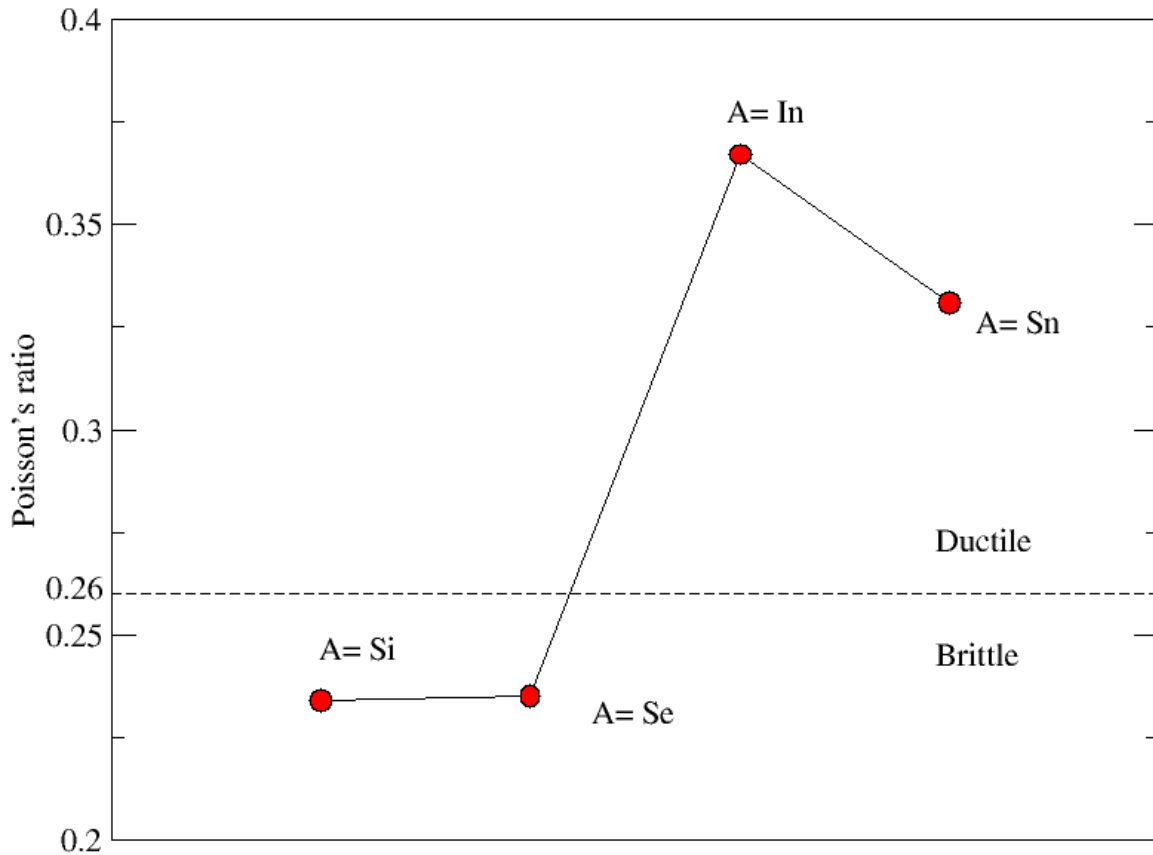
Figure 4. 19: Poisson's ratio (v) for the AFM phase of $FeMnP_{1-x}A_x$ (A= Si, Se, Sn, In, x = 0.33)

The results of the density functional theory of the calculations of the Poisson's ratio are shown in figure 4.19. This is the most important factor to be considered when selecting any material for use in stability sensitive devices. Materials with low Poisson's ratios are less likely to undergo large volume changes, contributing to stability in applications where volume conservation is important. It is calculated by getting the ratio of the lateral strain to that of the longitudinal strain in the direction of the stretching force. The ratio usually varies between 0 and 0.5. A material that has a Poisson ratio of 0.5 is perfectly incompressible in that it does not change volume as it deforms when subjected to stress.

A critical value of 0.26 separates a ductile material from a brittle material in that above this value materials are said to be ductile and below this value materials are said to be brittle. It can be noted that $FeMnP_{0.66}In_{0.33}$ and $FeMnP_{0.66}Sn_{0.33}$ are ductile whereas, $FeMnP_{0.66}Si_{0.33}$, $FeMnP_{0.66}Se_{0.33}$, are brittle. Materials with Poisson's ratio below the critical value of 0.26 also

imply that they are less likely to undergo large volume changes and therefore best in magnetocaloric applications since volume conservation is important. $FeMnP_{0.66}$ $In0._{33}$ is more suitable in applications requiring a significant amount of plastic deformation or extension along the direction of applied stress owing to its high value of Poisson's ratio.

The Debye Temperature of the selected materials in the AFM phase.

Column 6 of table 4.15 presents the results of the antiferromagnetic phase Debye temperature calculations for the selected materials by thermo PW interfaced with quantum espresso. This temperature provides insights into the stability, thermal properties, and phase behaviour of materials, especially at low temperatures. Materials with higher Debye temperatures may exhibit different stability and behaviour compared to those with lower Debye temperatures, influencing their suitability for various applications in practical devices. At temperatures much lower than the Debye temperature, the lattice vibrations or phonons are frozen out, and the material is said to be more stable thermally. This is because the thermal energy is insufficient to excite higher vibrational modes.

Table 4. 15: Compressional (V_P), bulk (V_B), shear (V_G), average Debye (VD) sound velocities in m/s, solid density (ρ) in g/cm3 and Debye temperature (θD) in Kelvin calculated by Voigt-Reuss-Hill average for the selected materials in AFM phase.

Material	V_P	V_B	V_G	V_D	ρ (g/cm^3)	θ_D
$FeMnP_{0.66}Si_{0.33}$	6487.682	4755.963	3821.404	4230.174	6.749	557.028
$FeMnP_{0.66}Se_{0.33}$	5806.168	4258.889	3417.615	3785.178	7.306	493.327
$FeMnP_{0.66}In_{0.33}$	5001.253	4243.000	2292.839	2576.545	7.142	324.677
$FeMnP_{0.66}Sn_{0.33}$	5265.187	4288.786	2645.068	2963.327	7.223	374.000

The Debye temperatures for the following materials $FeMnP_{0.66}$ $Si_{0.33}$, $FeMnP_{0.66}$ $Se_{0.33}$, $FeMnP_{0.66}$ $In_{0.33}$ and $FeMnP_{0.66}$ $Sn_{0.33}$ were found to be 557.028K, 493.327K, 324.677K and 374.000K respectively as indicated in table 4.15. This study was unable to compare these results

with any other since none was available in literature. Nonetheless, it can be easily seen that FeMnP$_{0.66}$In$_{0.33}$ has the lowest Debye temperature while FeMnP$_{0.66}$Si$_{0.33}$ has the highest Debye temperature implying that it has the highest interatomic bonding. This can be concluded from reported data of the Fe - A bond lengths on table 4.4, where A is the replacing atom. A careful analysis of the relationship between bond lengths and Debye temperature shows that a smaller bond length which corresponds to a higher interatomic bonding result to a higher Debye temperature and vice versa. The Debye temperature can also affect the thermal conductivity of materials, especially at low temperatures. Higher Debye temperatures are generally associated with higher thermal conductivities.

4.3 Vibrational Properties

The movement of an atom from its equilibrium position results to a rise in the forces on all the atoms in the structure. A sequence of phonon frequencies result from the investigation of these forces that are linked with an organised set of displacements. This brings about very valuable information in accounting for a number of properties and behaviour of crystalline structures, which include phonon dispersion, phonon density of state, thermal conductivity mechanical properties, phase transition and thermal properties (Togo & Tanaka, 2015).

4.3.1 Phonons

At the equilibrium point gamma, Γ (q=0), a crystal is alleged to be dynamically stable if its potential energy always rises against any combinations of atomic displacements. This is comparable to the condition that all phonons have actual and positive frequencies in the harmonic approximation (Togo & Tanaka, 2015). However, under computer-generated thermodynamic conditions, imaginary frequencies or undesirable eigenvalues can appear in the band structure. This symbolizes dynamical instability of the system, inferring that the atomic displacements decrease the potential energy in the neighborhood of the equilibrium atomic positions (Khandy *et al*., 2019).

Phonon dispersion spectra of the selected materials in the FM phase.

Figure 4.20, figure 4.21, figure 4.22 and figure 4.23 show the phonon dispersion spectra along the high symmetry paths for FeMnP$_{0.66}$Si$_{0.33}$, FeMnP$_{0.66}$Se$_{0.33}$, FeMnP$_{0.66}$Sn$_{0.33}$ and FeMnP$_{0.66}$In$_{0.33}$

respectively. Lack of imaginary frequencies in the respective dispersion spectra for both the acoustic and optical modes thus confirming the dynamical stability of these compounds. Moreover, the phonon dispersion curves for the four compounds in figures 4.20, 4.21,4.22 and 4.23 show some resemblance and this can only suggest that the bonding characteristics for these compounds are similar.

The phonon dispersion curves are characterised only by acoustic branches for one atom per unit cell. It has previously been well recognised that solids with more than one atom in the lowest unit cell display two types of phonons, the acoustic phonons which constitute the lower mode and optical phonons which are found in the upper mode (Maradudin *et al.*, 1963). The variation between acoustic and optical branches comes about because of a higher number of degrees of freedom resulting from the vibrations of atoms in the unit cell. Generally, a structure with N atoms per unit cell there are 3 acoustic branches (1 longitudinal and 2 transverse) and 3N-3 optical branches that is, N-1 longitudinal and 2N-2 transverse modes (Pavone *et al.*, 1993). This is displayed in figures 4.20, 4.21,4.22 and 4.23, whereby, they all show 27 modes of vibration out of which 3 are acoustic and 24 are optical branches. Of the optical branches, 8 are longitudinal and 16 are transverse.

Phonon dispersions are calculated along a given line of high symmetry of symmetry. Acoustic modes are shown to congregate at the gamma high symmetry point. The frequency of acoustic phonons approaches zero and reveal a linear relationship with phonon wave-vector for elongated wavelengths. Acoustic modes vibrate at a gentler frequency with two adjacent atoms vibrating at the same time in the same direction. Optical phonons have a positive frequency at the Brillouin zone center and express no dispersion close to the long wavelength limit Optical modes of vibration have a higher frequency compared to acoustic modes and two neighboring atoms vibrate in a direction conflicting each other. This happens if the lattice basis comprises of two or more atoms. They are called optical because in ionic fluctuations in displacement they generate an electrical polarisation that couples to the electromagnetic field (Dove, 2011).

Figure 4.20: Phonon dispersion spectra and the total density of state for FeMnP$_{0.66}$Si$_{0.33}$ in the FM phase.

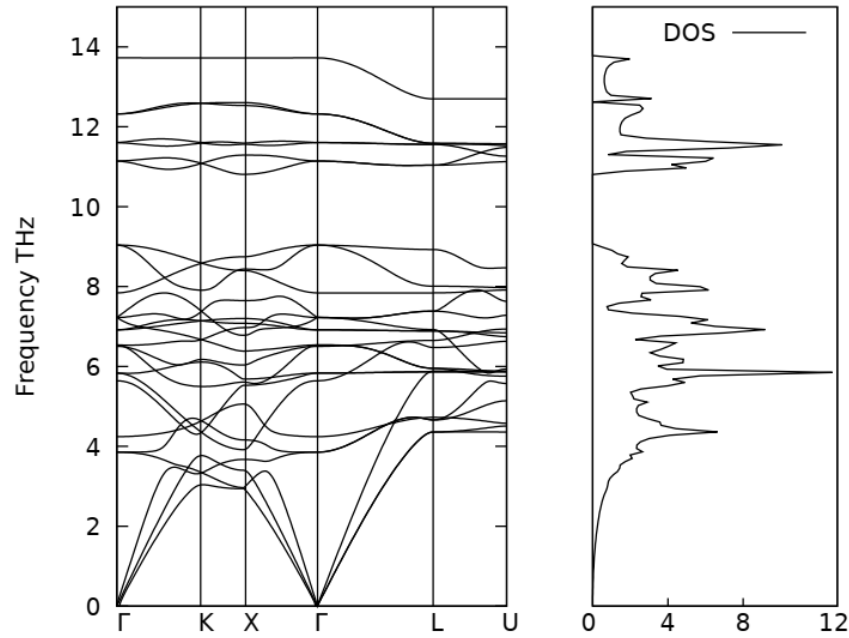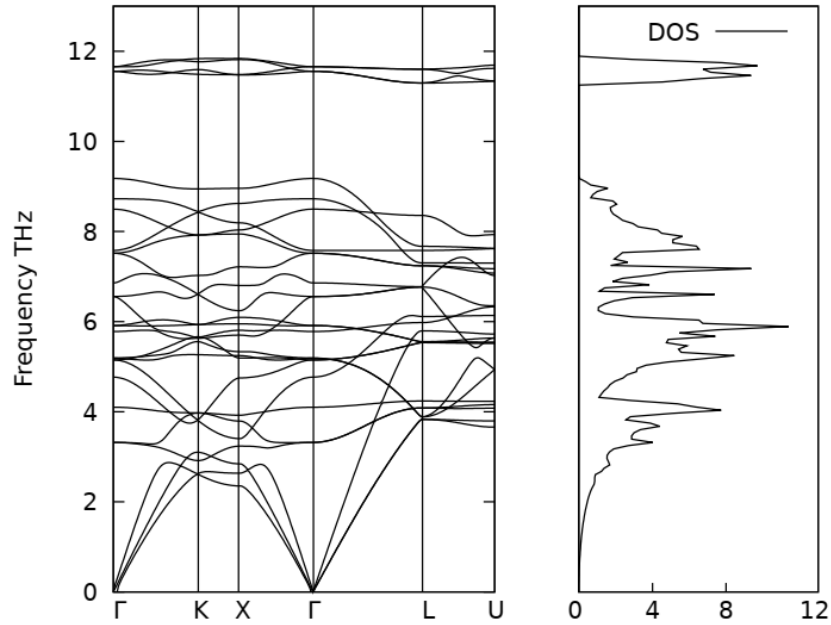**Figure 4. 21**: Phonon dispersion spectra and the total density of state for FeMnP$_{0.66}$Se$_{0.33}$ in the FM phase.
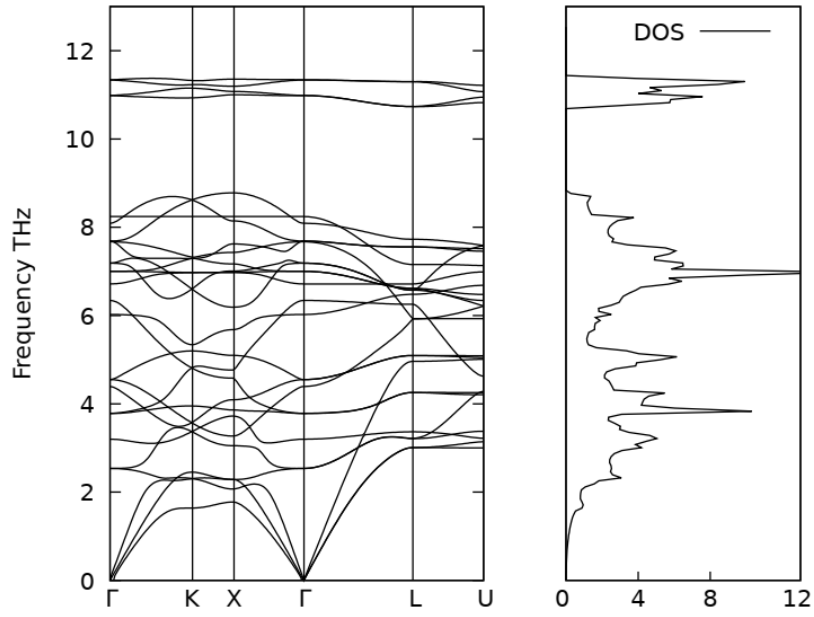
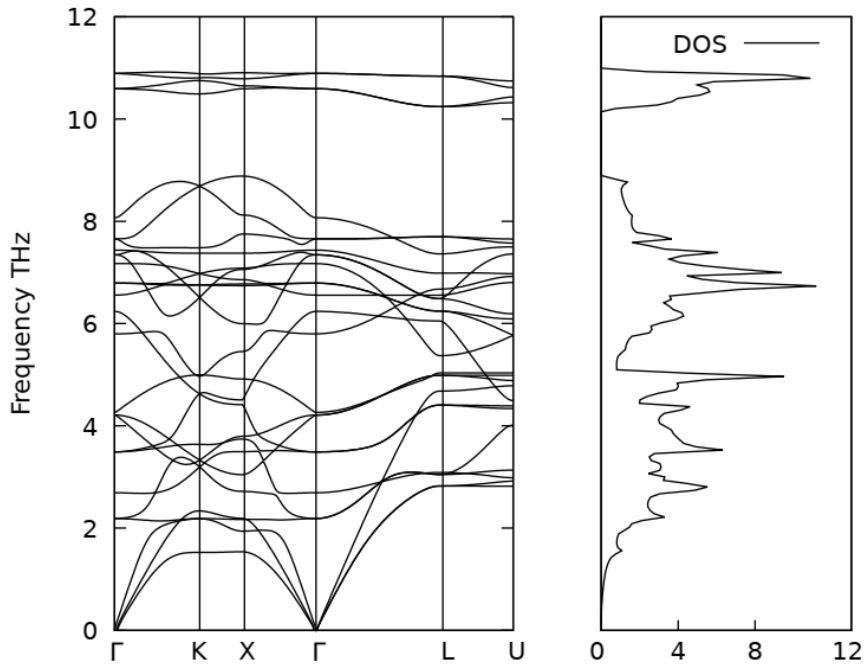**Figure 4. 22:** Phonon dispersion spectra and the total density of state for FeMnP$_{0.66}$Sn$_{0.33}$ in the FM phase.

Figure 4. 23: Phonon dispersion spectra and the total density of state for FeMnP$_{0.66}$In$_{0.33}$ in the FM phase.

A phonon bandgap between the optical and acoustic modes influences the phonon scattering process and thus lattice thermal conductivity. Gaps designate a higher rate of acoustic – optical phonon - phonon scattering resulting to low thermal conductivity. There was no band gap observed in the four compounds studied in this work hence their lattice thermal conductivity was relatively high. According to study done by Mackinnon *et al*. (2017), presence of phonon anomaly usually called a pseudo gap is fundamentally used as a measure of the superconductivity of solid structures. From figures 4.20, 4.21,4.22 and 4.23, between the frequency range of 9 THz -11Thz, it is clear that the upper and lower phonon branches are well separated which shows that the structures are good super conductors. However, the structure in figure 4.23 is a much better conductor due to a wider gap.

Phonon total density of states (DOS) of the selected materials in FM phase.

The phonon DOS represents the distribution of phonon frequencies at all wave vectors (k-points) in the Brillouin zone. It gives the density of vibrational states at different frequencies and provides insights into the material's thermal conductivity and heat capacity. Figure 4.20, figure 4.21, figure 4.22 and figure 4.23 presents the results of the total density of states for the selected materials in the FM phase. These graphs provide information about the number of vibrational modes at different frequencies, they also give insights into the distribution of vibrational frequencies and phonon energy levels in the material's vibrational spectrum. All the studied materials have high peak densities, higher phonon frequencies and longer phonon mean free paths and so possess higher thermal conductivity.

The Thermodynamic Properties.

At non-zero temperature, the energy of ions due to their vibration has major effects on a solid's thermal properties which include the entropy, heat capacity and the free energy. It is therefore essential to examine these properties for numerous applications, and in this case for materials to be used in near-room-temperature refrigeration. Using the thermodynamic relations, the heat capacity at constant volume (C_v), Helmholtz free energy (F) and entropy (S), can be computed as functions of temperature. The temperature dependence graphs of free energy, entropy, and specific heat capacity at constant volume of $FeMnP_{0.66}Si_{0.33}$, $FeMnP_{0.66}Se_{0.33}$, $FeMnP_{0.66}Sn_{0.33}$ and $FeMnP_{0.66}In_{0.33}$ are presented in figures 4.24, 4.25, 4.26, and 4.27 respectively.

The specific heat capacity at constant volume for the selected materials in the FM phase.

The Debye model approximates the phonon influence on the specific heat capacity of a solid. It forecasts that at low temperatures (temperatures below Debye temperature), the specific heat of crystals is proportionate to the cube of its temperature. This model also improves the Dulong-petit law at high temperatures which has it that above the Debye temperature, the gram-atomic specific heat capacity of solids is constant (Jasiukiewicz & Karpus, 2003). The green-coloured graph from the figures 4.24, 4.25, 4.26, and 4.27 show that for all the four compounds, the heat capacity curves show a sharp increase in the low-temperature region, and at high temperatures, C_v approaches a constant value (Dulong-Petit limit). This result is in good agreement with the Debye model of specific heat capacity, both for the low and high-temperature range.
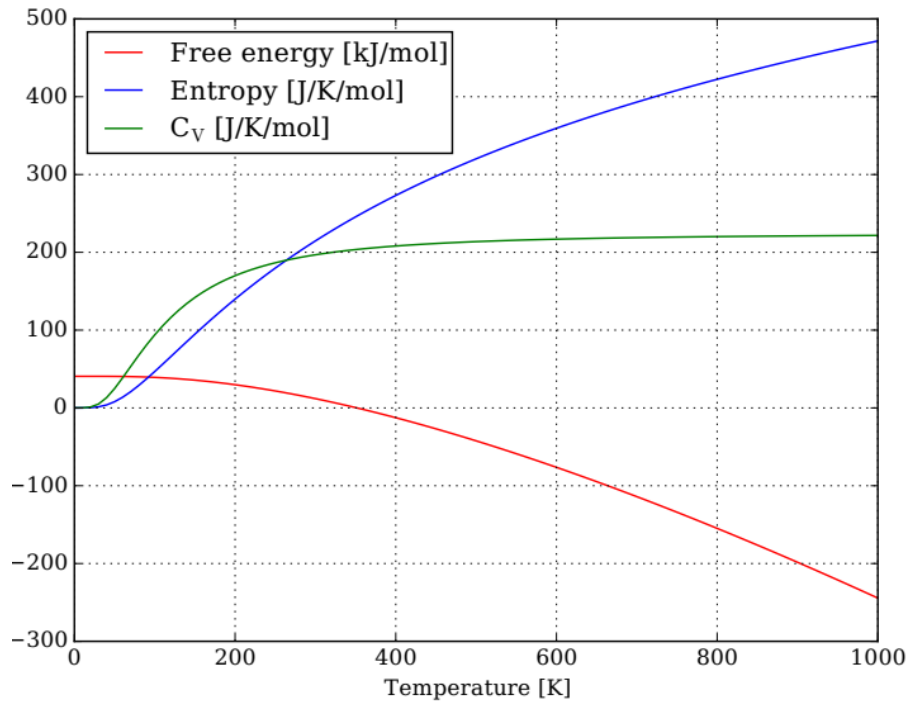
Figure 4.24: Graphs of free energy, entropy and specific heat capacity at constant volume against absolute temperature for the FM phase of FeMnP$_{0.66}$Si$_{0.33}$.
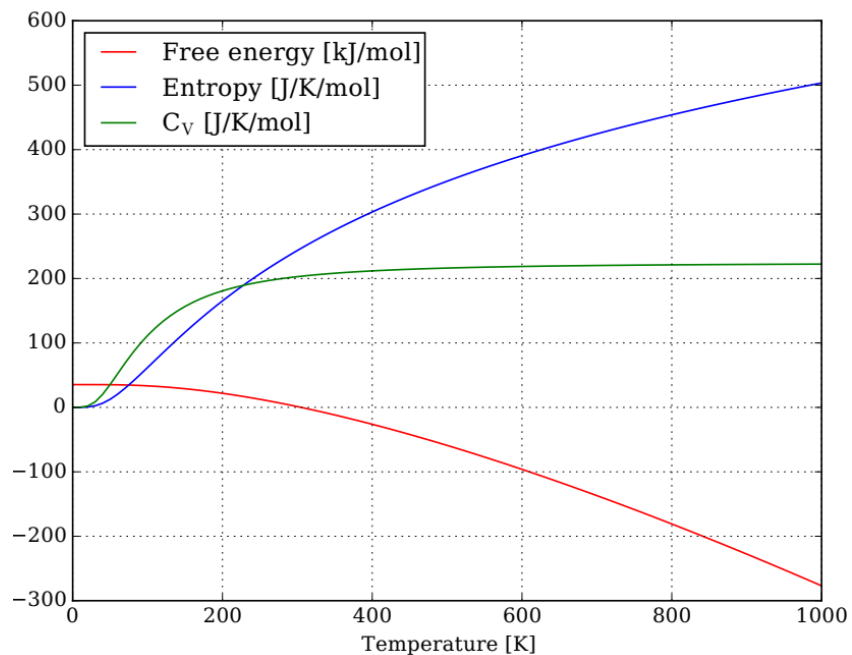
Figure 4.25: Graphs of free energy, entropy and specific heat capacity at constant volume against absolute temperature for the FM phase of FeMnP$_{0.66}$Se$_{0.33}$.
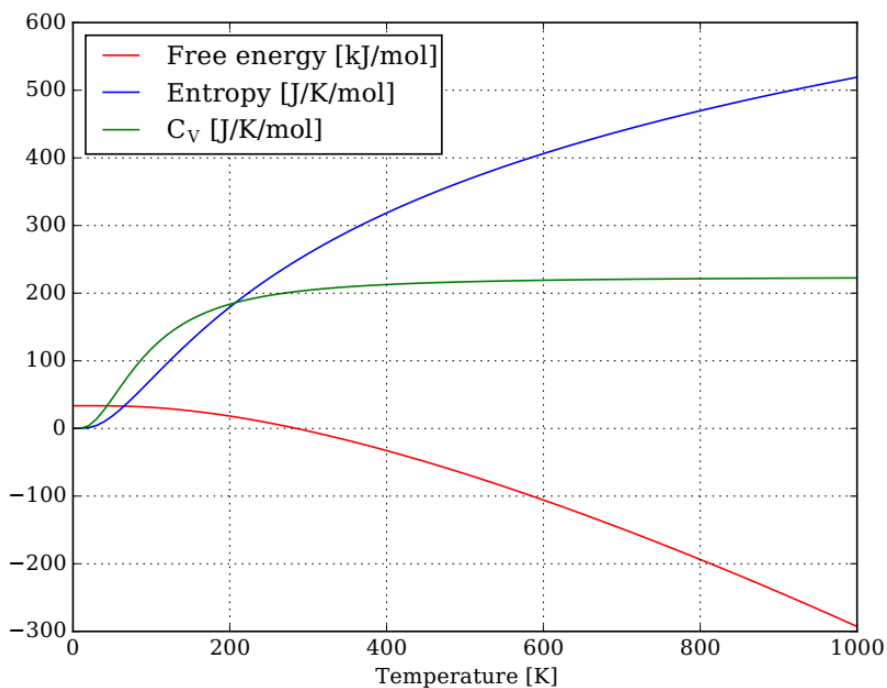
Figure 4. 26: Graphs of free energy, entropy and specific heat capacity at constant volume against absolute temperature for the FM phase of FeMnP$_{0.66}$Sn$_{0.33}$.
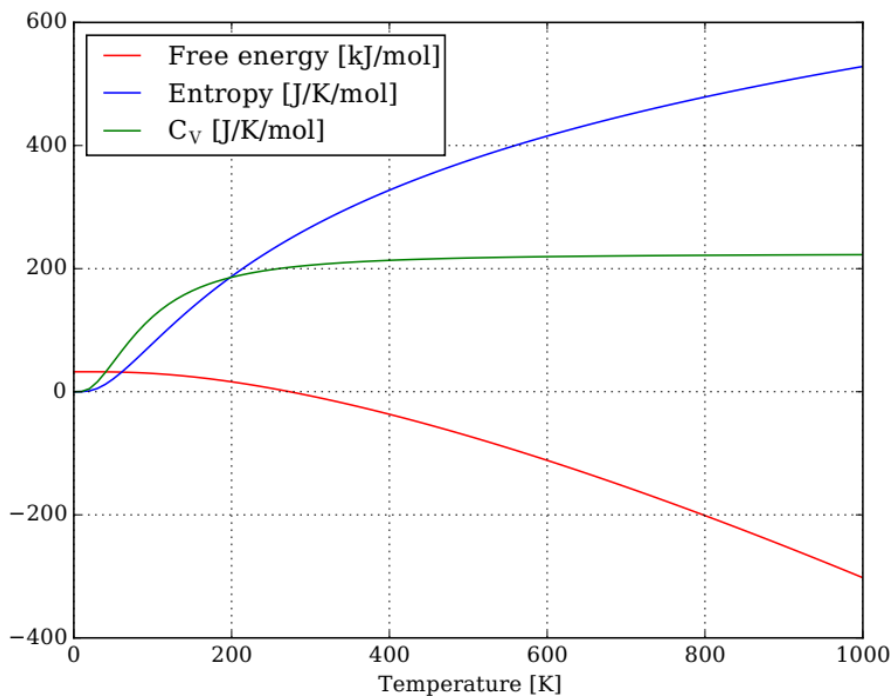
Figure 4. 27*: Graphs of free energy, entropy and specific heat capacity at constant volume against absolute temperature for the FM phase of FeMnP$_{0.66}$ In$_{0.33}$.

The classical equipartition law shows that $C_v = 3R$ at high temperatures, where C_v is the specific heat capacity at constant volume and R is the universal gas constant with the value of 8.314 J K^{-1} mol^{-1} (Gearhart, 1996). In this study, there are 9 atoms in one formula unit, which means the theoretical value of C_v should be 224.478 J K^{-1} mol^{-1}. From all the four graphs it is observed that the calculated C_v becomes a constant of 224 JK^{-1}mol^{-1} at high temperatures. This gives a negligible deviation of 0.213% implying that the calculated and theoretical C_v values show very good agreement. According to Fourier's law of heat conduction, the thermal conductivity of a solid is inversely proportional to its temperature. A high Debye temperature, therefore, implies that a crystal's thermal conductivity is low. This study established that the calculated Debye temperatures were 505.262 K, 476.259 K, 354.424 K and 291.571 K for the ferromagnetic phases of FeMnP$_{0.66}$Si$_{0.33}$, FeMnP$_{0.66}$Se$_{0.33}$, FeMnP$_{0.66}$Sn$_{0.33}$ and FeMnP$_{0.66}$ In$_{0.33}$ respectively. From these results, it is clear that FeMnP$_{0.66}$ In$_{0.33}$ is a better thermal conductor than the other compounds. It is however noted that a materials thermal conductivity cannot be purely drawn on the basis of Debye temperature only.

The entropy of the selected materials in the FM phase.

Entropy is another important thermal property that is commonly used in modelling the thermodynamic behaviour of solids. The blue-coloured graphs of figures 4.24, 4.25, 4.26, and 4.27 show the calculated entropy as a function of temperature for the selected alloys $FeMnP_{0.66}Si_{0.33}$, $FeMnP_{0.66}Se_{0.33}$, $FeMnP_{0.66}Sn_{0.33}$ and $FeMnP_{0.66}In_{0.33}$ respectively. It is an expected behaviour that the vibrational entropy curves increase as temperature increases due to the vibrational frequencies increasing with temperature (Fultz, 2010). This is clearly seen from the shape of the entropy graphs presented in figures 4.24, 4.25, 4.26, and 4.27. High entropy alloys (HEAs) are gaining substantial attention in material science and engineering. This is credited to their wanted qualities such as high tensile strength, better strength-to-weight ratio, high degree of fracture resistance as well as good resistance to corrosion and oxidation. From this work the entropies in J/K/Mol recorded for $FeMnP_{0.66}Si_{0.33}$, $FeMnP_{0.66}Se_{0.33}$, $FeMnP_{0.66}Sn_{0.33}$ and $FeMnP_{0.66}In_{0.33}$ at 1000K are approximately 470, 500,510 and 530 respectively. This suggests that $FeMnP_{0.66}In_{0.33}$ the best candidate for magnetic refrigeration owing to its high entropy value.

The Helmholtz's free energy of the selected materials in the FM phase.

Helmholtz free energy is a physical quantity that is of concern of concern to material physicists because it describes the amount of energy accessible to do work. This energy diminishes as temperature increases and this is confirmed by the formula F = U - TS where F is the Helmholtz free energy, U is the internal energy, T is the absolute temperature and S is the entropy. Following this equation, it is expected that if both T and S increase then F must decrease. The maximum amount of work done by a system is directly proportional to the decrease in the free energy. From the red-coloured graphs of figures 4.24, 4.25, 4.26, and 4.27, $FeMnP_{0.66}In_{0.33}$ has the highest decrease in Helmholtz free energy followed closely by $FeMnP_{0.66}Sn_{0.33}$. These two compounds therefore possess the highest amount of energy available to do work.

CHAPTER FIVE
CONCLUSIONS AND RECOMMENDATIONS

5.1 Conclusions

First principles calculation based on density functional theory was used to investigate the effect of alloying the A site of FeMnP$_{1-x}$A$_x$ (A = Si, x = 0.33) alternately with Se, Sn and in metalloids on the structural elastic and vibrational properties of these compounds. This work was done in the ferromagnetic, paramagnetic and antiferromagnetic phases and aimed at providing insights that would enable future studies to understand, predict and fabricate better magnetocaloric materials for magnetic refrigeration application.

The DFT calculated structural properties of FeMnP$_{0.66}$Si$_{0.33}$ including bond lengths, lattice parameters, bulk modulus and first-order pressure derivative of bulk modulus were in good agreement with available theoretical and experimental results. The small and acceptable percentage deviations of 2% and less, from the experimental data for the structural properties in the ferromagnetic phase of this alloy indicated the accuracy in these calculations. These deviations were a bit higher in the antiferromagnetic phase and this could be attributed to the fact that GGA approximations tend to underestimate some properties of solids due estimations made in the exchange correlation functionals. Moreover, theoretical calculations assume perfect structures while experiments could deal with polycrystalline samples which contain simple and extended defects thus leading to variations in the same parameters. Comparison of the structural parameters of FeMnP$_{1-x}$A$_x$ (A = Se, Sn, In; x = 0.33) alloys with experimental results was not done since there is no previous data available. However, the small and acceptable percentage deviation of the bond lengths of these compounds from those of FeMnP$_{0.66}$Si$_{0.33}$ confirmed that alloying did not significantly alter the structure of these materials.

Further, first principles DFT using Thermo PW software interfaced with the Quantum ESPRESSO code was used to investigate the elastic properties and hence mechanical stability of FeMnP$_{1-x}$A$_x$ (A= Si, Se, Sn, In, x = 0.33) as possible magnetocaloric materials. These materials were forced to undergo repeated magnetisation and demagnetisation cycles and so must exhibit mechanical stability at temperatures around their phase transition. The elastic constants, bulk modulus, shear modulus, young's modulus, Pugh's ratio, machinability index, elastic anisotropy factor and Debye temperature, which are essential for determining the long-term applicability of these materials in magnetic refrigeration were obtained. The calculated values for elastic constants

for all the materials were found to be in line with the Born and Huang conditions for mechanical stability. In addition, the values of the elastic constants were found to be relatively high indicating that the materials studied had good resistance against deformation. This study shows that in the ferromagnetic state $FeMnP_{0.66}In_{0.33}$ had the highest Poisson's ratio, Pugh's index, machinability index anisotropic ratio of all the selected materials. further proving that of the 4 compounds. This could imply that it is more stable mechanically and most suitable for sustainable operation as a magnetocaloric refrigerant. This finding is however, not conclusive because in addition to the elastic properties, there are other physical indicators of mechanical stability that have not been reported in this study.

The lack of negative frequencies on phonon dispersion curves of these compounds in the ferromagnetic phase, revealed that they are all dynamically stable. The temperature dependence graphs of the thermodynamic properties of $FeMnP_{0.66}Si_{0.33}$, $FeMnP_{0.66}Se_{0.33}$, $FeMnP_{0.66}Sn_{0.33}$ and $FeMnP_{0.66}In_{0.33}$ were calculated using the phonopy software. The calculated values of specific heat capacity, entropy and free energy are in excellent agreement with theoretical predictions. In particular, both the Dulong petit and Debye approximations of the specific heat capacities are realised at both the high and low temperature regions. The maximum amount of work done by a system is directly proportional to the decrease in the free energy. This study has also shown that $FeMnP_{0.66}In_{0.33}$ has the highest decrease in Helmholtz free energy and hence it possesses the highest amount of energy available to do work.

This study shows that alloying with Indium had better results in the structural, elastic and vibrational properties of the magnetocaloric material. This work can therefore be used as a reference to motivate further theoretical and experimental research on other physical properties of $FeMnP_{0.66}In_{0.33}$ for future use in magnetic refrigeration.

5.2 Recommendations

i. This study has dealt only with structural, elastic and vibrational and properties of $FeMnP_{1-x}A_x$ (A_x=Si, Se, In and Sn: x= 0.33) alloys. There is a need to study other physical properties including but not limited to; the magnetic properties, mechanical properties, optical properties and electronic properties of the same alloys since it gives a bond length, bond angles and lattice parameters which are reasonably closer to the experimental values and other theoretical findings as seen in the case of $FeMnP_{0.66}Si_{0.33}$.

ii.   This density functional theory study was done using the quantum ESPRESSO code to compute the structural, elastic and vibrational properties of $FeMnP_{1-x}A_x$ (A_x=Si, Se, Sn, In: x = 0.33) alloys. Other computational approaches like VASP and ABINIT can be used to compute the structural phonon, elastic and other physical properties of these materials in the same ratio. This will help determine the variations in these results if any and give more informed insights to these material properties.

iii.   This work dealt with the theoretical study of structural, elastic and vibrational properties of $FeMnP_{1-x}A_x$ (Si, Se, In and Sn: x= 0.33) alloys. Therefore, there is a need to conduct an experimental study on the same alloys in the same ratio. This will determine the variation of experimental results and theoretically calculated results from quantum ESPRESSO code, as well as the viability of using these alloys in near room temperature magnetic refrigeration.

iv.   This work did not present the vibrational properties of $FeMnP_{1-x}A_x$ (Si, Se, In and Sn: x= 0.33) alloys in the antiferromagnetic and paramagnetic phases. This was because of the heaviness of the calculations resulting to more use of computational resources and time since the phonopy software makes use of supercells. There is therefore a need to carry out calculations of this property in these two phases.

v.   Additional studies are needed to determine the vibrational, structural and mechanical properties of these materials in the same ratio using other *ab initio* calculation tools and also experimental investigations. Other alloying metalloids, those that have not been looked at by this study can also be investigated both theoretically and experimentally to shed more light on their properties and viability for use as magnetic refrigerants.

REFERENCES

Aksoy, S., Yucel, A., Elerman, Y., Krenke, T., Acet, M., Moya, X., & Mañosa, L. (2008). The influence of gallium on the magnetocaloric properties of Gd5Si2Ge2. *Journal of Alloys and Compounds*, *460*(1-2), 94-98. https://doi.org/10.1016/j.jallcom.2007.06.060

Alahmer, A., Al-Amayreh, M., Mostafa, A. O., Al-Dabbas, M., & Rezk, H. (2021). Magnetic refrigeration design technologies: State of the art and general perspectives. *Energies*, *14*(15), 4662. https://doi.org/10.3390/en14154662

Albertini, F., Bennati, C., Bianchi, M., Branchini, L., Cugini, F., Pascale, A. D., Fabbrici, S., Melino, F., Ottaviano, S., Peretto, A., Rosati, J., & Solzi, M. (2017). Preliminary investigation on a rotary Magnetocaloric refrigerator prototype. *Energy Procedia*, *142*, 1288-1293. https://doi.org/10.1016/j.egypro.2017.12.487

Alfè, D. (2009). PHON: A program to calculate phonons using the small displacement method. *Computer Physics Communications*, *180*(12), 2622-2633. https://doi.org/10.1016/j.cpc.2009.03.010

Andrade, V., Vivas, R. C., Pedro, S., Tedesco, J., Rossi, A., Coelho, A., Rocco, D., & Reis, M. (2016). Magnetic and magnetocaloric properties of La0.6Ca0.4MnO3 tunable by particle size and dimensionality. *Acta Materialia*, *102*, 49-55. https://doi.org/10.1016/j.actamat.2015.08.080

Anh, Kim D., Thuy, N., Duc, N., Nhien, T., & Nong, N. (2003). Magnetism and magnetocaloric effect in La1−yNdy(Fe0.88Si0.12)13 compounds. *Journal of Magnetism and Magnetic Materials*, *262*(3), 427-431. https://doi.org/10.1016/s0304-8853(03)00073-8

Aprea, C., Greco, A., & Maiorino, A. (2014). Magnetic refrigeration: A promising new technology for energy saving. *International Journal of Ambient Energy*, *37*(3), 294-313. https://doi.org/10.1080/01430750.2014.962088

Aprea, C., Greco, A., Maiorino, A., & Masselli, C. (2015). Magnetic refrigeration: An eco-friendly technology for the refrigeration at room temperature. *Journal of Physics: Conference Series*, *655*, 012026. https://doi.org/10.1088/1742-6596/655/1/012026

Armand, M., Endres, F., MacFarlane, D. R., Ohno, H., & Scrosati, B. (2009). Ionic-liquid materials for the electrochemical challenges of the future. *Nature Materials*, *8*(8), 621-629. https://doi.org/10.1038/nmat2448

Balema, V. P., Wiench, J. W., Pruski, M., & Pecharsky, V. K. (2002). Mechanically induced solid-state generation of phosphorus Ylides and the solvent-free Wittig reaction. *Journal of the American Chemical Society*, *124*(22), 6244-6245. https://doi.org/10.1021/ja017908p

Balli, M., Fruchart, D., & Gignoux, D. (2007). Optimization of La(Fe,Co) 13− xSix based compounds for magnetic refrigeration. *Journal of Physics: Condensed Matter*, *19*(23), 236230. https://doi.org/10.1088/0953-8984/19/23/236230

Balli, M., Sari, O., Mahmed, C., Besson, C., Bonhote, P., Duc, D., & Forchelet, J. (2012). A pre-industrial magnetic cooling system for room temperature application. *Applied Energy*, *98*, 556-561. https://doi.org/10.1016/j.apenergy.2012.04.034

Barcza, A., Gercsi, Z., Michor, H., Suzuki, K., Kockelmann, W., Knight, K. S., & Sandeman, K. G. (2013). Magnetoelastic coupling and competing entropy changes in substituted CoMnSi metamagnets. *Physical Review B*, *87*(6). https://doi.org/10.1103/physrevb.87.064410

Bejar, M., Dhahri, R., Dhahri, E., Balli, M., & Hlil, E. (2007). Large magnetic entropy change at room temperature in La0.7Ca0.3−xKxMnO3. *Journal of Alloys and Compounds*, *442*(1-2), 136-138. https://doi.org/10.1016/j.jallcom.2006.10.170

Beretta, D., Neophytou, N., Hodges, J. M., Kanatzidis, M. G., Narducci, D., Martin-Gonzalez, M., Beekman, M., Balke, B., Cerretti, G., Tremel, W., Zevalkink, A., Hofmann, A. I., Müller, C., Dörling, B., Campoy-Quiles, M., & Caironi, M. (2019). Thermoelectrics: From history, a window to the future. *Materials Science and Engineering: R: Reports*, *138*, 100501. https://doi.org/10.1016/j.mser.2018.09.001

Bleaney, B. (1990). Enhanced nuclear magnetic cooling: A new perspective. *Journal of Physics: Condensed Matter*, *2*(35), 7265-7273. https://doi.org/10.1088/0953-8984/2/35/002

Blöchl, P. E. (1994). Projector augmented-wave method. *Physical Review B*, *50*(24), 17953-17979. https://doi.org/10.1103/physrevb.50.17953

Blöchl, P. E., Jepsen, O., & Andersen, O. K. (1994). Improved tetrahedron method for brillouin-zone integrations. *Physical Review B*, *49*(23), 16223-16233. https://doi.org/10.1103/physrevb.49.16223

Bohigas, X., Tejada, J., Marínez-Sarrión, M., Tripp, S., & Black, R. (2000). Magnetic and calorimetric measurements on the magnetocaloric effect in La0.6Ca0.4MnO3. *Journal of*

Magnetism and Magnetic Materials, 208(1-2), 85-92. https://doi.org/10.1016/s0304-8853(99)00581-8

Born, M., Huang, K., & Lax, M. (1955). Dynamical theory of crystal lattices. *American Journal of Physics*, *23*(7), 474-474. https://doi.org/10.1119/1.1934059

Botoc, D., Siroux, M., & Salceanu, A. (2021). Magnetic refrigeration: Emerging technology for sustainable refrigeration. *E3S Web of Conferences*, *294*, 03001. https://doi.org/10.1051/e3sconf/202129403001

Brown, G. V. (1976). Magnetic heat pumping near room temperature. *Journal of Applied Physics*, *47*(8), 3673-3680. https://doi.org/10.1063/1.323176

Brück, E., Trung, N., Ou, Z., & Buschow, K. (2012). Enhanced magnetocaloric effects and tunable thermal hysteresis in transition metal pnictides. *Scripta Materialia,* 67(6), 590-593. https://doi.org/10.1016/j.scriptamat.2012.04.037

Brück, E. (2005). Developments in magnetocaloric refrigeration. *Journal of Physics D: Applied Physics*, *38*(23), R381-R391. https://doi.org/10.1088/0022-3727/38/23/r01

Brück, E., Tegus, O., Cam Thanh, D., Trung, N. T., & Buschow, K. (2008). A review on Mn based materials for magnetic refrigeration: Structure and properties. *International Journal of Refrigeration*, *31*(5), 763-770. https://doi.org/10.1016/j.ijrefrig.2007.11.013

Brück, E., Tegus, O., Zhang, L., Li, X., De Boer, F., & Buschow, K. (2004). Magnetic refrigeration near room temperature with fe2p-based compounds. *Journal of Alloys and Compounds*, *383*(1-2), 32-36. https://doi.org/10.1016/j.jallcom.2004.04.042

Burdett, J. K., & Miller, G. J. (1990). Fragment formalism in main-group solids: Applications to aluminum boride (AlB2), calcium aluminum silicide (CaAl2Si2), barium-aluminum (BaAl4), and related materials. *Chemistry of Materials*, *2*(1), 12-26. https://doi.org/10.1021/cm00007a004

Çakır, Ö., & Acet, M. (2012). Reversibility in the inverse magnetocaloric effect in Mn_3GaC studied by direct adiabatic temperature-change measurements. *Applied Physics Letters*, *100*(20), 202404. https://doi.org/10.1063/1.4717181

Capozzoli, A., & Primiceri, G. (2015). Cooling systems in data centers: State of art and emerging technologies. *Energy Procedia*, *83*, 484-493. https://doi.org/10.1016/j.egypro.2015.12.168

Carlin, R. L., & Van Duyneveldt, A. J. (1977). Magnetic properties of transition metal compounds. *Inorganic Chemistry Concepts*. (pp. 91-92) https://doi.org/10.1007/978-3-642-87392-8

Carrier, P., Wentzcovitch, R., & Tsuchiya, J. (2007). Erratum: First-principles prediction of crystal structures at high temperatures using the quasiharmonic approximation [Phys. Rev. B76, 064116 (2007)]. *Physical Review B*, *76*(18). https://doi.org/10.1103/physrevb.76.189901

Charif Alaoui, Y., Tahiri, N., El Bounagui, O., & Ez-Zahraouy, H. (2021). Magnetic properties and large magnetocaloric effect in the perovskite Mn3GeC compound: AB initio and Monte Carlo calculations. *Phase Transitions*, *95*(1), 10-18. https://doi.org/10.1080/01411594.2021.1999950

Chau, N., Nhat, H. N., Luong, N. H., Minh, D. L., Tho, N. D., & Chau, N. N. (2003). Structure, magnetic, magnetocaloric and magnetoresistance properties of La1−xPbxMnO3 perovskite. *Physica B: Condensed Matter*, *327*(2-4), 270-278. https://doi.org/10.1016/s0921-4526(02)01759-3

Chen, R., Wang, Q., Yang, Y., Guo, J., Su, Y., Ding, H., & Fu, H. (2018). Brittle–ductile transition during creep in nearly and fully lamellar high-NB TiAl alloys. *Intermetallics*, *93*, 47-54. https://doi.org/10.1016/j.intermet.2017.11.009

Chen, W., Zhong, W., Hou, D. L., Gao, R. W., Feng, W. C., Zhu, M. G., & Du, Y. W. (2002). Preparation and magnetocaloric effect of self-doped La0. 8− xNa0. 2xMnO3+ δ vacancies) polycrystal. *Journal of Physics: Condensed Matter*, *14*(45), 11889-11896. https://doi.org/10.1088/0953-8984/14/45/330

Chen, X., Chen, Y., & Tang, Y. (2012). Phase relation of Lafe 11·6 SI 1·4 compounds annealed at different high-temperature and the magnetic property of Lafe 11·6– X Co X SI 1·4 compounds. *Bulletin of Materials Science*, *35*(2), 175-182. https://doi.org/10.1007/s12034-012-0273-y

Chen, X., Niu, H., Li, D., & Li, Y. (2011). Modeling hardness of polycrystalline materials and bulk metallic glasses. *Intermetallics*, *19*(9), 1275-1281. https://doi.org/10.1016/j.intermet.2011.03.026

Chen, Y., Wang, F., Shen, B., Hu, F., Sun, J., Wang, G., & Cheng, Z. (2003). Magnetic properties and magnetic entropy change of LaFe11.5Si1.5H*y* interstitial compounds. *Journal of*

Physics: Condensed Matter, *15*(7), L161-L167. https://doi.org/10.1088/0953-8984/15/7/102

Chen, Y., Wang, F., Shen, B., Wang, G., & Sun, J. (2003). Magnetism and magnetic entropy change of LaFe11.6Si1.4Cx (x=0−0.6) interstitial compounds. *Journal of Applied Physics*, *93*(2), 1323-1325. https://doi.org/10.1063/1.1532930

Chepkoech, M., Joubert, D. P., & Amolo, G. O. (2020). A density functional theory study of the thermoelectric properties of K3AuO. *Computational Condensed Matter*, *24*, e00484. https://doi.org/10.1016/j.cocom.2020.e00484

Cherkaev, A., & Gibiansky, L. (1993). Coupled estimates for the bulk and shear moduli of a two-dimensional isotropic elastic composite. *Journal of the Mechanics and Physics of Solids*, *41*(5), 937-980. https://doi.org/10.1016/0022-5096(93)90006-2

Chung, P. C., Glynos, E., Sakellariou, G., & Green, P. F. (2016). Elastic mechanical response of thin supported star-shaped polymer films. *ACS Macro Letters*, *5*(4), 439-443. https://doi.org/10.1021/acsmacrolett.5b00944

Cohen, A. J., Mori-Sánchez, P., & Yang, W. (2008). Insights into current limitations of density functional theory. *Science*, *321*(5890), 792-794. https://doi.org/10.1126/science.1158722

Corso, A. D. (2018). SISSA, the International School for Advanced Studies, SISSA – Trieste, Italy, *https://dalcorso.github.io/thermo_pw/*

Cottenier, S., Vanhoof, V., Torumba, D., Bellini, V., Çakmak, M., & Rots, M. (2005). Ab initio calculation of hyperfine interaction parameters: Recent evolutions, recent examples. In *HFI/NQI 2004: Proceedings of the 13th International Conference on Hyperfine Interactions and 17th International Symposium on Nuclear Quadrupole Interactions (HFI/NQI 2004) Bonn, Germany, 22–27 August 2004* (pp. 9-18). Springer Berlin Heidelberg. https://doi.org/10.1007/3-540-30924-1_2

Ćwik, J., Koshkid'ko, Y., Małecka, M., Weise, B., Krautz, M., Mikhailova, A., & Kolchugina, N. (2021). Magnetocaloric prospects of mutual substitutions of rare-earth elements in pseudobinary Tb1−xHoxNi2 compositions (X = 0.25–0.75). *Journal of Alloys and Compounds*, *886*, 161295. https://doi.org/10.1016/j.jallcom.2021.161295

Dal Corso, A. (2014). Pseudopotentials periodic table: From H to Pu. *Computational Materials Science*, *95*, 337-350. https://doi.org/10.1016/j.commatsci.2014.07.043

Dan'kov, S. Y., Ivtchenko, V. V., Tishin, A. M., Gschneidner, K. A., & Pecharsky, V. K. (2000). Magnetocaloric effect in GdAl2 and Nd2Fe17. *Advances in Cryogenic Engineering Materials*, 397-404. https://doi.org/10.1007/978-1-4615-4293-3_51

Dan'kov, S. Y., Tishin, A. M., Pecharsky, V. K., & Gschneidner, K. A. (1998). Magnetic phase transitions and the magnetothermal properties of gadolinium. *Physical Review B*, *57*(6), 3478-3490. https://doi.org/10.1103/physrevb.57.3478

Daniels, L. M., Weber, M. C., Lees, M. R., Guennou, M., Kashtiban, R. J., Sloan, J., Kreisel, J., & Walton, R. I. (2013). Structures and magnetism of the rare-earth Orthochromite perovskite solid solution La$_x$sm$_{1-ixi}$CrO$_3$. *Inorganic Chemistry*, *52*(20), 12161-12169. https://doi.org/10.1021/ic402029u

Das, S., & Dey, T. K. (2006). Magnetocaloric effect in potassium doped lanthanum manganite perovskites prepared by a pyrophoric method. *Journal of Physics: Condensed Matter*, *18*(32), 7629-7641. https://doi.org/10.1088/0953-8984/18/32/011

Davarpanah, S. M., Ván, P., & Vásárhelyi, B. (2020). Investigation of the relationship between dynamic and static deformation moduli of rocks. *Geomechanics and Geophysics for Geo-Energy and Geo-Resources*, *6*(1). https://doi.org/10.1007/s40948-020-00155-z

Deltell, A., Mohamed, A. E., Álvarez-Alonso, P., Ipatov, M., Andrés, J., González, J., Sánchez, T., Zhukov, A., Escoda, M., Suñol, J., & López Antón, R. (2021). Martensitic transformation, magnetic and magnetocaloric properties of Ni–mn–Fe–Sn Heusler ribbons. *Journal of Materials Research and Technology*, *12*, 1091-1103. https://doi.org/10.1016/j.jmrt.2021.03.049

Demin, R. V., & Koroleva, L. I. (2004). Influence of a magnetic two-phase state on the magnetocaloric effect in the La1−x SrxMnO3 manganites. *Physics of the Solid State*, *46*(6), 1081-1083. https://doi.org/10.1134/1.1767248

Desideri, U., Proietti, S., & Sdringola, P. (2009). Solar-powered cooling systems: Technical and economic analysis on industrial refrigeration and air-conditioning applications. *Applied Energy*, *86*(9), 1376-1386. https://doi.org/10.1016/j.apenergy.2009.01.011

Dhahri, J., Dhahri, A., & Dhahri, E. (2009). Structural, magnetic and magnetocaloric properties of La0.7−xEuxBa0.3MnO3 perovskites. *Journal of Magnetism and Magnetic Materials*, *321*(24), 4128-4131. https://doi.org/10.1016/j.jmmm.2009.08.014

Dieckmann, J., Roth, K., & Brodrick, J. (2007). Magnetic refrigeration. *TC*, *ASHRAE Journal 10*, 5, 74-77.

Dixey, R. J., Manuel, P., Orlandi, F., Mukherjee, P., Dutton, S. E., Stenning, G. B., & Saines, P. J. (2020). *In situ* observation of the magnetocaloric effect through neutron diffraction in the Tb(DCO$_2$)$_3$ and TbODCO$_3$ frameworks. *Journal of Materials Chemistry C*, *8*(35), 12123-12132. https://doi.org/10.1039/d0tc03153d

Dove M. T & McConnell, J. D. (1995). Introduction to lattice dynamics Cambridge, (Cambridge University press), 1993. xvii + 258 pp., price £35. ISBN 0 521 39293 4. *Mineralogical Magazine*, *59*(396), 581-582. https://doi.org/10.1180/minmag.1995.059.396.24

Drake, F., Purvis, M., & Hunt, J. (2001). *Public Understanding of Science*, *10*(2), 187-211. https://doi.org/10.1088/0963-6625/10/2/303

Duan, J. F., Long, Y., Bao, B., Zhang, H., Ye, R. C., Chang, Y. Q., Wan, F. R., & Wu, G. H. (2008). Experimental and theoretical investigations of the magnetocaloric effect of Ni2.15Mn0.85−xCuxGa (x=0.05,0.07) alloys. *Journal of Applied Physics*, *103*(6), 063911. https://doi.org/10.1063/1.2899041

Duc, N., Shen, H., Clements, E., Thiabgoh, O., Sanchez Llamazares, J., Sanchez-Valdes, C., Huong, N., Sun, J., Srikanth, H., & Phan, M. (2019). Enhanced refrigerant capacity and Curie temperature of amorphous Gd60Fe20Al20 microwires. *Journal of Alloys and Compounds*, *807*, 151694. https://doi.org/10.1016/j.jallcom.2019.151694

Dung, N. H., Ou, Z. Q., Caron, L., Zhang, L., Thanh, D. T., De Wijs, G. A., De Groot, R. A., Buschow, K. H., & Brück, E. (2011). Mixed magnetism for refrigeration and energy conversion. *Advanced Energy Materials*, *1*(6), 1215-1219. https://doi.org/10.1002/aenm.201100252

Ekanth, V. P. & Kishor, F. (2016). New eco-friendly magnetic refrigeration system. *International Research Journal of Engineering and Technology*, 3, 1512-13.

Elveny, M., Sarjito, Jalil, A. T., Davarpanah, A., Alfakeer, M., Awadh Bahajjaj, A. A., & Ouladsmane, M. (2021). CFD-based simulation to reduce greenhouse gas emissions from industrial plants. *International Journal of Chemical Reactor Engineering*, *19*(11), 1179-1186. https://doi.org/10.1515/ijcre-2021-0063

Eraslan, D., Balcı, A., Çetin, B., Uçak, N., Çiçek, A., Yılmaz, O. D., & Davut, K. (2021). Machinability evaluations of austempered ductile iron and cast steel with similar

mechanical properties under eco-friendly Milling conditions. *Journal of Materials Research and Technology*, *11*, 1443-1456. https://doi.org/10.1016/j.jmrt.2021.01.123

Evdokimenko, V. I., & Kripyakevich, P. I. (1963). The crystal structures of magnesium-rich compounds in the systems La-Mg, Ce-Mg, and Nd-Mg. *Soviet Phys.-Cryst.(English Transl.)*, *8(1),* 44-49.

Fang, W., Yuan-Fu, C., Guang-Jun, W., Ji-Rong, S., & Bao-Gen, S. (2003). Large magnetic entropy change and magnetic properties in $La(Fe_{1-x}Mn_x)_{11.7}Si_{1.3}H_y$ compounds. *Chinese Physics*, *12*(8), 911-914. https://doi.org/10.1088/1009-1963/12/8/317

Fengxia, H., Baogen, S., Jirong, S., Zhaohua, C., & Xixiang, Z. (2000). Magnetic entropy change in $La(Fe_{0.98}Co_{0.02})_{11.7}Al_{1.3}$. *Journal of Physics. Condensed Matter*, *12(46),* L691. https://doi.org/10.1088/0953-8984/12/46/101

Fletcher, R. (1964). Function minimization by conjugate gradients. *The Computer Journal*, *7*(2), 149-154. https://doi.org/10.1093/comjnl/7.2.149

Franco, V., Blázquez, J. S., & Conde, A. (2006). Field dependence of the magnetocaloric effect in materials with a second order phase transition: A master curve for the magnetic entropy change. *Applied Physics Letters*, *89*(22), 27-39. https://doi.org/10.1063/1.2399361

Franco, V., Blázquez, J., Ipus, J., Law, J., Moreno-Ramírez, L., & Conde, A. (2018). Magnetocaloric effect: From materials research to refrigeration devices. *Progress in Materials Science*, *93*, 112-232. https://doi.org/10.1016/j.pmatsci.2017.10.005

Franco, V., Conde, A., Kuz'min, M. D., & Romero-Enrique, J. M. (2009). The magnetocaloric effect in materials with a second order phase transition: Are TC and Tpeak necessarily coincident? *Journal of Applied Physics*, *105*(7), 07A917. https://doi.org/10.1063/1.3063666

Fu, C., Wang, X., Ye, Y., & Ho, K. (1999). Phase stability, bonding mechanism, and elastic constants of Mo5Si3 by first-principles calculation. *Intermetallics*, *7*(2), 179-184. https://doi.org/10.1016/s0966-9795(98)00018-1

Fujieda, S, Fujita, A.,., Fukamichi, K., Yamazaki, Y., & Iijima, Y. (2002). Giant magnetic entropy change in hydrogenated La (Fe0. 88Si0. 12) 13Hy Compounds. *Materials Transactions*, *43*(5), 1202-1204. https://doi.org/10.2320/matertrans.43.1202

Fujieda, S., Hasegawa, Y., Fujita, A., & Fukamichi, K. (2004). Thermal transport properties of magnetic refrigerants La(FexSi1−x)13 and their hydrides, and Gd5Si2Ge2 and mnas. *Journal of Applied Physics*, *95*(5), 2429-2431. https://doi.org/10.1063/1.1643774

Fujita, A., Fujieda, S., Fukamichi, K., Yamazaki, Y., & Iijima, Y. (2002). Giant magnetic entropy changes in hydrogenated La (Fe0. 88Si0. 12) 13Hy Compounds. *Materials Transactions*, *43*(5), 1202-1204. https://doi.org/10.2320/matertrans.43.1202

Fultz, B. (2010). Vibrational thermodynamics of materials. *Progress in Materials Science*, *55*(4), 247-352. https://doi.org/10.1016/j.pmatsci.2009.05.002

Gamzatov, A. G., Kamilov, I. K., Aliev, A. M., Batdalov, A. B., Aliverdiev, A. A., Abdulvagidov, S. B., Melnikov, O. V., Gorbenko, O. Y., & Kaul, A. R. (2007). Magnetocaloric effect in La1− xAgyMnO3 (y⩽ x): Direct and indirect measurements. *Journal of Physics D: Applied Physics*, *40*(15), 4413-4417. https://doi.org/10.1088/0022-3727/40/15/004

Gao, N., Kamran, K., Quan, C., & Williams, P. T. (2020). Thermochemical conversion of sewage sludge: A critical review. *Progress in Energy and Combustion Science*, *79*, 100843. https://doi.org/10.1016/j.pecs.2020.100843

GaoFeng, W. (2012). *Magnetic and calorimetric study of the magnetocaloric effect in intermetallics exhibiting first-order magnetostructural transitions* (Vol. 99). Universidad de Zaragoza.

Gearhart, C. A. (1996). Specific heats and the equipartition law in introductory textbooks. *American Journal of Physics*, *64*(8), 995-1000. https://doi.org/10.1119/1.18316

Giannozzi, P., Baroni, S., Bonini, N., Calandra, M., Car, R., Cavazzoni, C., Ceresoli, D., Chiarotti, G. L., Cococcioni, M., Dabo, I., Dal Corso, A., De Gironcoli, S., Fabris, S., Fratesi, G., Gebauer, R., Gerstmann, U., Gougoussis, C., Kokalj, A., Lazzeri, M., Layla, M., & Wentzcovitch, R. M. (2009). Quantum espresso: A modular and open-source software project for quantum simulations of materials. *Journal of Physics: Condensed Matter*, *21*(39), 395502. https://doi.org/10.1088/0953-8984/21/39/395502

Giauque, W. F. (1927). A thermodynamic treatment of certain magnetic effects. A proposed method of producing temperatures considerably below 1° absolute. *Journal of the American Chemical Society*, *49*(8), 1864-1870. https://doi.org/10.1021/ja01407a003

Gjorgievski, V. Z., Markovska, N., Pukšec, T., Duić, N., & Foley, A. (2021). Supporting the 2030 agenda for sustainable development: Special issue dedicated to the conference on sustainable development of energy, water and environment systems 2019. *Renewable and Sustainable Energy Reviews*, *143*, 110920. https://doi.org/10.1016/j.rser.2021.110920

Görling, A. (1999). Density-functional theory beyond the Hohenberg-Kohn theorem. *Physical Review A*, *59*(5), 3359-3374. https://doi.org/10.1103/physreva.59.3359

Gottschall, T., Skokov, K. P., Fries, M., Taubel, A., Radulov, I., Scheibel, F., Benke, D., Riegg, S., & Gutfleisch, O. (2019). Making a cool choice: The materials library of magnetic refrigeration. *Advanced Energy Materials*, *9*(34), 1901322. https://doi.org/10.1002/aenm.201901322

Grimme, S., Ehrlich, S., & Goerigk, L. (2011). Effect of the damping function in dispersion corrected density functional theory. *Journal of Computational Chemistry*, *32*(7), 1456-1465. https://doi.org/10.1002/jcc.21759

Grunner, M. E., Keune, W., Cuenya, B. R., Weis, C., Landers, J., Makarov, S. I., & Krautz, M. (2015). Element-resolved thermodynamics of magnetocaloric LaFe $13-$ x Si x. *Physical Review Letters*, *114*(5), 057202-057208. https://doi.org/10.1103/physrevlett.114.057202

Gschneidner Jr., K., Pecharsky, V., Pecharsky, A., & Zimm, C. (1999). Recent developments in magnetic refrigeration. *Materials Science Forum*, *315-317*, 69-76. https://doi.org/10.4028/www.scientific.net/msf.315-317.69

Gschneidner, K. A., & Pecharsky, V. K. (2000). Magnetocaloric materials. *Annual Review of Materials Science*, *30*(1), 387-429. https://doi.org/10.1146/annurev.matsci.30.1.387

Gschneidner, K., & Pecharsky, V. (2008). Thirty years of near room temperature magnetic cooling: Where we are today and future prospects. *International Journal of Refrigeration*, *31*(6), 945-961. https://doi.org/10.1016/j.ijrefrig.2008.01.004

Guillou, F., Ollefs, K., Wilhelm, F., Rogalev, A., Yaresko, A. N., Yibole, H., ... & Brück, E. (2015). Electronic and magnetic properties of phosphorus across the first-order ferromagnetic transition of (Mn, Fe) 2 (P, Si, B) giant magnetocaloric materials. *Physical Review B*, *92*(22), 224427. https://doi.org/10.1103/physrevb.92.224427

Guillou, F., Yibole, H., Van Dijk, N., Zhang, L., Hardy, V., & Brück, E. (2014). About the mechanical stability of MnFe(P,Si,B) giant-magnetocaloric materials. *Journal of Alloys and Compounds*, *617*, 569-574. https://doi.org/10.1016/j.jallcom.2014.08.061

Guo, Z. B., Zhang, J. R., Huang, H., Ding, W. P., & Du, Y. W. (1997). Large magnetic entropy change in La0.75Ca0.25MnO3. *Applied Physics Letters*, *70*(7), 904-905. https://doi.org/10.1063/1.118309

Guo, Z., Yang, W., Shen, Y., & Du, Y. (1998). Magnetic entropy change in La0.75Ca0.25−xSrxMnO3 perovskites. *Solid State Communications*, *105*(2), 89-92. https://doi.org/10.1016/s0038-1098(97)10064-3

Gutfleisch, O., Willard, M. A., Brück, E., Chen, C. H., Sankar, S. G., & Liu, J. P. (2010). Magnetic materials and devices for the 21st century: Stronger, lighter, and more energy efficient. *Advanced Materials*, *23*(7), 821-842. https://doi.org/10.1002/adma.201002180

Gutfleisch, O., Yan, A., & Müller, K. (2005). Large magnetocaloric effect in melt-spun LaFe13−xSix. *Journal of Applied Physics*, *97*(10), 10M305. https://doi.org/10.1063/1.1847871

Hadimani, R. L., Melikhov, Y., Snyder, J. E., & Jiles, D. C. (2008). Estimation of second order phase transition temperature of the orthorhombic phase of Gd5(SixGe1−x)4 using Arrott plots. *Journal of Applied Physics*, *103*(3), 033906. https://doi.org/10.1063/1.2841728

Hafner, J. (2008). Ab-initio simulations of materials using VASP: Density-functional theory and beyond. *Journal of Computational Chemistry*, *29*(13), 2044-2078. https://doi.org/10.1007/3-540-35273-2_7

Hamann, D. R., Schlüter, M., & Chiang, C. (1979). Norm-conserving Pseudopotentials. *Physical Review Letters*, *43*(20), 1494-1497. https://doi.org/10.1103/physrevlett.43.1494

Han, M., & Miller, J. (2008). An application of the "Coloring Problem": Structure−Composition−Bonding Relationships in the Magnetocaloric Materials $LaFe_{13-x}Si_x$. *Inorganic Chemistry*, *47*(2), 515-528. https://doi.org/10.1021/ic701311b.s002

Hanh, V. T., Chau, L. H., Dong, V. L., & Chinh, P. D. (2019). Estimates for the elastic moduli of 2D aggregate of hexagonal-shape orthorhombic crystals with in-plane random crystalline orientations. *Vietnam Journal of Mechanics*, *41*(2), 171-177. https://doi.org/10.15625/0866-7136/13183

Hashimoto, T., Kuzuhara, T., Matsumoto, K., Sahashi, M., Imonata, K., Tomokiyo, A., & Yayama, H. (1987). A new method of producing the magnetic refrigerant suitable for the ericsson magnetic refrigeration. *IEEE Transactions on Magnetics*, *23*(5), 2847-2849. https://doi.org/10.1109/tmag.1987.1065717

He, J., Wu, Y., Chen, X., Lu, Y., Ma, C., Du, C., Liu, G., & Ma, R. (2015). Experimental study of a miniature vapor compression refrigeration system with two heat sink evaporators connected in series or in parallel. *International Journal of Refrigeration*, *49*, 28-35. https://doi.org/10.1016/j.ijrefrig.2014.10.010

Her, Jim Long, Keiichi Koyama, Kazuo Watanabe, Virgil Provenzano, Anqi Fu, Alexander J. Shapiro, and Robert D. Shull. "High-Magnetic Field X-ray Diffraction Studies on Gd5 (Ge2− xFex) Si2 (x= 0.05 and 0.2)." *Materials transactions* 46, no. 9 (2005): 2011-2014 https://doi.org/10.2320/matertrans.46.2011.

Hermes, C. J., Melo, C., Knabben, F. T., & Gonçalves, J. M. (2009). Prediction of the energy consumption of household refrigerators and freezers via steady-state simulation. *Applied Energy*, *86*(7-8), 1311-1319. https://doi.org/10.1016/j.apenergy.2008.10.008

Hernández-González, E. L., Palomares-Sánchez, S. A., Elizalde Galindo, J. T., & Mirabal-Garcia, M. (2014). Magnetocaloric effect near room temperature of La0.67Ca0.33−x SR X MnO3 (X = 0.06, 0.07, 0.08) manganites. *Journal of Superconductivity and Novel Magnetism*, *28*(5), 1635-1638. https://doi.org/10.1007/s10948-014-2932-2

Hien, N. T., & Thuy, N. P. (2002). Preparation and magneto-caloric effect of La1−xAgxMnO3 (x=0.10–0.30) perovskite compounds. *Physica B: Condensed Matter*, *319*(1-4), 168-173. https://doi.org/10.1016/s0921-4526(02)01118-3

Hillerbrand, R. (2018). Why affordable clean energy is not enough. A capability perspective on the sustainable development goals. *Sustainability*, *10*(7), 24-85.

Höglin, V., Cedervall, J., Andersson, M. S., Sarkar, T., Hudl, M., Nordblad, P., Andersson, Y., & Sahlberg, M. (2015). Phase diagram, structures and magnetism of the FeMnP1−xSix-system. *RSC Advances*, *5*(11), 8278-8284. https://doi.org/10.1039/c4ra15419c

Hou, D., Bai, Y., Xu, J., Tang, G., & Nie, X. (2004). Magnetic entropy change in La0.67−Ca0.33MnO3. *Journal of Alloys and Compounds*, *384*(1-2), 62-66. https://doi.org/10.1016/j.jallcom.2004.04.076 https://doi.org/10.3390/su10072485

Hu, F. X., Shen, B. G., Sun, J. R., Wang, G. J., & Gao, J. (2007). Magnetic properties and magnetocaloric effect around phase boundary in La(FexAl1−x)13 compounds. *Journal of Applied Physics*, *101*(9), 09C525. https://doi.org/10.1063/1.2713219

Hu, F., Shen, B., & Sun, J. (2000). Magnetic entropy change in Ni51.5Mn22.7Ga25.8 alloy. *Applied Physics Letters*, *76*(23), 3460-3462. https://doi.org/10.1063/1.126677

Hu, F., Shen, B., Sun, J., Cheng, Z., & Zhang, X. (2000). Magnetic entropy change in La(Fe0.98Co0.02)11.7 Al1.3. *Journal of Physics: Condensed Matter*, *12*(46), L691-L696. https://doi.org/10.1088/0953-8984/12/46/101

Hu, F., Shen, B., Sun, J., Wang, G., & Cheng, Z. (2002). Very large magnetic entropy change near room temperature in LaFe11.2Co0.7Si1.1. *Applied Physics Letters*, *80*(5), 826-828. https://doi.org/10.1063/1.1447592

Huang, B., Lai, J., Zeng, D., Zheng, Z., Harrison, B., Oort, A., Van Dijk, N., & Brück, E. (2019). Development of an experimental rotary magnetic refrigerator prototype. *International Journal of Refrigeration*, *104*, 42-50. https://doi.org/10.1016/j.ijrefrig.2019.04.029

Huang, S., Li, W., Lu, S., Tian, F., Shen, J., Holmström, E., & Vitos, L. (2015). Temperature dependent stacking fault energy of FeCrCoNiMn high entropy alloy. *Scripta Materialia*, *108*, 44-47. https://doi.org/10.1016/j.scriptamat.2015.05.041

Hueso, L. E., Sande, P., Miguéns, D. R., Rivas, J., Rivadulla, F., & López-Quintela, M. A. (2002). Tuning of the magnetocaloric effect in La[sub 0.67]Ca[sub 0.33]MnO[sub 3−δ] nanoparticles synthesized by Sol–gel techniques. *Journal of Applied Physics*, *91*(12), 9943. https://doi.org/10.1063/1.1476972

Jasiukiewicz, C., & Karpus, V. (2003). Debye temperature of cubic crystals. *Solid State Communications*, *128*(5), 167-169. https://doi.org/10.1016/j.ssc.2003.08.008

Jeong, S. (2014). AMR (Active magnetic regenerative) refrigeration for low temperature. *Cryogenics*, *62*, 193-201. https://doi.org/10.1016/j.cryogenics.2014.03.015

Jiang, D., Wu, M., Liu, D., Li, F., Chai, M., & Liu, S. (2019). Structural stability, electronic structures, mechanical properties and Debye temperature of transition metal impurities in tungsten: A first-principles study. *Metals*, *9*(9), 967. https://doi.org/10.3390/met9090967

Jiles, D. (2015). *Introduction to magnetism and magnetic materials*. https://doi.org/10.1201/b18948

Johnson, F., & Shull, R. D. (2006). Amorphous-fecocrzrb ferromagnets for use as high-temperature magnetic refrigerants. *Journal of Applied Physics*, *99*(8), 08K909. https://doi.org/10.1063/1.2172234

Jonker, G., & Van Santen, J. (1950). Ferromagnetic compounds of manganese with perovskite structure. *Physica*, *16*(3), 337-349. https://doi.org/10.1016/0031-8914(50)90033-4

Juan, Z., Lirong, L., & Gui, W. (2011). Synthesis and magnetocaloric properties of La0.85K0.15MnO3 nanoparticles. *Advanced Powder Technology*, *22*(1), 68-71. https://doi.org/10.1016/j.apt.2010.03.012

Jun, S., Yang-Xian, L., Ji-Rong, S., & Bao-Gen, S. (2009). Effect of R substitution on magnetic properties and magnetocaloric effects of La1− xRxFe11. 5Si1. 5 compounds with R= Ce, Pr and Nd. *Chinese Physics B*, *18*(5), 2058. https://doi.org/10.1088/1674-1056/18/5/055

Khandy, S. A., Islam, I., Gupta, D. C., Khenata, R., & Laref, A. (2019). Lattice dynamics, mechanical stability and electronic structure of FE-based Heusler semiconductors. *Scientific Reports*, *9*(1), 777-780. https://doi.org/10.1038/s41598-018-37740-y

Kim, J., Ulyanov, A., Kang, Y., Min, S., Yu, S., & Yoo, S. (2007). Influence of structural-phase transition on the magnetocaloric effects of lanthanum manganites. *Journal of Magnetism and Magnetic Materials*, *310*(2), 2818-2819. https://doi.org/10.1016/j.jmmm.2006.10.964

Kitanovski, A. (2020). Energy applications of Magnetocaloric materials. *Advanced Energy Materials*, *10*(10), 1903741. https://doi.org/10.1002/aenm.201903741

Kitanovski, A., & Egolf, P. W. (2009). Application of magnetic refrigeration and its assessment. *Journal of Magnetism and Magnetic Materials*, *321*(7), 777-781. https://doi.org/10.1016/j.jmmm.2008.11.078

Kitanovski, A., Plaznik, U., Tušek, J., & Poredoš, A. (2014). New thermodynamic cycles for magnetic refrigeration. *International Journal of Refrigeration*, *37*, 28-35. https://doi.org/10.1016/j.ijrefrig.2013.05.014

Kokalj, A. (1999). XCrySDen—a new program for displaying crystalline structures and electron densities. *Journal of Molecular Graphics and Modelling*, *17*(3-4), 176-179. https://doi.org/10.1016/s1093-3263(99)00028-5

Koubaa, M., Cheikh-Rouhou Koubaa, W., & Cheikhrouhou, A. (2009). Magnetocaloric effect in polycrystalline la 0.65 BA 0.3 M 0.05 MnO 3 (M =Na, Ag, K) manganites. *Journal of Magnetism and Magnetic Materials*, *321*(21), 3578-3584. https://doi.org/10.1016/j.jmmm.2009.05.002

Krenke, T., Duman, E., Acet, M., Wassermann, E. F., Moya, X., Mañosa, L., & Planes, A. (2005). Inverse magnetocaloric effect in ferromagnetic Ni–mn–Sn alloys. *Nature Materials*, *4*(6), 450-454. https://doi.org/10.1038/nmat1395

Kresse, G. (1995). AB initio molecular dynamics for liquid metals. *Journal of Non-Crystalline Solids*, *192-193*, 222-229. https://doi.org/10.1016/0022-3093(95)00355-x

Kresse, G., & Furthmüller, J. (1996). Efficiency of AB-initio total energy calculations for metals and semiconductors using a plane-wave basis set. *Computational Materials Science*, *6*(1), 15-50. https://doi.org/10.1016/0927-0256(96)00008-0

Kresse, G., & Joubert, D. (1999). From ultrasoft pseudopotentials to the projector augmented-wave method. *Physical Review B*, *59*(3), 1758-1775. https://doi.org/10.1103/physrevb.59.1758

Krypiakewytsch, P. I., Zaretschniuk, O. S., Gladyschewskyj, E. I., & Bodak, O. I. (1968). NaZn13 type alloys. *Z Anorg Chem*, *358*, 90. *Zeitschrift for anorganische und allgemeine Chemie*, *358*(1-2), 90-96. https://doi.org/10.1002/zaac.19683580110

Kulińska, A., Wodniecka, B., & Wodniecki, P. (2006). The perturbed angular correlation studies of Ag–Zr compounds with 111Cd probes. *Journal of Alloys and Compounds*. 426(2), 76-82. https://doi.org/10.1016/j.jallcom.2006.04.028

Kulińska, A., Wodniecka, B., & Wodniecki, P. (2006). The perturbed angular correlation studies of ag–zr compounds with 111Cd probes. *Journal of Alloys and Compounds*, *426*(1-2), 76-82. https://doi.org/10.1016/j.jallcom.2006.04.028

Laajimi, K., Khlifi, M., Hlil, E. K., Gazzah, M. H., & Dhahri, J. (2019). Enhancement of magnetocaloric effect by Nickel substitution in La0. 67Ca0. 33Mn0. 98Ni0. 02O3 manganite oxide. *Journal of Magnetism and Magnetic Materials*, *491*, 165625. https://doi.org/10.1016/j.jmmm.2019.165625

Le, T., Epa, V. C., Burden, F. R., & Winkler, D. A. (2012). Quantitative structure–property relationship modeling of diverse materials properties. *Chemical Reviews*, *112*(5), 2889-2919. https://doi.org/10.1021/cr200066h

Ledbetter, H. M. (1977). Elastic properties of zinc: A compilation and a review. *Journal of Physical and Chemical Reference Data*, *6*(4), 1181-1203. https://doi.org/10.1063/1.555564

Lemmon, E. W., & Span, R. (2015). Thermodynamic properties of R-227ea, R-365mfc, R-115, and R-13I1. *Journal of Chemical & Engineering Data*, *60*(12), 3745-3758. https://doi.org/10.1021/acs.jced.5b00684

Levin, E. M., Gschneidner Jr, K. A., & Pecharsky, V. K. (2002). Magnetic correlations induced by magnetic field and temperature in Gd 5 Ge 4. *Physical Review B*, *65*(21), 214427. https://doi.org/10.1103/physrevb.65.214427

Li, S., de La Cruz, C., Huang, Q., Chen, Y., Lynn, J. W., Hu, J., ... & Dai, P. (2009). First-order magnetic and structural phase transitions in Fe 1+ y Se x Te 1− x. *Physical Review B*, *79*(5), 054503. https://doi.org/10.1103/physrevb.79.054503

Lines, M. (1979). Elastic properties of magnetic materials. *Physics Reports*, *55*(2), 133-181. https://doi.org/10.1016/0370-1573(79)90039-5

Liu, D., Yue, M., Zhang, J., McQueen, T. M., Lynn, J. W., Wang, X., ... & Huang, Q. (2009). Origin and tuning of the magnetocaloric effect in the magnetic refrigerant Mn 1.1 Fe 0.9 (P0.8Ge0.2). *PhysicalReviewB*, *79*(1),014435. https://doi.org/10.1103/physrevb.79.014435

Liu, H., Tang, S., Ma, Y., Liu, W., & Liang, C. (2021). Short-range ordering governs brittleness and ductility in W-Ta solid solution: Insights from Pugh's shear-to-bulk modulus ratio. *Scripta Materialia*, *204*, 114136. https://doi.org/10.1016/j.scriptamat.2021.114136

Liu, J., Krautz, M., Skokov, K., Woodcock, T. G., & Gutfleisch, O. (2011). Systematic study of the microstructure, entropy change and adiabatic temperature change in optimized La–E–Sialloys. *ActaMaterialia*, *59*(9),3602-3611. https://doi.org/10.1016/j.actamat.2011.02.033

Liu, J., Zhang, P., Dai, F., & Yan, A. (2013). A new approach to prepare spherical La–FE–Si–Co magnetocaloric refrigerant particles. *Scripta Materialia*, *69*(6), 485-488. https://doi.org/10.1016/j.scriptamat.2013.06.009

Liu, X. B., Liu, X. D., & Altounian, Z. (2005). Phase formation and magnetocaloric effect in rapidly quenched La(Fe1−xCox)11.4Si1.6. *Journal of Applied Physics*, *98*(11), 113904. https://doi.org/10.1063/1.2137884

Liu, Z., Li, H., Fan, C., & Luo, W. (2017). Necessary and sufficient elastic stability conditions in 21 quasicrystal Laue classes. *European Journal of Mechanics - A/Solids*, *65*, 30-39. https://doi.org/10.1016/j.euromechsol.2017.02.007

Lobo, D. N., Priolkar, K. R., Emura, S., & Nigam, A. K. (2014). Ferromagnetic interactions and martensitic transformation in FE doped Ni-mn-In shape memory alloys. *Journal of Applied Physics*, *116*(18), 183903. https://doi.org/10.1063/1.4901469

Lozano, J. A., Capovilla, M. S., Trevizoli, P. V., Engelbrecht, K., Bahl, C. R., & Barbosa, J. R. (2016). Development of a novel rotary magnetic refrigerator. *International Journal of Refrigeration*, *68*, 187-197. https://doi.org/10.1016/j.ijrefrig.2016.04.005

Ma, S., Wurentuya, B., Wu, X., Jiang, Y., Tegus, O., Guan, P., & Narsu, B. (2017). AB initio mechanical and thermal properties of FeMnP1−xGa compounds as refrigerant for room-temperature magnetic refrigeration. *RSC Advances*, *7*(44), 27454-27463. https://doi.org/10.1039/c7ra04274d

Mackinnon, I. D., Talbot, P. C., & Alarco, J. A. (2017). Phonon dispersion anomalies and superconductivity in metal substituted MgB2. *Computational Materials Science*, *130*, 191-203. https://doi.org/10.1016/j.commatsci.2017.01.011

Maradudin, A. A. (1963). Lattice dynamics. *Annual Review of Physical Chemistry*, *14*(1), 89-116. https://doi.org/10.1146/annurev.pc.14.100163.000513

Mayrhofer, P. H., Music, D., & Schneider, J. M. (2006). Influence of the al distribution on the structure, elastic properties, and phase stability of supersaturated Ti1−xAlxN. *Journal of Applied Physics*, *100*(9), 094906. https://doi.org/10.1063/1.2360778

Methfessel, M., & Paxton, A. T. (1989). High-precision sampling for brillouin-zone integration in metals. *Physical Review B*, *40*(6), 3616-3621. https://doi.org/10.1103/physrevb.40.3616

Mezaal, N. A., Osintsev, K. V., & Zhirgalova, T. B. (2017). Review of magnetic refrigeration system as alternative to conventional refrigeration system. *IOP Conference Series: Earth and Environmental Science*, *87*, 032024. https://doi.org/10.1088/1755-1315/87/3/032024

Min, S., Kim, K., Yu, S., Suh, H., & Lee, S. (2005). undefined. *IEEE Transactions on Magnetics*, *41*(10), 2760-2762. https://doi.org/10.1109/tmag.2005.854823

Mira, J., Rivas, J., Hueso, L. E., Rivadulla, F., & López Quintela, M. A. (2002). Drop of magnetocaloric effect related to the change from first- to second-order magnetic phase transition in La[2/3](Ca[1−x]Sr[sub x])[1/3]MnO[3]. *Journal of Applied Physics*, *91*(10), 8903. https://doi.org/10.1063/1.1451892

Monkhorst, H. J., & Pack, J. D. (1976). Special points for brillouin-zone integrations. *Physical Review B*, *13*(12), 5188-5192. https://doi.org/10.1103/physrevb.13.5188

Morelli, D. T., Mance, A. M., Mantese, J. V., & Micheli, A. L. (1996). Magnetocaloric properties of doped lanthanum manganite films. *Journal of Applied Physics*, *79*(1), 373-375. https://doi.org/10.1063/1.360840

Morellon, L., Algarabel, P. A., Ibarra, M. R., Blasco, J., Garcia-Landa, B., Arnold, Z., & Albertini, F. (1998). Magnetic-field-induced structural phase transition in Gd 5 (S i 1.8 Ge 2.2). *Physical Review B*, *58*(22), R14721. https://doi.org/10.1103/physrevb.58.r14721

Mudryk, Y., & Pecharsky, V. K. (2020). 4.8 materials for solid state cooling. *Rare Earth Chemistry*, *6(4),* 487-510. https://doi.org/10.1515/9783110654929-031

Murnaghan, F. D. (1944, January). A modern presentation of quaternions. In Proceedings of the Royal Irish Academy. *Mathematical and Physical Sciences*. 10, 104-112.

Music, D., & Schneider, J. M. (2006). Elastic properties of MFe3N (M=Ni, PD, Pt) studied by *ab initio* calculations. *Applied Physics Letters*, *88*(3), 031914. https://doi.org/10.1063/1.2165285

Music, D., Takahashi, T., Vitos, L., Asker, C., Abrikosov, I. A., & Schneider, J. M. (2007). Elastic properties of FE–mn random alloys studied by *ab initio* calculations. *Applied Physics Letters*, *91*(19), 191904. https://doi.org/10.1063/1.2807677

Nagalakshmi, R., Kulkarni, R., Dhar, S., Thamizhavel, A., Krishnakumar, V., Reiffers, M., Čurlík, I., Hagemann, H., Lovy, D., & Nallamuthu, S. (2015). Magnetic properties of the tetragonal RCuGa3 (R=Pr, ND and Gd) single crystals. *Journal of Magnetism and Magnetic Materials*, *386*, 37-43. https://doi.org/10.1016/j.jmmm.2015.03.017

Nakashima, A. T., Fortkamp, F. P., De Sá, N. M., Dos Santos, V. M., Hoffmann, G., Peixer, G. F., Dutra, S. L., Ribeiro, M. C., Lozano, J. A., & Barbosa, J. R. (2021). A magnetic wine cooler prototype. *International Journal of Refrigeration*, *122*, 110-121. https://doi.org/10.1016/j.ijrefrig.2020.11.015

Nakashima, A., Peixer, G., Lozano, J., & Barbosa, J. (2022). A lumped-element magnetic refrigerator model. *Applied Thermal Engineering*, *204*, 117918. https://doi.org/10.1016/j.applthermaleng.2021.117918

Naumov, P., Karothu, D. P., Ahmed, E., Catalano, L., Commins, P., Mahmoud Halabi, J., Al-Handawi, M. B., & Li, L. (2020). The rise of the dynamic crystals. *Journal of the American Chemical Society*, *142*(31), 13256-13272. https://doi.org/10.1021/jacs.0c05440

Nayak, A. K., Suresh, K. G., & Nigam, A. K. (2009). Giant inverse magnetocaloric effect near room temperature in Co substituted NiMnSb Heusler alloys. *Journal of Physics D: Applied Physics*, *42*(3), 035009. https://doi.org/10.1088/0022-3727/42/3/035009

Newnham, R. E. (1975). Magnetic materials. *Structure-Property Relations*, 144-172. https://doi.org/10.1007/978-3-642-50017-6_6

Niu L. (2016). *Bayesian cluster expansion with lattice parameter dependence for studying surface alloys* [Doctoral dissertation]. Johns Hopkins University

Nye, J. (1985). *Physical properties of crystals: their representation by tensors and matrices*. Oxford university press.

Oesterreicher, H., & Parker, F. T. (1984). Magnetic cooling near Curie temperatures above 300 K. *Journal of Applied Physics*, *55*(12), 4334-4338. https://doi.org/10.1063/1.333046

Orestes, E., Capelle, K., Da Silva, A. B., & Ullrich, C. A. (2007). Generator coordinate method in time-dependent density-functional theory: Memory made simple. *The Journal of Chemical Physics*, *127*(12), 124101. https://doi.org/10.1063/1.2768368

Ou, Z., Zhang, L., Dung, N., Van Eijck, L., Mulders, A., Avdeev, M., Van Dijk, N., & Brück, E. (2013). Neutron diffraction study on the magnetic structure of fe2p-based $Mn_{0.66}Fe_{1.29}P_{1-x}Si_x$ melt-spun ribbons. *Journal of Magnetism and Magnetic Materials*, *340*, 80-85. https://doi.org/10.1016/j.jmmm.2013.03.028

Paier, J., Marsman, M., Hummer, K., Kresse, G., Gerber, I. C., & Ángyán, J. G. (2006). Screened hybrid density functionals applied to solids. *The Journal of Chemical Physics*, *124*(15), 154709. https://doi.org/10.1063/1.2187006

Park, I., & Jeong, S. (2017). Development of the active magnetic regenerative refrigerator operating between 77 K and 20 K with the conduction cooled high temperature superconducting magnet. *Cryogenics*, *88*, 106-115. https://doi.org/10.1016/j.cryogenics.2017.09.008

Park, J., Kim, S., Park, I., & Jeong, S. (2014). Experimental investigation of AC loss in a conduction-cooled layer-wound (RE)BCO magnet for continuous adiabatic demagnetization refrigerator (ADR). *Cryogenics*, *63*, 77-84. https://doi.org/10.1016/j.cryogenics.2014.07.008

Passamani, E. C., Xavier, F., Favre-Nicolin, E., Larica, C., Takeuchi, A. Y., Castro, I. L., & Proveti, J. R. (2009). Magnetic properties of nimn-based Heusler alloys influenced by FE atoms replacing Mn. *Journal of Applied Physics*, *105*(3), 033919. https://doi.org/10.1063/1.3075835

Pavone, P., Karch, K., Schütt, O., Strauch, D., Windl, W., Giannozzi, P., & Baroni, S. (1993). *Ab initio*lattice dynamics of diamond. *Physical Review B*, *48*(5), 3156-3163. https://doi.org/10.1103/physrevb.48.3156

Payne, M. C., Teter, M. P., Allan, D. C., Arias, T. A., & Joannopoulos, J. D. (1992). Iterative minimization techniques for*ab initio*total-energy calculations: Molecular dynamics and conjugate gradients. *Reviews of Modern Physics*, *64*(4), 1045-1097. https://doi.org/10.1103/revmodphys.64.1045

Pecharsky, V. K., & Gschneidner, Jr., K. A. (1997). Giant Magnetocaloric effect in $Gd_5(Si_2Ge_2)$. *Physical Review Letters*, *78*(23), 4494-4497. https://doi.org/10.1103/physrevlett.78.4494

Pecharsky, V. K., & Gschneidner, K. A. (1999). Magnetocaloric effect from indirect measurements: Magnetization and heat capacity. *Journal of Applied Physics*, *86*(1), 565-575. https://doi.org/10.1063/1.370767

Pecharsky, V. K., Cui, J., & Johnson, D. D. (2016). (Magneto)caloric refrigeration: Is there light at the end of the tunnel? *Philosophical Transactions of the Royal Society A: Mathematical, Physical and Engineering Sciences*, *374*(2074), 20150305. https://doi.org/10.1098/rsta.2015.0305

Peixer, G. F., Dutra, S. L., Calomeno, R. S., Sá, N. M., Lang, G. B., Lozano, J. A., & Barbosa, J. R. (2022). Influence of heat exchanger design on the thermal performance of a domestic wine cooler driven by a magnetic refrigeration system. *Anais da Academia Brasileira de Ciências*, *94*(1), e20200563. https://doi.org/10.1590/0001-3765202220200563

Pękała, M., & Drozd, V. (2008). Magnetocaloric effect in nano- and polycrystalline La0.8Sr0.2MnO3 manganites. *Journal of Non-Crystalline Solids*, *354*(47-51), 5308-5314. https://doi.org/10.1016/j.jnoncrysol.2008.06.112

Perdew, J. P., Burke, K., & Ernzerhof, M. (1998). Perdew, Burke, and Ernzerhof reply:. *Physical Review Letters*, *80*(4), 891-891. https://doi.org/10.1103/physrevlett.80.891

Perdew, J. P., Ruzsinszky, A., Tao, J., Staroverov, V. N., Scuseria, G. E., & Csonka, G. I. (2005). Prescription for the design and selection of density functional approximations: More constraint satisfaction with fewer fits. *The Journal of Chemical Physics*, *123*(6), 062201. https://doi.org/10.1063/1.1904565

Phan, M., & Yu, S. (2007). Review of the magnetocaloric effect in manganite materials. *Journal of Magnetism and Magnetic Materials*, *308*(2), 325-340. https://doi.org/10.1016/j.jmmm.2006.07.025

Phan, M., Peng, H., Yu, S., & Hwi Hur, N. (2005). Large magnetic entropy change above 300K in a La0.7Ca0.2Sr0.1MnO3 single crystal. *Journal of Magnetism and Magnetic Materials*, *290-291*, 665-668. https://doi.org/10.1016/j.jmmm.2004.11.330

Phan, M., Yu, S., & Hur, N. (2003). Magnetic and magnetocaloric properties of (La1−x)0.8Ca0.2MnO3 (x=0.05, 0.20) single crystals. *Journal of Magnetism and Magnetic Materials*, *262*(3), 407-411. https://doi.org/10.1016/s0304-8853(03)00071-4

Planes, A., Mañosa, L., Moya, X., Krenke, T., Acet, M., & Wassermann, E. (2007). Magnetocaloric effect in Heusler shape-memory alloys. *Journal of Magnetism and Magnetic Materials*, *310*(2), 2767-2769. https://doi.org/10.1016/j.jmmm.2006.10.1041

Podmiljsak, B., J. McGuiness, P., & Kobe, S. (2015). Complex metallic alloys for applications in magnetic refrigeration. *Recent Patents on Materials Science*, *8*(2), 129-154. https://doi.org/10.2174/1874464808666150427223327

Protocol, M. (1987). Montreal protocol on substances that deplete the ozone layer. *Washington, DC: US Government Printing Office*, *26*, 128-136.

Pugh, S. (1954). XCII. Relations between the elastic moduli and the plastic properties of polycrystalline pure metals. *The London, Edinburgh, and Dublin Philosophical Magazine and Journal of Science*, *45*(367), 823-843. https://doi.org/10.1080/14786440808520496

Purvis, M., Hunt, J., & Drake, F. (2001). Global atmospheric change and the UK refrigeration industry: Redefining problems and contesting solutions. *Geoforum*, *32*(2), 143-156. https://doi.org/10.1016/s0016-7185(00)00010-5

Qiu, L., Zhu, N., Feng, Y., Michaelides, E. E., Żyła, G., Jing, D., Zhang, X., Norris, P. M., Markides, C. N., & Mahian, O. (2020). A review of recent advances in thermophysical properties at the nanoscale: From solid state to colloids. *Physics Reports*, *843*, 1-81. https://doi.org/10.1016/j.physrep.2019.12.001

Ramli, M., Nuawi, M., Rasani, M., Ngatiman, N., Basar, M., & Ghani, A. A. (2020). Analysis of young modulus and Poisson ratio using I-kaz 4d analysis method through piezofilm sensor. *Journal of Physics: Conference Series*, *1529*(4), 042025. https://doi.org/10.1088/1742-6596/1529/4/042025

Romero Gómez, J., Ferreiro Garcia, R., De Miguel Catoira, A., & Romero Gómez, M. (2013). Magnetocaloric effect: A review of the thermodynamic cycles in magnetic refrigeration. *Renewable and Sustainable Energy Reviews*, *17*, 74-82. https://doi.org/10.1016/j.rser.2012.09.027

Roy, P., Torun, E., & De Groot, R. A. (2016). Effect of doping and elastic properties in (Mn, Fe) (Si,P). *Physical Review B*, *93*(9), 094110. https://doi.org/10.1103/physrevb.93.094110

Roy, S., Chattopadhyay, M., Manekar, M., Sokhey, K., & Chaddah, P. (2006). First order magneto-structural transition in functional magnetic materials: Phase-coexistence and metastability. *Bulletin of Materials Science*, *29*(6), 623-631. https://doi.org/10.1007/s12034-006-0014-1

Sasaki, T., Sonoda, S., Yamamoto, Y., Suga, K., Shimizu, S., Kindo, K., & Hori, H. (2002). Magnetic and transport characteristics on high Curie temperature ferromagnet of mn-doped Gan. *Journal of Applied Physics*, *91*(10), 7911-7913. https://doi.org/10.1063/1.1451879

Sato, H., Sugawara, H., Aoki, Y., & Harima, H. (2009). Chapter one magnetic properties of filled skutterudites. *Handbook of Magnetic Materials*, 1-110. https://doi.org/10.1016/s1567-2719(09)01801-0

Shamberger, P. J., & Ohuchi, F. S. (2009). Hysteresis of the martensitic phase transition in magnetocaloric-effect Ni-mn-Sn alloys. *Physical Review B*, *79*(14), 777-780. https://doi.org/10.1103/physrevb.79.144407

Shao, Y., Liu, Y., Wang, K., Zhang, M., & Liu, J. (2020). Impact of interface structure on functionality in hot-pressed La-FE-Si/FE magnetocaloric composites. *Acta Materialia*, *195*, 163-171. https://doi.org/10.1016/j.actamat.2020.04.042

Sharma, P., & Verma, V. (2015). Structural, magnetic and electrical properties of la and Mn Co-substituted BFO samples prepared by the Sol–gel technique. *Journal of Magnetism and Magnetic Materials*, *374*, 18-21. https://doi.org/10.1016/j.jmmm.2014.08.002

Shen, J., Gao, B., Dong, Q., Li, Y., Hu, F., Sun, J., & Shen, B. (2008). Magnetocaloric effect in La1− xPrxFe10. 7Co0. 8Si1. 5 compounds near room temperature. *Journal of Physics D: Applied Physics*, *41*(24), 245005. https://doi.org/10.1088/0022-3727/41/24/245005

Shen, J., Li, Y., Hu, F., & Sun, J. (2009). Effect of substitution of Co for FE on the magnetic hysteresis loss and the refrigerant capacity in the La0.5Pr0.5Fe11.5Si1.5 compounds. *Journal of Applied Physics*, *105*(7), 07A901. https://doi.org/10.1063/1.3055188

Shi, Y., & Wasserman, A. (2021). Inverse Kohn–sham density functional theory: Progress and challenges. *The Journal of Physical Chemistry Letters*, *12*(22), 5308-5318. https://doi.org/10.1021/acs.jpclett.1c00752

Shobana, M., & Meher, S. (2019). Effect of Cobalt doping on the structural, optical and magnetic properties of Sol-gel derived ZnS nanocrystalline thin films and AB initio studies. *Thin Solid Films*, *683*, 97-110. https://doi.org/10.1016/j.tsf.2019.05.037

Sholl, D. & Steckel, J. (2011). *Density functional theory: a practical introduction*. John Wiley and Sons.

Shoukourian, H., & Kranzlmüller, D. (2020). Forecasting power-efficiency related key performance indicators for modern data centers using LSTMs. *Future Generation Computer Systems*, *112*, 362-382. https://doi.org/10.1016/j.future.2020.05.014

Shull, R. D., Provenzano, V., Shapiro, A. J., Fu, A., Lufaso, M. W., Karapetrova, J., Kletetschka, G., & Mikula, V. (2006). The effects of small metal additions (Co,Cu,Ga,Mn,Al,Bi,Sn) on the magnetocaloric properties of the Gd5Ge2Si2 alloy. *Journal of Applied Physics*, *99*(8), 08K908. https://doi.org/10.1063/1.2173632

Smaïli, A., & Chahine, R. (1997). Composite materials for ericsson-like magnetic refrigeration cycle. *Journal of Applied Physics*, *81*(2), 824-829. https://doi.org/10.1063/1.364166

Smedley, K., & Abravomitz, A. (2011). Development of fault current controller technology.

Smith, A. (2013). Who discovered the magnetocaloric effect? *The European Physical Journal H*, *38*(4), 507-517. https://doi.org/10.1140/epjh/e2013-40001-9

Sözen, A., Menlik, T., & Özbaş, E. (2012). The effect of ejector on the performance of diffusion absorption refrigeration systems: An experimental study. *Applied Thermal Engineering*, *33-34*, 44-53. https://doi.org/10.1016/j.applthermaleng.2011.09.009

Srivastava, G. P. (1984). Broyden's method for self-consistent field convergence acceleration. *Journal of Physics A: Mathematical and General*, *17*(6), L317-L321. https://doi.org/10.1088/0305-4470/17/6/002

Srivastava, G. P. (2022). Phonons in liquid helium. *The Physics of Phonons*, (pp. 375-386). https://doi.org/10.1201/9781003141273-14

Steyert, W. A. (1978). Stirling-cycle rotating magnetic refrigerators and heat engines for use near room temperature. *Journal of Applied Physics*, *49*(3), 1216-1226. https://doi.org/10.1063/1.325009

Sun, W., Li, J., Ao, W., Tang, J., & Gong, X. (2006). Hydrothermal synthesis and magnetocaloric effect of La0.7Ca0.2Sr0.1MnO3. *Powder Technology*, *166*(2), 77-80. https://doi.org/10.1016/j.powtec.2006.05.015

Sun, Z., Li, S., Ahuja, R., & Schneider, J. M. (2004). Calculated elastic properties of M2AlC (M=Ti, V, CR, NB and Ta). *Solid State Communications*, *129*(9), 589-592. https://doi.org/10.1016/j.ssc.2003.12.008

Sun, Z., Zhu, T., Wang, X., Mei, Y., & Zhang, J. Z. (2017). Optimization of convergence criteria for fragmentation methods. *Chemical Physics Letters*, *687*, 163-170. https://doi.org/10.1016/j.cplett.2017.08.059

Szewczyk, A., Szymczak, H., Wiśniewski, A., Piotrowski, K., Kartaszyński, R., Dąbrowski, B., Koleśnik, S., & Bukowski, Z. (2000). Magnetocaloric effect in La[sub 1−x]Sr[sub x]MnO[sub 3] for x=0.13 and 0.16. *Applied Physics Letters*, *77*(7), 1026. https://doi.org/10.1063/1.1288671

Szymczak, R., Kolano, R., Kolano-Burian, A., Pietosa, J., & Szymczak, H. (2010). Cooling by adiabatic pressure application in La0.7Ca0.3MnO3 magnetocaloric effect material. *Journal of Magnetism and Magnetic Materials*, *322*(9-12), 1589-1591. https://doi.org/10.1016/j.jmmm.2009.09.020

Tang, T., Gu, K., Cao, Q., Wang, D., Zhang, S., & Du, Y. (2000). Magnetocaloric properties of ag-substituted perovskite-type manganites. *Journal of Magnetism and Magnetic Materials*, *222*(1-2), 110-114. https://doi.org/10.1016/s0304-8853(00)00544-8

Tegus, O., Brück, E., Buschow, K. H., & De Boer, F. R. (2002). Transition-metal-based magnetic refrigerants for room-temperature applications. *Nature*, *415*(6868), 150-152. https://doi.org/10.1038/415150a

Thanh, D. T. C. (2009). *Magnetocalorics and magnetism in MnFe (P, Si, Ge) materials*. Universiteit van Amsterdam [Host].

Thol, M., Rutkai, G., Köster, A., Dubberke, F. H., Windmann, T., Span, R., & Vrabec, J. (2016). Thermodynamic properties of Octamethylcyclotetrasiloxane. *Journal of Chemical & Engineering Data*, *61*(7), 2580-2595. https://doi.org/10.1021/acs.jced.6b00261

Tian, N., Zhang, N. N., You, C. Y., Gao, B., & He, J. (2013). Magnetic hysteresis loss and corrosion behavior of LaFe LaFe11. 5Si1. 5 particles coated with Cu. *Journal of Applied Physics*, *113*(10), 103909. https://doi.org/10.1063/1.4795265

Tishin, M., & Spichkin, Y. (2016). *The magnetocaloric effect and its applications*. CRC Press.

Togo, A., & Tanaka, I. (2015). First principles phonon calculations in materials science. *Scripta Materialia*, *108*, 1-5. https://doi.org/10.1016/j.scriptamat.2015.07.021

Toulouse, J. (2005). Simple model of the static exchange-correlation kernel of a uniform electron gas with long-range electron-electron interaction. *Physical Review B*, *72*(3), 035117 . https://doi.org/10.1103/physrevb.72.035117

Tozri, A., Dhahri, E., & Hlil, E. (2010). Magnetic transition and magnetic entropy changes of La0.8Pb0.1MnO3 and La0.8Pb0.1Na0.1MnO3. *Materials Letters*, *64*(19), 2138-2141. https://doi.org/10.1016/j.matlet.2010.06.051

Trung, N. T., Biharie, V., Zhang, L., Caron, L., Buschow, K. H., & Brück, E. (2010). From single- to double-first-order magnetic phase transition in magnetocaloric Mn1−xCrxCoGe compounds. *Applied Physics Letters*, *96*(16), 162507. https://doi.org/10.1063/1.3399774

Trung, N. T., Ou, Z. Q., Gortenmulder, T. J., Tegus, O., Buschow, K. H., & Brück, E. (2009). Tunable thermal hysteresis in MnFe(P,Ge) compounds. *Applied Physics Letters*, *94*(10), 102513. https://doi.org/10.1063/1.3095597

Tsvetkov, O. B., Mitripov, V. V., Laptev, Y. A., Baranov, I. V., & Kustikova, M. A. (2021). Global allergens and refrigeration alarmism. *IOP Conference Series: Earth and Environmental Science*, *866*(1), 012021. https://doi.org/10.1088/1755-1315/866/1/012021

Vanderbilt, D. (1990). Soft self-consistent pseudopotentials in a generalized eigenvalue formalism. *Physical Review B*, *41*(11), 7892-7895. https://doi.org/10.1103/physrevb.41.7892

Vanov, A. O., Kantorovich, S. S., Zverev, V. S., Elfimova, E. A., Lebedev, A. V., & Pshenichnikov, A. F. (2016). Temperature-dependent dynamic correlations in suspensions

of magnetic nanoparticles in a broad range of concentrations: A combined experimental and theoretical study. *Physical Chemistry Chemical Physics*, *18*(27), 18342-18352. https://doi.org/10.1039/c6cp02793h

Varshney, D., Khan, E., & Choudhary, D. (2014). Interpretation of temperature-dependent thermoelectric power behaviour of La0. 67Ba0. 33MnO3 manganites. *Molecular Physics*, *112*(24), 3183-3188. https://doi.org/10.1080/00268976.2014.936920

Vincent, O., Mulwa, W. M., & Kirui, M. (2021). Investigation of magnetic properties of femnp1-xax (A = in, se and Sn, where X = 0.33) by use of GGA functionals. *Physica B: Condensed Matter*, *613*, 412777. https://doi.org/10.1016/j.physb.2020.412777

Vinh, T., Hien, N., Nong, V., Long, T., Tai, L., Thuy, P., & Duijn, M. (1999). Determination of the magneto-caloric effects in Gd5 (Ge1-xSix) compounds from magnetisation isotherms. *Proceedings of the Third International Workshop on Materials Science, Hanoi,* 2-4

Vitos, L., Korzhavyi, A., & Johansson, B. (2003). Stainless steel optimization from quantum mechanical calculations. *Nature Materials*, *2*(1), 25-28.

Von Ranke, P. J., Lima, A. L., Nobrega, E. P., Da Silva, X. A., Guimarães, A. P., & Oliveira, I. S. (2000). Anomalous magnetocaloric effect in YbAs associated with the giant quadrupolar interaction. *Physical Review B*, *63*(2). https://doi.org/10.1103/physrevb.63.024422

Wali, M., Skini, R., Khlifi, M., Dhahri, E., & Hlil, E. K. (2015). A giant magnetocaloric effect with a tunable temperature transition close to room temperature in Na-deficient La $_{0.8}$ Na $_{0.2-}$ $_x$ square x MnO$_3$ manganites. *Dalton Transactions*, *44*(28), 12796-12803. https://doi.org/10.1039/c5dt01254f

Wang Dun-Hui, Yin Jin-Hua, Tang Shao-Long, Shen Ya-Tao, & Du You-Wei. (1999). Study on the Magnetocaloric of alloy gd3al2-xgax. *Acta Physica Sinica*, *48*(13), 116. https://doi.org/10.7498/aps.48.116

Wang, F., Chen, Y. F., Wang, G. J., Sun, J. R., & Shen, B. G. (2004). The large magnetic entropy change and the change in the magnetic ground state of the antiferromagnetic compound LaFe11. 5Al1. 5 caused by carbonization. *Journal of Physics: Condensed Matter*, *16*(12), 2103-2108. https://doi.org/10.1088/0953-8984/16/12/019

Wang, S. Q., & Ye, H. Q. (2003). First-principles study on elastic properties and phase stability of III–V compounds. *Physica Status Solidi (b)*, *240*(1), 45-54. https://doi.org/10.1002/pssb.200301861

Wang, Y., & Bi, X. (2009). The role of Zr and B in room temperature magnetic entropy change of FeZrB amorphous alloys. *Applied Physics Letters*, *95*(26), 262501. https://doi.org/10.1063/1.3276558

Webster, P. J., Ziebeck, K. R., Town, S. L., & Peak, M. S. (1984). Magnetic order and phase transformation in Ni_2MnGa. *Philosophical Magazine B*, *49*(3), 295-310. https://doi.org/10.1080/13642817408246515

Willie S. & Pearce R. R, the paramagnetism of the ferromagnetic elements. (1938). *Proceedings of the Royal Society of London. Series A. Mathematical and Physical Sciences*, *167*(929), 189-204. https://doi.org/10.1098/rspa.1938.0126

Xiao, G., He, W., Yang, T., Huang, G., Wang, T., & Huang, J. (2019). Effect of Co-doping on structural, magnetic and magnetocaloric properties of la0.67ca0.13ba0.2mn1-xcoxo3 (X = 0, 0.02, 0.04, 0.06, 0.08, 0.1) manganites. *Current Applied Physics*, *19*(4), 424-435. https://doi.org/10.1016/j.cap.2019.01.011

Xu, Q. Y., Gu, K. M., Liang, X. L., Ni, G., Wang, Z. M., Sang, H., & Du, Y. W. (2001). Magnetic entropy change in La 0.54 Ca 0.32MnO 3−δ. *Journal of Applied Physics*, *90*(1), 524-526. https://doi.org/10.1063/1.1379047

Yan, A., Müller, K., & Gutfleisch, O. (2008). Magnetocaloric effect in LaFe11.8−xCoxSi1.2 melt-spun ribbons. *Journal of Alloys and Compounds*, *450*(1-2), 18-21. https://doi.org/10.1016/j.jallcom.2006.10.093

Yan, H., Deng, H., Ding, N., He, J., Peng, L., Sun, L., Yang, P., & Chu, J. (2013). Influence of transition elements doping on structural, optical and magnetic properties of BiFeO3 films fabricated by magnetron sputtering. *Materials Letters*, *111*, 123-125. https://doi.org/10.1016/j.matlet.2013.08.075

Yibole, H., Pathak, A., Mudryk, Y., Guillou, F., Zarkevich, N., Gupta, S., Balema, V., & Pecharsky, V. (2018). Manipulating the stability of crystallographic and magnetic sub-lattices: A first-order magnetoelastic transformation in transition metal based laves phase. *Acta Materialia*, *154*, 365-374. https://doi.org/10.1016/j.actamat.2018.05.048

Yin, C., Liu, Q., Decourt, R., Pollet, M., Gaudin, E., & Toulemonde, O. (2011). Unusual oxidation states give reversible room temperature magnetocaloric effect on perovskite-related oxides SrFe0.5Co0.5O3. *Journal of Solid State Chemistry*, *184*(12), 3228-3231. https://doi.org/10.1016/j.jssc.2011.10.002

You, K., Kim, C., Nahm, K., Ryu, M. & Pelzl, J. (1996). Structural Phase Transition of Cubic Ferromagnetic Materials. *Journal of the Korean Physical Society*, *29*(5), 609-613.

Yu, B., Gao, Q., Zhang, B., Meng, X., & Chen, Z. (2003). Review on research of room temperature magnetic refrigeration. *International Journal of Refrigeration*, *26*(6), 622-636. https://doi.org/10.1016/s0140-7007(03)00048-3

Yu, X., Zhou, N., Liu, R., Wang, L., Xu, Z., Gong, H., Zhao, T., Sun, J., Hu, F., & Shen, B. (2023). Effect of zn2+-sn4+ Co-substitution on structural and magnetic properties of srfe12-2xznxsnxo19 (X = 0–2) M-type strontium ferrite. *Physica B: Condensed Matter*, *653*, 414676. https://doi.org/10.1016/j.physb.2023.414676

Zhang, X. X., Tejada, J., Xin, Y., Sun, G. F., Wong, K. W., & Bohigas, X. (1996). Magnetocaloric effect in La0. 67Ca0. 33MnOδ and La0. 60Y0. 07Ca0. 33MnOδ bulk materials. *Applied Physics Letters*, *69*(23), 3596-3598. https://doi.org/10.1063/1.117218

Zhang, Y., Lampen, P. J., Phan, T., Yu, S., Srikanth, H., & Phan, M. (2012). Tunable magnetocaloric effect near room temperature in $La_{0.7-x}Pr_xSr0._3MnO_3$ (0.02≤ x≤ 0.30) manganites. *Journal of Applied Physics*, *111*(6), 063918. https://doi.org/10.1063/1.3698346

Zhang, Z., Luo, Q., Shao, L., Xue, L., Chen, B., & Shen, B. (2022). Tuning magnetocaloric effect of Gd-Co-Al-Si bulk metallic glass via controlling degree of structural order. *Journal of Magnetism and Magnetic Materials*, *545*, 168769. https://doi.org/10.1016/j.jmmm.2021.168769

Zhong, X., Peng, D., Dong, X., Huang, J., Zhang, H., Huang, Y., Wu, S., Yu, H., Qiu, W., Liu, Z., & Ramanujan, R. (2021). Improvement in mechanical and magnetocaloric properties of hot-pressed La(Fe,Si)13/La70Co30 composites by grain boundary engineering. *Materials Science and Engineering: B*, *263*, 114900. https://doi.org/10.1016/j.mseb.2020.114900

Zhong, X., Shen, X., Mo, H., Jiao, D., Liu, Z., Qiu, W., Zhang, H., & Ramanujan, R. (2018). Table-like magnetocaloric effect and large refrigerant capacity in gd65mn25si10-gd composite materials for near room temperature refrigeration. *Materials Today Communications*, *14*, 22-26. https://doi.org/10.1016/j.mtcomm.2017.12.005

Zhou, X., Li, W., Kunkel, H. P., & Williams, G. (2004). A criterion for enhancing the giant magnetocaloric effect: (Ni–mn–Ga)—a promising new system for magnetic refrigeration.

Journal of Physics: Condensed Matter, *16*(6), L39-L44. https://doi.org/10.1088/0953-8984/16/6/l02

Zhu, X., Zhou, X., Yu, S., Wei, C., Xu, J., & Wang, Y. (2017). Effects of annealing on the microstructure and magnetic property of the mechanically alloyed FeSiBAlNiM (M=Co, CU, Ag) amorphous high entropy alloys. *Journal of Magnetism and Magnetic Materials*, *430*, 59-64. https://doi.org/10.1016/j.jmmm.2017.01.028

Zhu, Y., Xie, K., Song, X., Sun, Z., & Lv, W. (2005). Magnetic phase transition and magnetic entropy change in melt-spun La1−xNdxFe11.5Si1.5 ribbons. *Journal of Alloys and Compounds*, *392*(1-2), 20-23. https://doi.org/10.1016/j.jallcom.2004.09.021

Zimm, C., Jastrab, A., Sternberg, A., Pecharsky, V., Gschneidner, K., Osborne, M., & Anderson, I. (1998). Description and performance of a near-room temperature magnetic refrigerator. *Advances in Cryogenic Engineering*, 1759-1766. https://doi.org/10.1007/978-1-4757-9047-4_222

Zoontjens, L., Howard, C., Zander, A., & Cazzolato, B. (2009). Numerical study of flow and energy fields in thermoacoustic couples of non-zero thickness. *International Journal of Thermal Sciences*, *48*(4), 733-746. https://doi.org/10.1016/j.ijthermalsci.2008.06.007

Zverev, V., & Tishin, A. (2016). Magnetocaloric effect: From theory to practice. *Reference Module in Materials Science and Materials Engineering*. https://doi.org/10.1016/b978-0-12-803581-8.02813-7.

APPENDICES

Appendix I: Sample of an input file used for Self-consistent field calculation

```
*FeP_scf1.in - Notepad
File  Edit  Format  View  Help

&control
    calculation='scf'
    pseudo_dir = './',
    outdir='./temp'
    prefix='Fe2P'
 /
 &system
    ibrav = 4,
    celldm(1) = 10.4325
    celldm(3) = 0.5605
    nat= 9, ntyp= 4,
    ecutwfc = 90, ecutrho = 1080
    occupations='smearing', smearing='gaussian',
    degauss=0.05, nspin=2
    starting_magnetization(1)=0.5
    starting_magnetization(2)=0.5

 /
 &electrons
    mixing_beta = 0.7
 /
ATOMIC_SPECIES
Fe1 55.85  fe_pbe_v1.5.uspp.F.UPF
Mn2 54.94  mn_pbe_v1.5.uspp.F.UPF
P   30.97  p_pbe_v1.5.uspp.F.UPF
Si 28.09   si_pbe_v1.uspp.F.UPF


ATOMIC_POSITIONS {crystal}
Mn2   0.000000  0.408468  0.500000
Mn2   0.591532  0.591532  0.500000
Mn2   0.408468  0.000000  0.500000
Fe1   0.743444  0.000000  0.000000
Fe1   0.256556  0.256556  0.000000
Fe1   0.000000  0.743444  0.000000
P    0.666667  0.333333  0.000000  |
P    0.333333  0.666667  0.000000
Si   0.000000  0.000000  0.500000

K_POINTS (automatic)
3 3 5 0 0 0
```

Appendix II: Elastic properties of the selected materials in the FM, PM and PM phases

Material (FM)	B_V	B_R	B_H	G_V	G_R	G_H	E	ν	B_H/G_H
$FeMnP_{0.66}Si_{0.33}$	1608.981	1598.343	1603.662	842.060	763.336	802.698	2063.234	0.285	1.998
$FeMnP_{0.66}Se_{0.33}$	1560.731	1560.591	1560.661	790.682	784.937	787.810	2023.023	0.284	1.981
$FeMnP_{0.66}In_{0.33}$	1220.319	1036.992	1128.656	389.772	162.226	275.997	759.674	0.376	4.089
$FeMnP_{0.66}Sn_{0.33}$	1358.422	1336.805	1347.614	494.698	409.574	452.136	1219.153	0.348	2.978

Material (PM)	B_V	B_R	B_H	G_V	G_R	G_H	E	ν	B_H/G_H
$FeMnP_{0.66}Si_{0.33}$	1979.555	1969.550	1974.552	1127.274	1118.538	1122.906	2831.896	0.261	1.758
$FeMnP_{0.66}Se_{0.33}$	2043.070	2042.638	2043.304	1007.386	987.502	997.444	2573.538	0.290	2.049
$FeMnP_{0.66}In_{0.33}$	1582.652	2856.448	2219.550	485.268	2529.402	1507.335	3589.832	0.191	1.472
$FeMnP_{0.66}Sn_{0.33}$	1634.574	1627.062	1630.818	503.703	498.399	501.051	1363.511	0.361	3.255

Material (AFM)	B_V	B_R	B_H	G_V	G_R	G_H	E	ν	B_H/G_H
$FeMnP_{0.66}Si_{0.33}$	1549.553	1500.741	1525.147	999.384	969.911	984.647	2430.822	0.234	1.549
$FeMnP_{0.66}Se_{0.33}$	1328.678	1328.558	1328.618	858.829	852.305	855.567	2113.113	0.235	1.553
$FeMnP_{0.66}In_{0.33}$	1283.303	1281.185	1282.244	381.668	367.194	374.431	1023.625	0.367	3.425
$FeMnP_{0.66}Sn_{0.33}$	1334.180	1318.375	1326.277	511.076	497.873	504.475	1343.122	0.331	2.629

Appendix III: Absolute magnetisation and total magnetisation of the selected materials in the FM, AFM and PM phases.

Material (FM)	Absolute magnetization (μ_B)	Total magnetization (μ_B)
$FeMnP_{0.66}Si_{0.33}$	17.00	16.17
$FeMnP_{0.66}Se_{0.33}$	17.79	17.03
$FeMnP_{0.66}In_{0.33}$	22.33	21.37
$FeMnP_{0.66}Sn_{0.33}$	20.55	20.64

Material (PM)	Absolute magnetization (μ_B)	Total magnetization (μ_B)
$FeMnP_{0.66}Si_{0.33}$	0.00	-0.00
$FeMnP_{0.66}Se_{0.33}$	0.00	-0.00
$FeMnP_{0.66}In_{0.33}$	0.11	-0.02
$FeMnP_{0.66}Sn_{0.33}$	0.04	0.00

Material (AFM)	Absolute magnetization (μ_B)	Total magnetization (μ_B)
$FeMnP_{0.66}Si_{0.33}$	17.00	-0.00
$FeMnP_{0.66}Se_{0.33}$	17.79	0.00
$FeMnP_{0.66}In_{0.33}$	22.33	-0.01
$FeMnP_{0.66}Sn_{0.33}$	20.55	0.00

Appendix IV: Snapshot of the abstract of the first publication

Ab Initio Study of Structural and Vibrational Properties of Fe₂P-Type Materials for Near - Room - Temperature Refrigeration

Anne Mwende Thirika[1,*], Winfred Mueni Mulwa[1],
Nicholus Wambua Makau[2], Adentuji Bamidele Ibrahim[3]

[1]Egerton University, Nakuru, Kenya
[2]University of Eldoret, Eldoret, Kenya
[3]Bells University of Technology, Ota Ogun State, Nigeria
*Corresponding author: annethirika@gmail.com

Abstract This work has applied density functional theory (DFT) based calculations to investigate the structural and vibrational properties of $FeMnP_{1-x}A_x$ (A= Si, Se, Sn and In, x = 0.33) within the first-principles pseudopotential technique. The exchange correlation potentials were treated within generalized gradient approximation (GGA), in the Quantum ESPRESSO code. The Perdew, Burke, Ernzerhof (PBE) functional as implemented in Vanderbilt's ultra-soft pseudo potential (USPP) was used for all the calculations. Vibrational properties were calculated using phonopy code with $1 \times 1 \times 2$ supercell of the conventional unit cell. Thermodynamic properties were predicted using the phonon density of states. The dependence of lattice thermal conductivity on temperature was determined using Debye theory. The optimized structural parameters and corresponding graphical values fit within available experimental data and other theoretical reports. There were no imaginary phonon modes in the phonon dispersion curves revealing that these materials are dynamically stable for magnetic refrigeration.

Keywords: Fe₂P-type materials, magnetic refrigeration, density functional theory, phonons, quantum ESPRESSO, thermodynamic

Cite This Article: Anne Mwende Thirika, Winfred Mueni Mulwa, Nicholus Wambua Makau, and Adentuji Bamidele Ibrahim, "*Ab Initio* Study of Structural and Vibrational Properties of Fe₂P-Type Materials for Near - Room - Temperature Refrigeration." *International Journal of Physics*, vol. 10, no. 1 (2022): 49-58. doi: 10.12691/ijp-10-1-3.

Appendix V: Snapshot of an abstract of the second publication

The Elastic Properties of $F_e m_n P_{1-x} A_x$ (A= Si, Se, Sn, In, x = 0.33) Materials: A DFT Study

Anne Mwende Thirika[1,*], Winfred Mueni Mulwa[2],
Nicholus Wambua Makau[3], Adentuji Bamidele Ibrahim[4]

[1]Egerton University, Nakuru, Kenya,
[2]Egerton University, Nakuru, Kenya
[3]University of Eldoret, Eldoret, Kenya
[4]Bells University of Technology, Ota Ogun State, Nigeria
*Corresponding author: annethirika@gmail.com

Abstract Hexagonal Fe_2P-type magnetocaloric materials have been attracting a lot of research interest lately as a result of their promising application in magnetic refrigeration. These materials work under repeated magnetic and thermal cycles which results to large local strains in the polycrystalline samples and so they need to be mechanically stable across the phase transition. Hence, there is a need to conduct extensive investigations in order to obtain materials which may have better performance in magnetic refrigeration. In this study the elastic properties of $FeMnP_{1-x}A_x$ (A= Si, Se, Sn, In, x = 0.33) were investigated using first principles density functional theory within the generalized gradient approximations as expressed in Quantum Espresso code. The work conclusively shows that $FeMnP_{0.66}In_{0.33}$ has the highest Poisson's ratio, Pugh's and machinability index hence most ductile of the selected materials. Moreover, it had the highest anisotropic ratio further proving that of the four compounds, it is the most suitable for sustainable operation as a magnetocaloric refrigerant.

Keywords: machinability, ductile, phase transition, hexagonal, mechanical stability, elastic

Cite This Article: Anne Mwende Thirika, Winfred Mueni Mulwa, Nicholus Wambua Makau, and Adentuji Bamidele Ibrahim, "The Elastic Properties of $F_e m_n P_{1-x} A_x$ (A= Si, Se, Sn, In, x = 0.33) Materials: A DFT Study." *Journal of Materials Physics and Chemistry*, vol. 10, no. 1 (2022): 10-16. doi: 10.12691/jmpc-10-1-2.

Appendix VI: Snapshot of the research permit

Ref No: 645004

Date of Issue: 09/September/2021

RESEARCH LICENSE

This is to Certify that Miss.. Anne Mwende Thirika of Egerton University, has been licensed to conduct research in Nakuru on the topic: AB INITIO STUDY OF STRUCTURAL, ELASTIC AND VIBRATIONAL PROPERTIES OF Fe_2P-TYPE MATERIALS FOR NEAR -ROOM -TEMPERATURE REFRIGERATION for the period ending : 09/September/2022.

License No: NACOSTI/P/21/12874

645004

Applicant Identification Number

Director General
NATIONAL COMMISSION FOR
SCIENCE,TECHNOLOGY &
INNOVATION

Verification QR Code

NOTE: This is a computer generated License. To verify the authenticity of this document,
Scan the QR Code using QR scanner application.

160